AD-A158 229 THEORETICAL STUDIES OF TWO-DIMENSIONAL EFFECTS IN FREE ELECTRON LASERS(U) AUSTIN RESEARCH ASSOCIATES INC TX M N ROSENBLUTH ET AL. DEC 84 I-ARA-84-U-121 1/2

UNCLASSIFIED AFOSR-TR-85-0493 F/G 20/5 NL

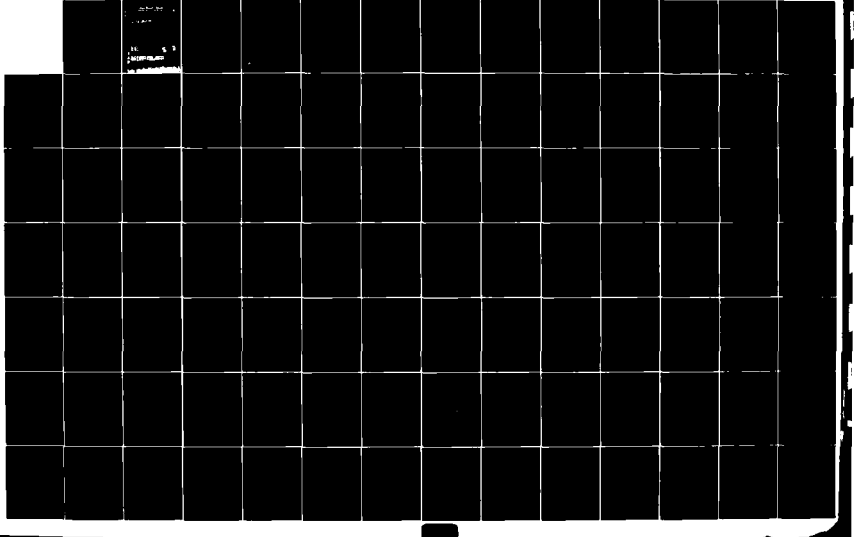

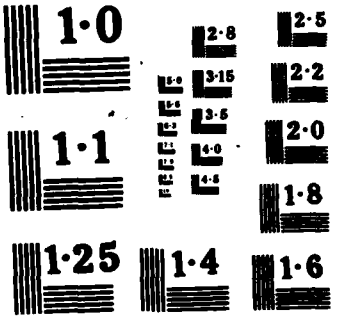
1·0
1·1
1·25
2·8
3·15
3·5
4·0
4·5
1·4
2·5
2·2
2·0
1·8
1·6

UNCLASSIFIED

SECURITY CLASSIFICATION OF THIS PAGE

REPORT DOCUMENTATION PAGE

1a. REPORT SECURITY CLASSIFICATION: UNCLASSIFIED	1b. RESTRICTIVE MARKINGS
2a. SECURITY CLASSIFICATION AUTHORITY: n/a	3. DISTRIBUTION/AVAILABILITY OF REPORT: Approved for public release; distribution unlimited.
2b. DECLASSIFICATION/DOWNGRADING SCHEDULE: n/a	
4. PERFORMING ORGANIZATION REPORT NUMBER(S): I-ARA-84-U-121 (ARA-525)	5. MONITORING ORGANIZATION REPORT NUMBER(S): AFOSR-TR- 85-0493
6a. NAME OF PERFORMING ORGANIZATION: Austin Research Associates; 6b. OFFICE SYMBOL (If applicable):	7a. NAME OF MONITORING ORGANIZATION: AFOSR/NP
6c. ADDRESS (City, State and ZIP Code): 1901 Rutland Drive, Austin, Texas 78758	7b. ADDRESS (City, State and ZIP Code): Building 410, Bolling AFB, DC 20332
8a. NAME OF FUNDING/SPONSORING ORGANIZATION: Defense Advanced Research Projects Agency; 8b. OFFICE SYMBOL (If applicable): DARPA	9. PROCUREMENT INSTRUMENT IDENTIFICATION NUMBER: F49620-84-C-0011
8c. ADDRESS (City, State and ZIP Code): 1400 Wilson Boulevard, Arlington, VA 22209	10. SOURCE OF FUNDING NOS. — PROGRAM ELEMENT NO.: 61102F; PROJECT NO.: 2301; TASK NO.: A1; WORK UNIT NO.:
11. TITLE (Include Security Classification): Final Technical Report on Theoretical Studies of Two-Dimensional Effects in Free Electron Lasers (U)	
12. PERSONAL AUTHOR(S): M. N. Rosenbluth, H. Vernon Wong and B. N. Moore	
13a. TYPE OF REPORT: Final Technical; 13b. TIME COVERED: FROM 2/1/84 TO 10/31/84; 14. DATE OF REPORT (Yr., Mo., Day): December 1984; 15. PAGE COUNT: 145	
16. SUPPLEMENTARY NOTATION	

17. COSATI CODES			18. SUBJECT TERMS (Continue on reverse if necessary and identify by block number)
FIELD	GROUP	SUB. GR.	free electron laser (FEL); two-dimensional effects; variable parameter wiggler

19. ABSTRACT (Continue on reverse if necessary and identify by block number)

This report describes the development of a two-dimensional numerical simulation free electron laser code which includes pass-to-pass electromagnetic pulse evolution, wave diffraction, transverse betatron motion of the electrons, and frequency discrimination to suppress the growth of unstable sidebands. The code was used to simulate the experiment recently completed at TRW, the experiment being done at LANL, and the proposed MSNW experiment. The TRW simulations are in qualitative agreement with experimental results. The LANL simulations are similar to the one-dimensional simulations (1-D) previously done. The MSNW simulations exhibit general trends which are similar to those of the MSNW 1-D simulations; in both, frequency discrimination improves the trapping efficiency and produces a smooth optical pulse.

(Continued on back)

20. DISTRIBUTION/AVAILABILITY OF ABSTRACT: UNCLASSIFIED/UNLIMITED ☐ SAME AS RPT. ☒ DTIC USERS ☐	21. ABSTRACT SECURITY CLASSIFICATION: UNCLASSIFIED
22a. NAME OF RESPONSIBLE INDIVIDUAL: [redacted], Capt., USAF Dr. Schloerb	22b. TELEPHONE NUMBER (Include Area Code): (202) 767-[redacted]4906; 22c. OFFICE SYMBOL: NP

DD FORM 1473, 83 APR EDITION OF 1 JAN 73 IS OBSOLETE.

UNCLASSIFIED

SECURITY CLASSIFICATION OF THIS PAGE

A

19. This report also discusses the feasibility of steady state operation of tapered wigglers in storage rings. Long smooth optical pulses are necessary to reduce energy spreading in the wiggler. Conventional tapered wigglers appear to require lower circulating power levels than phase area displacement wigglers. Additional

Keywords: Various parameter wiggler ...

TABLE OF CONTENTS

FINAL REPORT ON
THEORETICAL STUDIES OF TWO-DIMENSIONAL
EFFECTS IN FREE ELECTRON LASERS

During the nine-month period extending from February 1, 1984 through October 31, 1984, the following tasks were undertaken:

I. The development of a two-dimensional (2-D) numerical simulation FEL code which includes pass-to-pass electromagnetic (EM) pulse evolution, frequency discrimination, wave diffraction, and transverse betatron motion of the electrons. This effort represents the beginning of an attempt to obtain more accurate simulations of realistic FEL configurations than can be achieved with one-dimensional 1-D analyses. The 2-D FEL code was used to simulate the TRW and LANL experiments, and the proposed MSNW experiment. A steady state version of the code, suitable for studying amplifiers (e.g., ETA and ATA) has been developed but not yet tested for convergence of the mode expansion under the large expected gains of these experiments.

II. The study of the operation of FELs in conjunction with storage rings, using phase area displacement wigglers and conventionally tapered wigglers with adiabatic electron trapping, deceleration, and detrapping.

I. 2-D SIMULATIONS

The main focus of the investigation was the 2-D FEL simulations. The 1-D FEL model is lacking in several respects.[1] It neglects the transverse spatial variations of the EM pulse, magnetic wiggler and electron beam micropulse, and hence does not include the effects of EM pulse diffraction radial detrapping and the transverse electron betatron motion produced by the focusing fields of the wiggler. These effects can modify the 1-D results. They can influence not only the growth of sideband instabilities, but also the efficiency of electron trapping. Electron detrapping can become significant when there is resonance coupling of the "bounce" motion of the trapped electrons (in the FEL ponderomotive potential well) with the transverse betatron motion.[2] These additional effects are linked to the transverse spatial variations of the fields of the EM pulse and wiggler and are present to some degree in any FEL configuration. They can be properly described only by a 2-D FEL model.

In the simulations described in this report, resonance detrapping of electrons does not appear to be significant. However, the importance of this resonance will be enhanced if different focusing schemes (e.g., quadrupole focusing) are employed. These will be incorporated into the code shortly.

A. Simulation Code

In formulating the 2-D FEL equations, the EM pulse is represented as a superposition of cylindrically symmetric Gaussian resonator modes of an optical cavity formed by two spherical mirrors.[3] (The generalization to three dimensions is, in principle, trivial.) Each Gaussian mode is approximated by a wave packet propagating in the z-direction, with amplitude and phase varying slowly with time t and the longitudinal spatial variable z. The magnetic wiggler is approximated by a superposition of two plane-polarized wigglers, and this configuration is adopted to provide for focusing of the electrons inside the wiggler. (No quadrupole focusing magnetic fields are considered although such fields will be incorporated into the code in the future.) A variable parameter wiggler is modeled by introducing a constant accelerating electric field. The transverse spatial variations of the wiggler field induce transverse betatron motion of the electrons passing through it. This transverse betatron motion is approximated as a simple harmonic motion. The longitudinal electron motion can then be reduced to a pair of coupled equations for the electron energy and relative phase in the EM pulse, analogous to the "pendulum" equation in the 1-D limit. The analogous ponderomotive potential well depends on the transverse as well as the longitudinal electron position and involves a sum over the Gaussian modes. The temporal and spatial evolution of each Gaussian mode, determined from Maxwell's equations, is similar in form to the

1-D limit. The derivation of these equations are discussed in Appendix A, Section II.

The FEL oscillator equations, incorporating multiple reflections of the EM pulse by the spherical mirrors, energy losses on reflection at the mirrors, and frequency discrimination by passing the pulse through a band-pass filter, are formulated by following the same procedure previously described in the 1-D limit.[1] The only additional complication is the relative phase shifts between the Gaussian modes which occur on reflection.

The difference equations which approximate the FEL equations are discussed in Appendix A, Section III. They are correct to first order in the steplengths, and are adequate to simulate FEL oscillators with modest peak current densities and weakly tapered, short wigglers; for example, the FEL oscillator experiments of TRW and LANL. The detailed simulation results of the TRW and LANL experiment are presented in Appendix A, Section IV.

These difference equations are, however, not sufficiently accurate for practical steplengths to simulate the MSNW experiment and have recently been modified to be correct to second order in the steplengths by making use of the centered difference approximation. The MSNW FEL experiment involves higher peak current densities, stronger wiggler taper, and a longer wiggler. The details of this improved numerical

algorithm will be reported elsewhere. The detailed simulation results of the MSNW experiment is presented in Appendix B.

Due to computer time constraints, the electron micropulses used in the simulations were only two to three slippage lengths and hence were shorter than the experimental lengths. Longer micropulses are planned for future investigations.

The principal results of these simulations may be summarized as follows:

B. TRW FEL Simulation

In the TRW experiment, the peak current is 2.5 amp, the electron energy 66 MeV, the wiggler taper 1%, and the wavelength of the EM pulse 1.57 microns. A notable feature of this experiment is the narrow single peaked spectrum of the Em pulse at saturation, the full width $\Delta\omega$ at half maximum being $\Delta\omega/\omega_s \sim 0.13\%$, where ω_s is the frequency of the EM pulse.

The FEL simulations are in qualitative agreement with this experimental result. The EM pulse shape is smooth, there is no evidence of any unstable sideband activity, and the frequency spectrum at saturation consists of a single narrow peak. The simulation spectral width $\Delta\omega_{sim}$ is, however, smaller in magnitude $\Delta\omega_{sim}/\omega_s \sim 0.05\%$.

The somewhat wider experimental width could be due to time averaging over changing parameters. The essential feature

of our results is that for these low currents and tapers no sidebands are predicted or observed.

The effective fraction of trapped electrons is 33% and the average output power is

$$\left\langle P_{output} \right\rangle \sim 0.47 \text{ megawatts.}$$

While this output is in reasonable agreement with the experiment, it should be noted that for 2% taper we predict a near doubling of output, which was not observed perhaps due to lack of time for optimizing the experiment.

C. LANL FEL Experiment

In the LANL experiment, the peak current is 25 or 80 amps for different runs, the electron energy 21 MeV, the wiggler taper 6%, and the wavelength of the EM pulse 10 microns.

The linear gain per pass in the simulation is negligibly small when the peak current is 25 amps, and ~5% when the peak current is 80 amps.

The EM pulse shape at saturation is not smooth. It is characterized by several maxima and minima. At the same time, the frequency spectrum of the pulse exhibits appreciable growth of sideband frequencies. This pulse distortion is due to the growth of unstable sideband modes, and has previously been observed in 1-D FEL simulations. The growth of sideband modes

can be suppressed by frequency discrimination.[1] However, such frequency discriminated simulations with the LANL parameters have not yet been done with the 2-D simulation code, although they are planned for future investigations.

Despite the pulse distortion, the effective electron trapping fraction is still appreciable, ~40% at saturation. The average output power is

$$\left\langle P_{output} \right\rangle \sim 21 \text{ megawatts.}$$

The condition for resonance coupling of the electron "bounce" motion to the betatron motion is satisfied at an intermediate stage of the pulse evolution, but no significant resonance detrapping has been observed. However, it should be noted that the radial electron focusing method employed in the code is not that used in the experiment.

D. MSNW FEL Simulation

In the proposed MSNW experiment, the peak current is 200 amps, the electron energy is 120 MeV, the wiggler taper is 12.5%, and the wavelength of the EM pulse is 0.5 microns.

The simulations were done both without and with frequency discrimination. In the absence of frequency discrimination, the EM pulse shape at saturation is highly irregular and characterized by random peaks. The frequency spectrum is broad and exhibits considerable activity at

sideband frequencies. When frequency discrimination is present to suppress unstable sideband modes, a smooth saturated pulse shape and a narrow single peaked spectrum are obtained. In addition, the effective electron trapping fraction and the average output power are significantly higher.

With frequency discrimination, the linear gain for zero mirror losses is ~8.5% per pass. The effective electron trapping fraction with power reflectivity of 0.9 is ~22% and the average output power is

$$\left\langle P_{output} \right\rangle \sim 660 \text{ megawatts.}$$

Significant effects associated with the 2-D structure of the EM pulse are present in these simulations. For example, two Gaussian modes were allowed to evolve, and the pulse energy of the higher order Gaussian mode was about 2% of the energy in the lowest order Gaussian mode at saturation.

Since electrons are trapped at EM pulse amplitudes above the critical amplitude for resonance coupling to the betatron motion, resonance detrapping effects do not appear to be important in these simulations. Again, it will be interesting to study the effects of proposed quadrupole focusing.

II. STORAGE RING OPREATION

A. Phase Area Displacement Wiggler

In a previous investigation, it was concluded that high FEL efficiency is theoretically possible for FEL oscillators using a phase area displacement wiggler in conjunction with a storage ring. The operation of such a device has yet to be demonstrated experimentally. It has been suggested that it may be possible to design a proof of principle experiment for the Stanford storage ring under construction.

In the Stanford storage ring, the electron energy is 1 GeV and the peak current is 270 amps. The stored electron beams are 1 cm in length and ~ 0.05 cm in radius. The synchrotron energy loss is less than 0.1% per round trip. The space available to accommodate FEL wigglers is ~ 20 meters long.

With the above constraints and assuming that the wavelength of the EM pulse to be generated is 0.5 microns, it has been concluded on the basis of the analysis discussed in Appendix C that steady state operation is impractical because:

1. Very good "power reflectivities" > 0.999 per pass are required since the electron beam and EM pulse can only be allowed to interact infrequently to avoid excessive beam energy spread;

2. Long electron beams of the order of 100 cm are required in order to produce long smooth EM pulses so as to minimize nonadiabatic electron trapping;

3. Steady state circulating peak power levels of 100 GeV are required, which imply the added complication of having to grow the pulse from lower levels.

4. An extremely steady optical pulse would be required to avoid electron trapping.

Thus, a practical device appears to be impossible unless the wiggler performance can be considerably enhanced.

An interesting modification in this direction, suggested by D. A. G. Deacon, is to "phase bunch" the electrons in a "pre-buncher" prior to entry into the wiggler. With careful "phase-bunching," the electron interaction can be optimized to further reduce the energy spreading, in which case steady state operation may be possible at lower pulse power levels and for shorter electron beam lengths. However, this modification has not yet been explored in any detail, and success will certainly require long steady EM pulses.

B. Conventional Variable Parameter Wiggler

An alternative wiggler for use in a storage ring, discussed in Appendix D, is a conventionally tapered wiggler designed to adiabatically trap electrons at the front, decelerate the trapped electrons inside the wiggler, and then

detrap the electrons at the back. In this scheme, negligible increase in the energy spread is produced during adiabatic deceleration. The critical task is then to minimize the increase in the energy spread during trapping and detrapping. This separation of energy extraction from energy spreading introduces a degree of flexibility which can be exploited to reduce the ratio of energy spreading to energy extraction to desirable levels.

Preliminary estimates suggest that it should be possible to design a conventionally tapered wiggler to be used with the Stanford storage ring, with steady state circulating power levels of the order of 1 GW, which are considerably lower than that required for a phase area displacement wiggler.

Furthermore, growth from low noise levels would be easier since conventionally tapered wigglers typically have higher linear gain.

Thus, conventionally tapered wigglers appear to be more favorable than phase area displacement wigglers, although many of the same problems arise; in particular, the need for a very smooth EM pulse.

REFERENCES

1. W. B. Colson and S. K. Ride, "The Free Electron Laser: Maxwell's Equations Driven by Single Particle Currents," Free Electron Generators of Coherent Radiation, Physics of Quantum Electronics, Vol. 7 (Addison-Wesley, 1980), p. 377.

   J. C. Goldstein, "Evolution of Long Pulses in a Tapered Wiggler Free Electron Laser," Free Electron Generators of Coherent Radiation, SPIE, Vol. 453 (June 1983), p. 2.

   M. N. Rosenbluth, H. V. Wong and B. N. Moore, "Free Electron Laser (Oscillator) - Linear Gain and Stable Pulse Propagation," Free Electron Generators of Coherent Radiation, SPIE, Vol. 453 (June 1983), p. 11.

   M. N. Rosenbluth, H. Vernon Wong and B. N. Moore, "Annual Technical Report for Theoretical Studies on Free Electron Lasers," ARA Report No. I-ARA-82-U-89 (NTIS No. AD-A121673), August 1982.

   M. N. Rosenbluth, H. Vernon Wong and B. N. Moore, "Final Technical Report for Theoretical Studies on Free Electron Lasers," ARA Report No. I-ARA-83-U-62 (NTIS No. AD-136333), November 1983.

2. M. N. Rosenbluth, "Two-Dimensional Effects in Free Electron Lasers," Journal of Quantum Electronics (to be published in 1985), Appendix E, ARA Report No. I-ARA-83-U-62 (NTIS No. AD-136333), November 1983.

   W. M. Fawley, D. Prosnitz and E. T. Schorlemann, submitted to Phys. Rev. A (1985), Lawrence Livermore National Laboratory Report UCRL-90838 (1984).

3. H. Kogelnik and T. Li, "Laser Beams and Resonators," Applied Optics, Vol. 5, No. 10, 1550-1567.

   C. M. Tang and P. Sprangle, "Semi-analytic Formulation of the Two-Dimensional Pulse Propagation in the Free Electron Laser Oscillator," Free Electron Generators of Coherent Radiation, SPIE, Vol. 453 (June 1983), p. 11.

A P P E N D I X A

SIMULATION OF TRW AND LANL EXPERIMENTS

I. INTRODUCTION

In this report, we describe the development of a two-dimensional (2-D) numerical simulation free electron laser (FEL) code which includes pass-to-pass electromagnetic (EM) pulse evolution, frequency discrimination, wave diffraction, and transverse betatron motion of the electrons. This effort represents the beginning of an attempt to obtain more accurate simulations of realistic FEL configurations than can be achieved with one-dimensional (1-D) analysis.

In one-dimensional investigations of the FEL, transverse spatial variations of the EM pulse, magnetic wiggler, and electron beam micropulses are neglected. The EM pulse is represented as a plane wave with amplitude and phase varying slowing in the direction of propagation (z-direction); the wiggler amplitude and wavelength varies slowly with z; and the electron equations of motion are reduced to the "pendulum" equation for the electron energy and relative phase in the EM pulse.[1] The wiggler couples the electrons to the EM pulse, and

in the Compton regime may be viewed in terms of the interaction of electrons with a one-dimensional ponderomotive potential well produced by the combined wiggler and EM pulse fields. Maxwell's equations, with the transverse electron currents as sources, determine the temporal and spatial evolution of the EM pulse.

This model has served as the basis for many theoretical analyses and numerical simulations of FEL operation.[1] These investigations have discussed: The linear gain of small amplitude EM pulses, the growth of the EM pulse into the nonlinear regime when electrons become trapped in the ponderomotive potential, the "breakup" of large amplitude EM pulses due to the onset of "sideband" instabilities, the suppression of "sideband" instabilities by frequency discrimination.

However, the one-dimensional FEL model is lacking in several respects. It does not include the effects of the diffraction of the EM pulse and the electron betatron motion produced by the focusing fields of the wiggler. These effects will modify somewhat the one-dimensional results. They can influence not only the growth of sideband instabilities, but also the efficiency of electron trapping. Electron detrapping may become significant when the ponderomotive potential amplitude reaches a value where resonance coupling of the "bounce" and betatron motion can occur.[2] The strength of this coupling depends on the geometry of the focusing magnetic wiggler fields as well as the curvature of the wave front.

Quadrupole focusing fields appear to induce unacceptably strong coupling, while that due to wave front curvature may be weakened by any flattening of the wave front produced by interaction with electrons.[3] These additional effects are linked to the transverse spatial variations of the fields of the EM pulse and wiggler which are always present to some degree in any FEL configuration, and they can be properly described only by a two-dimensional FEL model.

In Section II, we derive the electron equations of motion and the EM pulse evolution equations, and we formulate the basic 2-D FEL oscillator equations which are incorporated in the numerical simulation code. The EM pulse is considered to be axisymmetric and is represented as a sum of the Gaussian modes of a cavity formed by spherical mirrors symmetrically positioned on either side of the wiggler. The wiggler is modeled by the superposition of two plane polarized wigglers. No quadrupole focusing magnetic fields are included in this investigation, although we intend to incorporate such fields into the code in the near future.

In Section III, we describe the numerical algorithms implemented in the code. The code is used to simulate the experiment recently completed at TRW, and the experiment being done at LANL. (A modified version of the code was used for simulation of MSNW parameters [see Appendix B]). These results are presented in Section IV, but have not yet been analyzed in detail. A preliminary survey indicates the following:

1. The 2-D simulation of the TRW experiments yielded results which were consistent with the observation. The spectrum of the EM pulse was singly peaked with no evidence of sideband activity. The output power levels at saturation were within a factor of two of the observed levels, the differences probably due to uncertainty in the value of the detuning parameter. The 2-D and the 1-D simulation results were essentially the same.

2. In the 2-D simulation of the LANL experiment, the EM pulse shape at saturation was not smooth, but exhibited several maxima and minima due to the growth of unstable sideband modes. Despite this distortion of the pulse shape, the effective electron trapping efficiency is still appreciable ~40%. Detrapping due to resonance coupling between the "bounce" motion and the betatron motion does not appear to be appreciable.

II. BASIC EQUATIONS

A. Electron Equation of Motion

In the free electron laser (FEL) oscillator, a relativistic electron beam is propagated through a transverse periodic magnetic field wiggler where the electrons acquire transverse oscillatory motion which enables them to couple to the transverse electric field of an electromagnetic (EM) pulse. The EM pulse is reflected many times through the wiggler by spherical mirrors positioned on either side of the wiggler. Electron micropulses are injected into the wiggler at periodic intervals so that on each forward pass of the EM pulse through the wiggler, there is overlap of the EM pulse and the electron micropulse (Fig. A1). The EM pulse amplitude grows on each pass and in this way can be grown to large amplitudes after a finite number of passes.

We consider the limit of very energetic, low current electron micropulses, where the electrostatic self-fields may be neglected nd the electron current is a sum of the single particle currents. The EM pulse is approximated by the vacuum solutions of Maxwell's equations. It is represented as a sum of the Gaussian modes of the cavity formed by spherical mirrors:

$$A_{sy} = \frac{1}{2} \sum A_{ns}(z,t)\ \chi_n(r,z)\ e^{-i\omega_s t + i k_s z + i \zeta_n(z)} + \text{complex conjugate} \qquad \text{(A1)}$$

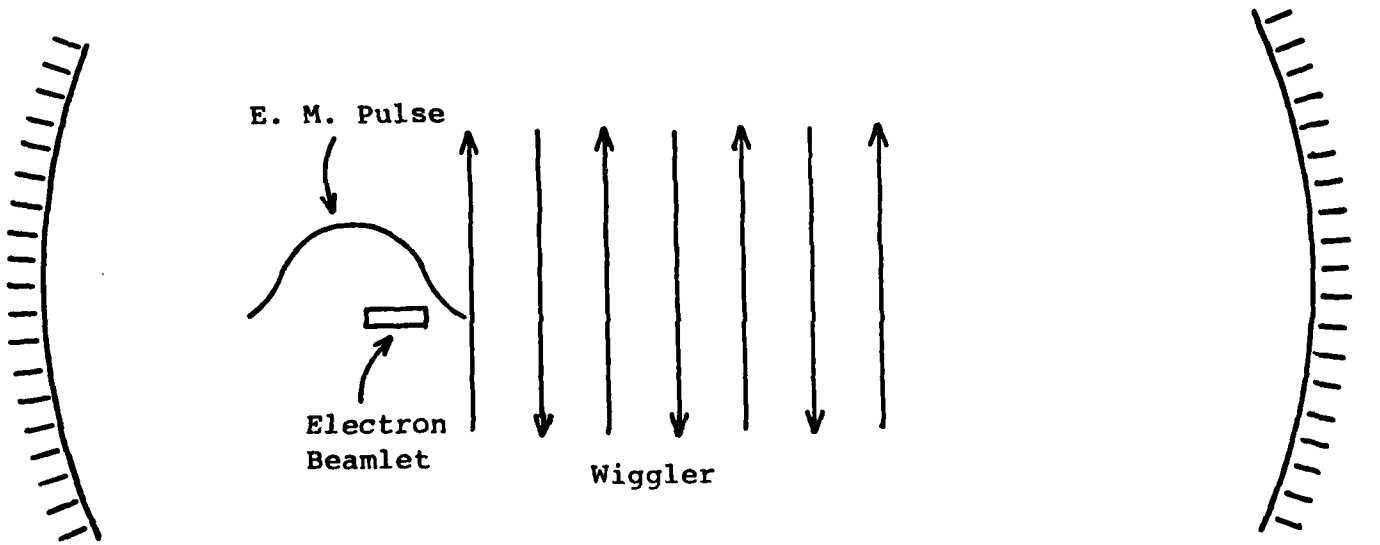

Figure A1. FEL Configuration

where

$$\chi_n(r,z) = \hat{\chi}_n(r,z)\, e^{+\frac{ik_s r^2}{2R(z)} - i(2n+1)\tan^{-1}\frac{z}{z_R}}$$

$$\hat{\chi}_n = \frac{L_n\left(\frac{2r^2}{w^2(z)}\right) e^{-r^2/w^2(z)}}{\left(1 + \frac{z^2}{z_R^2}\right)^{\frac{1}{2}}}$$

$$w^2(z) = r_p^2\left(1 + \frac{z^2}{z_R^2}\right)$$

$$r_p^2 = \frac{2z_R}{k_s}$$

$$R(z) = \frac{\left(z^2 + z_R^2\right)}{z}$$

$$z_R = \left(\frac{LR_o}{2}\right)^{\frac{1}{2}}\left(1 - \frac{L}{2R_o}\right)^{\frac{1}{2}}$$

$L_n\left(\frac{2r^2}{w^2}\right) \equiv$ Laguerre polynomial

$$\omega_s = k_s c$$

$$k_s z_R >> 1$$

$X_n(r,z)$ is a solution of the equation:

$$\frac{1}{r}\frac{\partial}{\partial r}\, r \frac{\partial}{\partial r} \chi_n - 2i k_s \frac{\partial}{\partial z} \chi_n = 0$$

A_{sy} is the vector potential of the EM pulse. It is considered to be cylindrically symmetric (r,θ,z are the usual cylindrical coordinates), plane polarized in the y-direction, and propagating in the z-direction. The mirrors have radius of curvature R_o and the mirror separation is L. Each Gaussian mode is approximated by a wave packet with amplitude $A_{ns}(z,t)$ and phase $\zeta_n(z,t)$ varying slowly in space and time,

$$\left\{\frac{1}{A_{ns}}\frac{\partial A_{ns}}{\partial z}, \frac{\partial \zeta_n}{\partial z}\right\} << k_s, \left\{\frac{1}{A_{ns}}\frac{\partial A_{ns}}{\partial t}, \frac{\partial \zeta_n}{\partial t}\right\} << \omega_s .$$

The dependence of frequency ω_s and wave number k_s on mode number n is ignored.

The wave front is plane at $z = 0$ where the minimum "spot" size radius is r_p. Away from $z = 0$, the "spot" size increases and the wave front becomes spherical with radius of curvature $R(z = \pm L/2) = R_o$.

The vector potential of the magnetic wiggler is approximated by:

$$A_w = -\hat{y} A_{wy}\left(1 + \frac{k_{wy}^2 x^2}{2}\right)\cos\int^z k_{wy}\,dz$$

$$-\hat{x} A_{wx}\left(1 + \frac{k_{wx}^2 y^2}{2}\right)\cos\int^z k_{wx}\,dz \qquad \text{(A2)}$$

where $\left\{k_{wy}x,\ k_{wx}y\right\} << 1$.

This arrangement consists of a superposition of two plane-polarized wigglers and is adopted to provide for "focusing" of the electron micropulses inside the wiggler. The amplitudes A_{wx}, A_{wy} and wave numbers k_{wx}, k_{wy} are slowly varying in z. Their magnitudes are chosen so that the electron micropulses can be in resonance with one (A_{wy}, k_{wy}) but not the other (A_{wx}, k_{wx}), and that the betatron motion of the electrons in the x- and y-directions have the same frequency.

The electron equations of motion can be derived from the Hamiltonian

$$H = H(x, P_x, y, P_y, (-\mathcal{E}), t, z)$$

$$= -\left[\frac{(\mathcal{E} - e\phi_o)^2}{c^2} - m^2c^2 - \left(P_x - \frac{e}{c}A_x\right)^2 - \left(P_y - \frac{e}{c}A_y\right)^2\right]^{\frac{1}{2}} - \frac{e}{c}A_z \tag{A3}$$

where the electron energy $(-\mathcal{E})$ plays the role of the momentum conjugate to t, and z is the independent variable.

ϕ_o is the electrostatic potential of an accelerating electric field $-\partial\phi_o/\partial z$. Its presence is used to model the effect of a variable parameter wiggler in a simple way.

$\underline{A} = \underline{A}_w + \underline{A}_s$ is the sum of the vector potentials of the wiggler and EM pulse.

If we introduce as new variables the energy parameter $\gamma = (\mathcal{E} - e\phi_o)/mc^2$ and the relative phase

$$\psi = \int^{z} k_{wy}\, dz + k_s z - \omega_s t + \frac{k_s r^2}{2R}$$

the Hamiltonian takes the form

$$H\left(P_x,\ x,\ P_y,\ y,\ (-\mathcal{E}),\ t;\ z\right)$$

$$= - mc\gamma$$

$$+ \frac{mc}{2\gamma}\left[\mu^2 + \frac{P_x^2 + P_y^2}{m^2 c^2} + \frac{a_{wx}^2 k_{wx}^2 y^2}{2} + \frac{a_{wy}^2 k_{wy}^2 x^2}{2}\right.$$

$$+ \frac{a_{wx}^2}{2}\cos 2\int^{z} k_{wx}\, dz + \frac{a_{wy}^2}{2}\cos 2\int^{z} k_{wy}\, dz$$

$$+ \frac{2P_x a_{wx}}{mc}\cos\int^{z} k_{wx}\, dz + \frac{2P_y a_{wy}}{mc}\cos\int^{z} k_{wy}\, dz$$

$$-\sum_n a_{wy}\, a_{ns}\, \hat{\chi}_n \left\{\cos\left(\psi - (2n+1)\ \tan^{-1}\frac{z}{z_R} + \zeta_n\right)\right.$$

$$+ \cos\left(\psi - 2k_s z + 2\omega_s t - \frac{k_s r^2}{R}\right.$$

$$\left.\left. + (2n+1)\ \tan^{-1}\frac{z}{z_R} - \zeta_n\right)\right\}$$

$$\left. + \ldots\right]$$

where

$$\underline{a}_w = \frac{e}{mc^2} \underline{A}_w ,$$

$$a_{ns} = \frac{e}{mc^2} A_{ns} ,$$

$$\mu^2 = 1 + \frac{a_{wy}^2}{2} + \frac{a_{wx}^2}{2} ,$$

$$|\underline{a}_w| >> a_{ns} , \quad \gamma^2 >> \mu^2 .$$

Let $p_1 = p_x$, $q_1 = x$, $p_2 = p_y$, $q_2 = y$, $p_3 = -\mathcal{E}$, $q_3 = t$. Then consider the following canonical transformation $p_i, q_i \rightarrow P_i, Q_i$ produced by the generating function G:

$$G(Q,p,z) = - Q_i p_i + \frac{mc^2}{p_3 + e\phi_o} \left(p_1 \frac{a_{wx}}{k_{wx}} \sin \int^z k_{wx}\, dz + p_2 \frac{a_{wy}}{k_{wy}} \sin \int^z k_{wy}\, dz \right) + \frac{m^2c^2}{p_3 + e\phi_o} \left(\frac{a_{wx}^2}{k_{wx}} \sin 2 \int^z k_{wx}\, dz + \frac{a_{wy}^2}{k_{wy}} \sin \int^z k_{wy}\, dz \right)$$

The new variables P_i, Q_i are related to the old variables p_i, q_i by

$$q_i = - \frac{\partial G}{\partial P_i}$$

$$P_i = - \frac{\partial G}{\partial Q_i}$$

and the new Hamiltonian is

$$\bar{H} = H + \frac{\partial G}{\partial z} .$$

Thus:

$$P_1 = P_x,\ P_2 = P_y,\ P_3 = -\mathcal{E}$$

$$x = \bar{x} + \frac{a_{wx}}{\gamma k_{wx}} \sin \int^z k_{wx}\, dz$$

$$y = \bar{y} + \frac{a_{wy}}{\gamma k_{wy}} \sin \int^z k_{wy}\, dz$$

$$t = \bar{t} + \frac{1}{m\gamma^2 c^2} \left\{ \frac{P_x a_{wx}}{k_{wx}} \sin \int^z k_{wx}\, dx + \frac{P_y a_{wy}}{k_{wy}} \sin \int^z k_{wy}\, dz \right\}$$

$$+ \frac{1}{8\gamma^2 c} \left\{ \frac{a_{wx}^2}{k_{wx}} \sin 2 \int^z k_{wx}\, dz + \frac{a_{wy}^2}{k_{wy}} \sin 2 \int^z k_{wy}\, dz \right\}$$

where

$$Q_1 \equiv \bar{x},\ Q_2 \equiv \bar{y},\ Q_3 = \bar{t}$$

and in the limit of

$$\frac{k_s a_{wx} P_x}{k_{wx} m\gamma^2 c} ,\ \frac{k_s}{k_{wy}} \frac{a_{wy} P_y}{m\gamma^2 c} << 1$$

$$\frac{k_s a_{wx}^2}{k_{wx} 8\gamma^2} ,\ \frac{k_s a_{wy}^2}{k_{wy} 8\gamma^2} << 1$$

$\bar{H}$ may be approximated by:

$$\bar{H}(P_x, \bar{x}, P_y, \bar{y}, -\mathcal{E}, \bar{t}; z)$$

$$= -mc\gamma + \frac{mc\mu^2}{2\gamma}$$

$$+ \frac{P_x^2 + P_y^2}{2\gamma mc} + \frac{mc}{4\gamma}\left(a_{wx}^2 k_{wx}^2 \bar{y}^2 + a_{wy}^2 k_{wy}^2 \bar{x}^2\right)$$

$$- \frac{mc}{2\gamma}\sum_n a_{wy}\, a_{ns}\, \hat{\chi}_n \cos\left(\bar{\psi} - (2n+1)\tan^{-1}\frac{z}{z_R} + \zeta_n\right) \quad \text{(A5)}$$

where

$$\bar{\psi} = \int^z k_{wy}\, dz + k_s z - \omega_s \bar{t} + \frac{k_s r^2}{2R(z)}$$

$$r^2 = \bar{x}^2 + \bar{y}^2 \quad \text{(A6)}$$

$\bar{\psi}$ is assumed to be slowly varying in z and the remaining oscillatory terms have been neglected.

The electron equations of motion may therefore be approximated as follows:

$$\frac{d\bar{\psi}}{dz} = k_{wy} + k_s + \frac{d}{dz}\left\{\frac{k_s r^2}{2R(z)}\right\} + \frac{k_s}{mc}\frac{\partial \bar{H}}{\partial \gamma}$$

$$= k_{wy} - \frac{k_s \mu^2}{2\gamma^2} + \frac{d}{dz}\left\{\frac{k_s r^2}{2R}\right\}$$

$$- \frac{k_s}{2}\left\{k_\beta^2 (\bar{x}^2 + \bar{y}^2) + \frac{\left(P_x^2 + P_y^2\right)}{m^2 c^2 \gamma^2}\right\} \qquad \text{(A7)}$$

$$\frac{d\gamma}{dz} = -\frac{e}{mc^2}\frac{d\phi_o}{dz} + \frac{1}{mc^2}\frac{\partial \bar{H}}{\partial \bar{t}} \qquad \text{(A8)}$$

$$= -\frac{e}{mc^2}\frac{d\phi_o}{dz} - \frac{k_s}{2\gamma}\sum_n a_{wy}\, a_{ns}\, \hat{\chi}_n \sin\left(\bar{\psi} - (2n+1)\tan^{-1}\frac{z}{z_R} + \zeta_n\right)$$

$$\frac{d\bar{x}}{dz} = \frac{P_x}{\gamma mc}$$

$$\frac{dP_x}{dz} = -mc\gamma\, k_\beta^2\, \bar{x} + \cdots$$

$$\frac{d\bar{y}}{dz} = \frac{P_y}{\gamma mc}$$

$$\frac{dP_y}{dz} = -mc\gamma\, k_\beta^2\, \bar{y} + \cdots$$

where

$$k_\beta^2 \equiv \frac{a_{wx}^2 k_{wx}^2}{2\gamma^2} = \frac{a_{wy}^2 k_{wy}^2}{2\gamma^2}$$

The approximate solutions for $\bar{x}$ and $\bar{y}$ when k_β is constant and

$$k_\beta >> \left|\frac{1}{\gamma}\frac{d\gamma}{dz}\right|$$

are

$$\bar{x} = \alpha_x \sin(k_\beta z + q_x) \qquad \text{(A9-a)}$$

$$\bar{y} = \alpha_y \sin(k_\beta z + q_y) \qquad \text{(A9-b)}$$

and they describe the betatron motion of the electron in the transverse direction. The betatron frequency in the x- and y-direction has been chosen equal. α_x, q_x and α_y, q_y are the amplitudes, phases of the betatron motion.

The relative phase $\bar{\psi}$ varies slowly for electrons with values of γ close to γ_R (the resonant energy) defined by:

$$\gamma_R = \left(\frac{k_s}{2k_{wy}}\right)^{\frac{1}{2}} \mu$$

These electrons interact strongly with the EM pulse and will exchange net energy with it. Electrons with values of γ far from γ_R have negligible effects.

It is therefore convenient to introduce the variable $\tilde{\gamma} = \gamma - \gamma_R$. Then in the limit of $\tilde{\gamma} << \gamma_R$, the electron equations of motion for $\bar{\gamma}$ and $\bar{\psi}$ may finally be approximated by:

$$\frac{d\bar{\psi}}{dz} = \frac{2k_{wy}\tilde{\gamma}}{\gamma_R} + \frac{d}{dz}\left\{\frac{k_s r^2}{2R}\right\} - \frac{k_s k_\beta^2}{2}\left(\alpha_x^2 + \alpha_y^2\right) \quad \text{(A10)}$$

$$\frac{d\tilde{\gamma}}{dz} = -\frac{d\gamma_R}{dz} - \frac{e}{mc^2}\frac{d\phi_o}{dz} \quad \text{(A11)}$$

$$- \frac{k_s}{2\gamma_R}\sum_n a_{wy}\, a_{ns}\, \hat{\chi}_n \sin\left(\bar{\psi} - (2n+1)\tan^{-1}\frac{z}{z_R} + \zeta_n\right)$$

where the transverse motion is assumed to be adequately described by Equation (A9).

Equations (A9), (A10) and (A11) constitute the electron equations of motion which are implemented in the simulation code to be described in subsequent sections.

In a variable parameter wiggler, γ_R is allowed to vary spatially, $d\gamma_R/dz \neq 0$. However, the presence of an accelerating electric field $d\phi_o/dz$ affects the electron phase space $(\tilde{\gamma}, \bar{\psi})$ trajectories in a manner similar to spatial variations of

γ_R, and in some problems it is adequate to model a variable parameter wiggler by $d\gamma_R/dz = 0$, $d\Phi_o/dz \neq 0$.

B. Electromagnetic Field Equations

The transverse electron beam current density $\underline{J}$ determines the time and spatial evolution of the optical pulse through Maxwell's equations:

$$\nabla^2 A_{sy} - \frac{1}{c^2} \frac{\partial^2}{\partial t^2} A_{sy} = - \frac{4\pi}{c} J_y \qquad \text{(A12)}$$

If the assumed form of A_{sy} [Eq. (A1)] is substituted in Equation (A12), we obtain

$$\sum_m i k_s \chi_m \left\{ \frac{\partial A_{ms}}{\partial z} + \frac{1}{c} \frac{\partial A_{ms}}{\partial t} + i A_{ms} \left(\frac{\partial \zeta_m}{\partial z} + \frac{1}{c} \frac{\partial \zeta_m}{\partial t} \right) \right\}$$

$$e^{-i\omega_s t + i k_s z + i \zeta_m}$$

$$+ \text{complex conjugate}$$

$$= - \frac{4\pi}{c} J_y \qquad \text{(A13)}$$

Multiplying both sides of the equation by

$$\exp \left\{ i\omega_s t - i k_s z - \frac{i k_s r^2}{2R(z)} \right\}$$

and averaging in t over a time $T_o > \frac{1}{\omega_s}$:

$$\sum_m i k_s \hat{\chi}_m \left\{ \frac{\partial A_{ms}}{\partial z} + \frac{1}{c} \frac{\partial A_{ms}}{\partial t} + i A_{ms} \left(\frac{\partial \zeta_m}{\partial z} + \frac{1}{c} \frac{\partial \zeta_m}{\partial t} \right) \right\}$$

$$e^{-i(2m+1) \tan^{-1} \frac{z}{z_R} + i \zeta_m}$$

$$= - \frac{1}{T_o} \int_{t - \frac{T_o}{2}}^{t + \frac{T_o}{2}} dt \, \frac{4\pi}{c} J_y \, e^{i \omega_s t - i k_s z - \frac{i k_s r^2}{2R(z)}} \qquad \text{(A14)}$$

Then multiplying by $\hat{\chi}_n(r,z)$ and integrating in r,

$$\int_o^\infty \frac{4r \, dr}{r_p^2}$$

$$i \left[\left(\frac{\partial A_{ns}}{\partial z} + \frac{1}{c} \frac{\partial A_{ns}}{\partial t} \right) - A_{ns} \left(\frac{\partial \zeta_n}{\partial z} + \frac{1}{c} \frac{\partial \zeta_n}{\partial t} \right) \right] e^{i \zeta_n}$$

$$= - \int_o^\infty \frac{4r \, dr}{r_p^2} \, \hat{\chi}_n(r,z) \qquad \text{(A15)}$$

$$\frac{1}{T_o} \int_{t - \frac{T_o}{2}}^{t + \frac{T_o}{2}} dt \, \frac{4\pi}{k_s c} J_y \, e^{i \omega_s t - i k_s z - \frac{i k_s r^2}{2R} + i(2n+1) \tan^{-1} \frac{z}{z_R}}$$

where we have used the orthogonality relation:

$$\int_0^\infty \hat{\chi}_n \, \hat{\chi}_m \, \frac{4r\,dr}{r_p^2} = \delta_{n,m}$$

Let the electron distribution function F on entry at $z = z_{in}$ into the wiggler be:

$$F = F\left(\tilde{\gamma}_o,\ \bar{t}_o,\ P_{ox},\ \bar{x}_o,\ P_{oy},\ \bar{y}_o\right)$$

$$= \frac{H(\bar{t}_o)\ F_o(\tilde{\gamma}_o)\ \exp\left[-\left(\alpha_x^2 + \alpha_y^2\right)/r_b^2\right]}{\pi r_b^2\, m^2\, \tilde{\gamma}_o^2\, c^2\, k_\beta^2}$$

The electron density is

$$N(x,y,t;z) = \langle\langle F\ \delta(x-X)\ \delta(y-Y)\ \delta(t-T)\rangle\rangle$$

$$\equiv \int d\tilde{\gamma}_o\ d\bar{t}_o\, dP_{ox}\ dx_o\, dP_{oy}\, d\bar{y}_o\, F$$

$$\delta(x-X)\ \delta(y-Y)\ \delta(t-T) \qquad \text{(A16)}$$

where $X(\tilde{\gamma}_o,\bar{t}_o,P_{ox},\bar{x},P_{oy},\bar{y}_o;z)$, $Y(\tilde{\gamma}_o,\bar{t}_o,P_{ox},\bar{x}_o,P_{oy},\bar{y}_o;z)$, $T(\tilde{\gamma}_o,\bar{t}_o,P_{ox},\bar{x}_o,P_{oy},\bar{y}_o;z)$ are the values of x,y,t at z for an electron with initial phase space variables $\tilde{\gamma}_o,\bar{t}_o,P_{ox},\bar{x}_o,P_{oy},\bar{y}_o$ at $z = z_{in}$.

At $z = z_{in}$

$$N(x,y,t;z_{in})$$

$$= \frac{1}{\pi r_b^2} \int d\tilde{\gamma}_o \, d\bar{t}_o \, d\alpha_x \, dq_x \, d\alpha_y \, dq_y \, \alpha_x \, \alpha_y \, H(\bar{t}_o) \, F_o(\tilde{\gamma}_o)$$

$$\exp\left[-(\alpha_x^2 + \alpha_y^2)/r_b^2\right]$$

$$\delta(x - \alpha_x \sin q_x) \, \delta(y - \alpha_y \sin q_y)$$

$$\delta(t - T)$$

$$= \int d\tilde{\gamma}_o \, d\bar{t}_o \, H(\bar{t}_o) \, F_o(\tilde{\gamma}_o) \, \exp\left(-\frac{r^2}{r_b^2}\right)$$

$$\delta(t - T)$$

Let $F(\tilde{\gamma}_o)$ be normalized so that

$$\int_o^\infty d\tilde{\gamma}_o \, F_o(\tilde{\gamma}_o) = 1 \qquad \text{(A18)}$$

Then

$$N = H\left(t - \frac{z}{V}\right) \exp\left(-\frac{r}{r_b^2}\right) \qquad \text{(A19)}$$

where T has been approximated by $T \approx \bar{t}_o + z/V$ with

$$V = \frac{C}{1 + \mu^2/2\gamma_R^2} \qquad \text{(A20)}$$

r_b is the root mean square beam radius. $H(t - z/V)$ is related to the electron beam current

$$I_b = HeV\ \pi r_b^2 \tag{A21}$$

The transverse electron current density J_y is:

$$J_y = \left\langle\!\!\left\langle \frac{e}{m\gamma} \left(P_y - \frac{e}{c} A_y\right) F \right.\right.$$

$$\left.\left. \delta(x - X)\ \delta(y - Y)\ \delta(t - T) \right\rangle\!\!\right\rangle \tag{A22}$$

Substituting for J_y in Equation (A15):

$$\left(\frac{\partial}{\partial z} + \frac{1}{c}\frac{\partial}{\partial t}\right)\ a_{ns}\ e^{i\zeta_n}$$

$$= i\left\langle\!\!\left\langle \int_0^\infty r\,dr \int_0^{2\pi} d\theta \int_{t-\frac{T_o}{2}}^{t+\frac{T_o}{2}} \frac{dt}{T_o} \frac{8e^2 a_{wy}}{m\gamma_R k_s c^2 r_p^2} \cos\int^z k_{wy}\,dz \right.\right.$$

$$\hat{\chi}_n(r,z)\ \exp\left[i\omega_s t - i k_s z - \frac{i k_s r^2}{2R} + i(2n+1)\ \tan^{-1}\frac{z}{z_R}\right]$$

$$\left.\left. F\,\delta(x - X)\ \delta(y - Y)\ \delta(t - T) \right\rangle\!\!\right\rangle$$

$$\approx i \frac{e^2 a_{wy}}{m\gamma_R k_s c^2 r_p^2} \int d\tilde{\gamma}_o \, d\alpha_x^2 \, d\alpha_y^2 \, dq_x \, dq_y \int_{t-\frac{z}{v}-\frac{T_o}{2}}^{t-\frac{z}{v}+\frac{T_o}{2}} d\bar{t}_o/T_o$$

$$\frac{1}{\pi r_b^2} H(\bar{t}_o) \; F_o(\tilde{\gamma}_o) \; \exp\left(- \frac{\alpha_x^2 + \alpha_y^2}{r_b^2}\right)$$

$$\hat{\chi}_n \; \exp\left\{- i\bar{\psi} + i(2n+1) \; \tan^{-1} \frac{z}{z_R}\right\}$$

$$\approx i \frac{4e^2 a_{wy} \pi r_b^2}{m\gamma_R k_s c^2 r_p^2} H\left(t - \frac{z}{v}\right) \qquad \text{(A23)}$$

$$\left\langle \hat{\chi}_n \; \exp\left\{- i\psi + i(2n+1) \; \tan^{-1} \frac{z}{z_R}\right\} \right\rangle$$

where

$$\left\langle \left(\quad \right) \right\rangle \equiv \int d\tilde{\gamma}_o \, d\alpha_x^2 \, d\alpha_y^2 \, dq_x \, dq_y \; \frac{1}{r_b^4 \, 4\pi^2}$$

$$\int \frac{d\bar{\psi}_o}{2\pi} \; F_o(\tilde{\gamma}_o) \; \exp\left(- \frac{\alpha_x^2 + \alpha_y^2}{r_b^2}\right)\left(\quad \right)$$

This equation determines the temporal and spatial evolution of the amplitude A_{ns} and phase ζ_n of each Gaussian mode of the EM pulse.

C. FEL Equations

The FEL equations are most conveniently formulated after introducing the new independent variables u and v:

$$u = \frac{c}{L_w\left(\frac{c}{V} - 1\right)}\left(\frac{z + \frac{L_w}{2}}{V} - t\right) \qquad \text{(A24-a)}$$

$$v = \frac{c}{L_w\left(\frac{c}{V} - 1\right)}\left(t - \frac{z + \frac{L_w}{2}}{c}\right) \qquad \text{(A24-b)}$$

to replace t and z.

It will be assumed that the wiggler amplitude and wave number are constant. γ_R and hence the longitudinal electron resonant velocity V are independent of z. A variable parameter wiggler is modeled by a finite value of the accelerating field $d\Phi_o/dz$.

The wiggler, total length L_w, is positioned symmetrically between the mirrors, the front being at $z = -L_w/2$ and the back at $z = L_w/2$. The line $z = -L_w/2$ in $z - t$ space maps into the line $u + v = 0$ in $u - v$ space and $z = L_w/2$ into $u + v = 1$ (see Figure A2).

In $u - v$ space, the electrons move on lines of constant u, and the "photons" of the EM pulse propagating in the direction of the electrons move on lines of constant v. The EM pulse interacts with the electrons only inside the

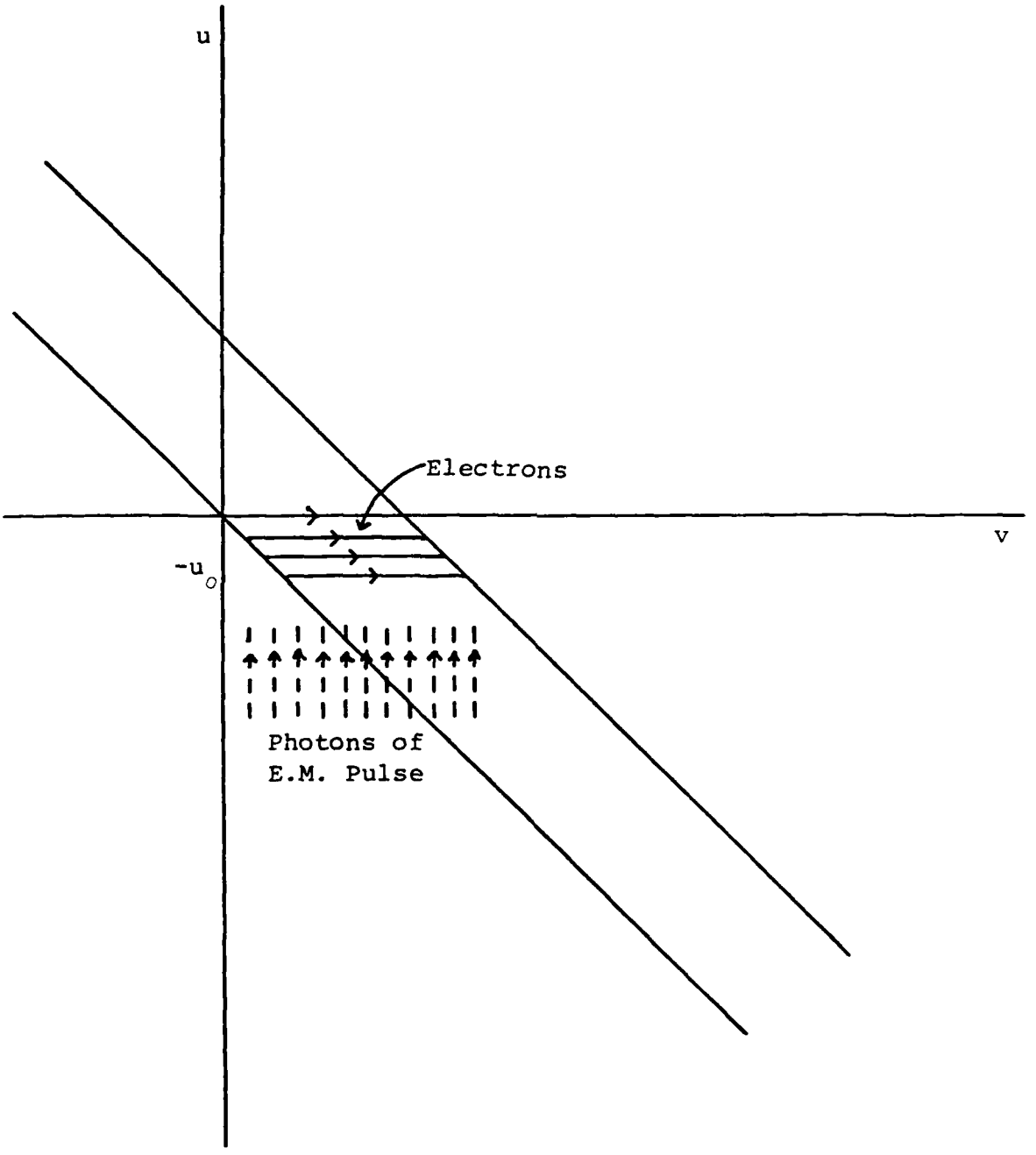

Figure A2. Electron and Photon Trajectories in u - v plane

region of the $u - v$ plane bounded by the lines $u + v = 0$ and $u + v = 1$.

The electron equations of motion, Equations (A9), (A10) and (A11), now take the following forms:

$$\frac{\partial \bar{\psi}}{\partial v} = \hat{\gamma} + \frac{\partial}{\partial v} \frac{k_s r^2}{2R} - \frac{k_s L_w}{2} k_\beta^2 r_b^2 \left(\hat{\alpha}_x^2 + \hat{\alpha}_y^2 \right) \tag{A25}$$

$$\frac{\partial \hat{\gamma}}{\partial v} = \Gamma - \sum_n \hat{a}_n \hat{\chi}_n \sin\left(\bar{\psi} - (2n+1) \tan^{-1} \frac{z}{z_R} + \zeta_n \right) \tag{A26}$$

$$r^2 = \bar{x}^2 + \bar{y}^2 = r_b^2 \left\{ \hat{\alpha}_x^2 \sin^2\left(k_\beta \left(z + \frac{L_w}{2} \right) + q_x \right) + \hat{\alpha}_y^2 \sin^2\left(k_\beta \left(z + \frac{L_w}{2} \right) + q_y \right) \right\} \tag{A27}$$

$$z = \left(u + v - \frac{1}{2}\right) L_w$$

$$\hat{\chi}_n = \frac{L_n\left(\frac{2r^2}{w^2}\right) \exp\left(-\frac{r^2}{w^2}\right)}{\left(1 + \frac{z^2}{z_R^2}\right)^{\frac{1}{2}}}$$

and the EM pulse evolution equation, Equation (A23), can be written as follows:

$$\frac{\partial}{\partial u} \hat{a}_n e^{i\zeta_n}$$

$$= i\eta h(u) \left\langle \hat{\chi}_n \exp\left\{-i\bar{\psi} + i(2n+1) \tan^{-1} \frac{z}{z_R}\right\}\right\rangle \quad \text{(A28)}$$

where

$$\hat{\gamma} = \frac{2k_{wy} L_w}{\gamma_R} \tilde{\gamma}$$

$$\hat{a}_n = \frac{k_s k_{wy} L_w^2 a_{wy} a_{ns}}{\gamma_R^2}$$

$$\Gamma = -\frac{2k_{wy} L_w}{\gamma_R} \frac{e}{mc^2} \frac{\partial \Phi_o}{\partial v}$$

$$\equiv \frac{2k_{wy} L_w}{\gamma_R} \Delta\gamma_R$$

$$\eta = \frac{8(k_{wy} L_w)^2 a_{wy}^2}{\gamma_R \mu^2} \frac{e\langle I_b \rangle}{mc^2 v} \frac{u_o L_w}{k_s r_p^2}$$

$$\langle I_b \rangle = \frac{1}{\ell} \int dz\, I_b\, dz$$

$$h(u) = \frac{L_w\left(1 - \frac{V}{c}\right) I_b}{\ell \langle I_b \rangle}$$

$$u_o = \ell \Big/ L_w\left(1 - \frac{V}{c}\right)$$

I_b is the beam current

ℓ is the nominal electron micropulse length

$$\int h(u)\, du = 1$$

$$\langle\langle \quad \rangle\rangle$$

$$= \frac{1}{(2\pi)^3} \int d\tilde{\gamma}_o\, d\bar{\psi}_o\, d\hat{\alpha}_x^2\, d\hat{\alpha}_y^2\, dq_x\, dq_y\, F_o(\tilde{\gamma}_o)$$

$$\exp\left(-\hat{\alpha}_x^2 - \hat{\alpha}_y^2\right)(\quad)$$

h(u) is a form factor determined by the current profile of the electron micropulse.

For the N^{th} pass of the EM pulse through the wiggler, the electron phase space trajectories are determined by the solutions of Equations (A25) and (A26) with initial condition $\hat{\gamma}_o$, $\bar{\psi}_o$, $\hat{\alpha}_x$, q_x, $\hat{\alpha}_y$, q_y at $v = -u$. The initial phases

$\bar{\psi}_o$, q_x, q_y are uncorrelated with that of the EM pulse and thus are distributed uniformly between 0 and 2π. The electrons are assumed to occupy the area $0 > u > -u_o$.

The pulse amplitude after interaction with the electrons is

$$\hat{a}_n^N(v,o) = \hat{a}_n^N(v, -u_o) + \Delta\hat{a}_n^N(v) \qquad \text{(A29)}$$

where $\Delta\hat{a}_n^N(v)$ is determined by integrating Equation (A28) from $u = -v$ to $u = 1 - v$ through the wiggler.

The EM pulse is reflected backwards and then forwards for the $(N+1)^{th}$ pass through the wiggler.

Between passes, the EM pulse is filtered to attenuate the unstable sideband frequencies which can grow when the pulse amplitude is large enough to trap electrons. This filtering is accomplished by a band-pass filter, modeled by the equation:

$$\frac{\partial\hat{\hat{a}}_n^N(v,o)}{\partial v} + \nu\hat{\hat{a}}_n^N(v,o) = \nu\hat{a}_n^N(v,o) \qquad \text{(A30)}$$

where $\hat{\hat{a}}_n^N$ is the filtered pulse amplitude, and the frequency half-width $\Delta\omega$ of the band-pass filter is related to the parameter ν by

$$\Delta\omega = \frac{\nu c}{L_w(c/V - 1)} \qquad \text{(A31)}$$

If $\mathcal{R} < 1$ is the effective amplitude reflectivity, accounting for the energy losses on reflection at the mirrors, and β represents the tunable pass-to-pass shift in the position of the pulse relative to the front of the electron micropulse at the moment of entry into the wiggler, the pulse amplitude at the beginning of the $(N+1)^{th}$ pass is:

$$\hat{a}_n^{N+1}(v - \beta, -u_o) = \mathcal{R}\,\hat{\hat{a}}_n^{N}(v,o) \tag{A32}$$

Thus, the pass-to-pass change in pulse amplitude after interaction with the electrons, filtering, and reflection at the mirrors is given by:

$$\frac{1}{\nu}\frac{\partial}{\partial v}\hat{a}_n^{N+1}(v - \beta, -u_o) + \hat{a}_n^{N+1}(v - \beta, -u_o)$$

$$= \mathcal{R}\left[\hat{a}_n^{N}(v, -u_o) + \Delta\hat{a}_n^{N}(v)\right] \tag{A33}$$

An additional complication not present in the one-dimensional formulation of the FEL equations is the relative phase shifts between the Gaussian modes introduced by reflection at the mirrors. On each reflection, the phase shift introduced between the n^{th} Gaussian mode and the lowest (n=0) mode is $-4n \tan^{-1}(L/2z_R)$. Thus, the pass-to-pass phase change of each Gaussian mode of the EM pulse is given by:

$$\zeta_n^{N+1}(v - \beta, -u_o)$$

$$= \zeta_n^N(v, -u_o) + \Delta\zeta_n^N(v) - 8n \tan^{-1} \frac{L}{2z_R} \quad \text{(A34)}$$

where $\Delta\zeta_n^N(v)$ is the phase change due to the interaction of the EM pulse with the electrons inside the wiggler.

Equations (A25), (A26), (A27), (A28), (A33) and (A34) govern the operation of the FEL oscillator.

III. CODE DESCRIPTION

The code PZD is a two-dimensional, time dependent, long pulse FEL simulation code which includes the effects of radial structure in the optical mode and betatron dynamics of the electron beam. The modular structure and organization of PZD are similar to that of the one-dimensional simulation code LPULSE.[1] The main driver program makes successive passes through a set of specialized subroutines which process the large blocks of field and particle data held in COMMON. The subroutines include packages for data input (DATIN), code initialization (INIT), integration of particle equations of motion (PHSADV), integration of the optical mode equations (FLDADV), and simulation of the pass-to-pass optical events; e.g., desynchronization and frequency discrimination (NXTPLS).

There is a basic diagnostics package (DIAGNOS), but it is anticipated that much more work will be done on it. At present, pass-to-pass histories of pulse power, growth rate and field and particle energy bookkeeping are provided. Provision has been made for a restart of the code in order to handle unusually long simulations, but a renormalizing version has not been completed.

The following discussions will concern the most important numerical implementations of the model equations described in Section II. It should be noted that the wiggler

model, while more detailed than that of the 1-D codes for it includes betatron effects, is not as detailed in its emulation of the ponderomotive forces as VWIG.[1]

Data Input

The intention was to design PZD to be invoked by a single command file which: (1) Completes a batch edit task to make custom modifications to the reference code file, and (2) compiles, links, and runs the modified code. Typically, the modifications would include a complete set of data and any special modifications to the basic algorithms or diagnostics. The input parameters fall into the four groups indicated in Table A1.

The code models the focusing of the electron beam as the combined betatron motion due to two crossed-plane polarized wigglers. Only one of the wigglers produces a resonant ponderomotive force on the electrons, the other having a wiggler wavelength not equal to the resonant wavelength. However, the betatron wavelength for the two wigglers is identical because the ratio of the wiggler wavelength to the peak B-field is equal. This is a restriction of parameter space which simplified the betatron dynamics and reduces the particle phase space which must be sampled. The input radius and the betatron wavelength imply a specific beam emittance.

TABLE A1

PZD INPUT PARAMETERS

Optical Parameters

Wavelength
Mirror Separation
Mirror Curvature
Effective Reflectivity
Cutoff Frequency for Discrimination
Initial Amplitude

Wiggler Parameters

Wavelength (at entrance)
B-field (at entrance)
Total Length
Fractional Length of Constant Parameter Section
Taper
Wavelength of Focusing Wiggler

Beam Parameters

Current
Energy
Radius
Micropulse Length
Desynchronization Length

Numerical and Control Parameters

Integration Step
Number of Optical Modes
Bounds for Simulated Optical Mode
Number of Electrons
Length of Simulated Electron Beamlet
Current Profile
Restart Dump and Read Flags
Diagnostic Pass Flags

Initialization

The particle arrays which represent the beam and the amplitude arrays for the optical pulse are initialized in INIT, along with miscellaneous numerical parameters and arrays. The following description refers to Figure A2, which is a diagram of the interaction region in u-v space. The variables u and v are determined from z and t by the transformation equations (A24-a) and (A24-b), whose inverses are

$$z = L_w (u + v - \tfrac{1}{2}) \qquad \text{(A35-a)}$$

$$t = \frac{L_w}{c} (u + \frac{c}{V} v) \qquad \text{(A35-b)}$$

The physical significance of this transformation is discussed in the paragraphs on FEL equations in Section II. As noted there, the electrons enter the interaction region on the line segment $u + v = 0$, between $u = 0$ and $u = u_F < 0$, and move right on horizontal trajectories to exit on the segment $u + v = 1$, again between $u = 0$ and $u = u_F$. The first electrons to enter the wiggler are those near $u = 0$ and the last are those near $u = u_F$. The photons enter the interaction region along $u + v = 0$ between $u = 0$ and $u = u_F$ (and along $u = u_F$ between $v = -u_F$ and $v = 1 - u_F$). [The first photons to enter are those near $v = 0$ and the last are those near $v = 1 - u_F$.] The photons move on vertical trajectories and exit the interaction region on $u = 0$ between $v = 0$ and

$v = 1$ and on $u + v = 1$ between $v = 1$ and $v = 1 - u_F$. Additionally, on a given pass there are some noninteracting photons to the left of $v = 0$ and the right of $v = 1 - u_F$, and these must be handled correctly because the desynchronization process (Eq. A32) will bring those on the right into play on succeeding passes. Also, the frequency discrimination filter (Eq. A30) will fold information from those photons to the left into all of the amplitudes.

The fields are initialized as individual uniform pulses with specified amplitudes and phases for each mode. These are defined from V_{min} to V_{max} along the line $u + v = 0$, but INIT must transform these into code quantities along the line segment $u + v = 0$, $v_{min} < v < -u_F$, $u = 0$, $-u_F < v < 1 - u_F$, and $u + v = 0$, $1 - u_F < v < V_{max}$. This involves some manipulation of the mode amplitudes as discussed in the following section on NXTPLA. Also, see Equation (A34).

Particle-associated quantities which must be handled in INIT include those associated with the betatron dynamics. Since the betatron solution (Eq. A27) is numerically integrated, as is the associated Gaussian exponential function, a table of initial conditions for these O.D.E.s is set up for each particle at each u in INIT. The motivation for these numerical integrations is discussed in the following section on PHSADV. Because Laguerre polynomials are required in calculating ponderomotive forces and evaluating currents for

each Gaussian mode, INIT sets up the starting values for evaluation by a recurrence relation.

The initial conditions required to start the integration of the axial (ponderomotive) equations (A26) are tabulated for all particles at all u's in INIT. Random numbers are used to insure that the particle phases at one u are uncorrelated with those at another u. The particles are tabulated with fixed energy and with Gaussian-distributed radial positions. The particles are loaded in pairs with phases differing by π to insure zero initial current.

Driver

Upon completion of initialization, the process of pass-to-pass integration of the 2-D FEL oscillator equations begins as a nested DO loop in the main program. The subroutines PHSADV (particle integration), FLDADV (field integration) and NXT (array bookkeeping) are called successively for each u, beginning with $u = u_F < 0$ and ending with $u = 0$. After the last u integration, the subroutine NXTPLS (pass-to-pass optics) is called and the whole sequence is repeated for the succeeding passes. Within PHSADV and FLDADV, the various quantities are evaluated for v increasing from $u + v = 0$ to $u + v = 1$. The integration sequence is not identical to the temporal sequence, but physical causality is not violated. This is because photons overrun trailing electrons, are

amplified by them, and in turn affect the dynamics of the leading electrons.

Particle Dynamics (PHSADV)

The betatron and axial ponderomotive equations are integrated in PHSADV. Although the analytic solutions (Eq. A27) are available, the betatron equations are integrated in order to reduce run time by eliminating multiple calls to the trigonometric and exponential routines.

A leapfrog (semi-implicit) algorithm is used

$$\left[\frac{d}{dv}\left(\frac{r^2}{r_p^2}\right)\right]^{n+\frac{1}{2}} = \left[\frac{d}{dv}\left(\frac{r^2}{r_p^2}\right)\right]^{n-\frac{1}{2}} + 4k_\beta^2 L_w^2 \left[\frac{\hat{\alpha}_x^2 + \hat{\alpha}_y^2}{2} - \left(\frac{r^2}{r_p^2}\right)^n\right]\Delta v$$

$$\left(\frac{r^2}{r_p^2}\right)^{n+1} = \left(\frac{r^2}{r_p^2}\right)^n + \left[\frac{d}{dv}\left(\frac{r^2}{r_p^2}\right)\right]^{n+\frac{1}{2}} \Delta v \qquad \text{(A36)}$$

The electron axial equations are advanced next. The algorithm is a noncentered version of that used in the 1-D code and is an approximation to Equations (A25) and (A26) in Section II.

$$\left[\delta\hat{\gamma} - \int^v \Gamma\, dv\right]^{n+\frac{1}{2}} = \left[\delta\hat{\gamma} - \int^v \Gamma\, dv\right]^{n-\frac{1}{2}} \qquad \text{(A37)}$$

$$- \Delta v \sum_m \hat{a}_m \hat{\chi}_m \sin\left(\bar{\psi}^n - (2m+1)\tan^{-1}\frac{z}{z_R} + \zeta_m\right)$$

The algorithm for advancing the $\sin\bar{\psi}$ and $\cos\bar{\psi}$ was selected to conserve $\sin^2\bar{\psi} + \cos^2\bar{\psi}$.

$$\left(\cos\bar{\psi}\right)^{n+1} = \left(\frac{1-\alpha^2}{1+\alpha^2}\right)\left(\cos\bar{\psi}\right)^n - \left(\frac{2\alpha}{1+\alpha^2}\right)\left(\sin\bar{\psi}\right)^n$$

$$\left(\sin\bar{\psi}\right)^{n+1} = \left(\frac{2\alpha}{1+\alpha^2}\right)\left(\cos\bar{\psi}\right)^n + \left(\frac{1-\alpha^2}{1+\alpha^2}\right)\left(\sin\bar{\psi}\right)^n \qquad \text{(A38)}$$

where

$$\alpha = \frac{\Delta v}{2}\left\{\left[\delta\hat{\gamma} - \int^{v} \Gamma\, dv'\right]^{n+\frac{1}{2}} + \int^{v} \Gamma\, dv' + \left[\frac{\partial}{\partial v}\left(\frac{k_s r^2}{2R}\right)\right]^{n+\frac{1}{2}} - \frac{k_s L_w}{2} k_\beta^2 r_b^2 \left(\hat{\alpha}_x^2 + \hat{\alpha}_y^2\right)\right\} \qquad \text{(A39)}$$

The integration of $\hat{\gamma}$ involves a sum over the optical modes, and after the integration of $\sin\bar{\psi}$ and $\cos\bar{\psi}$, another sum over modes is required to evaluate the R.H.S. of

Equation (A23), the source term for each mode of the fields. The loop is completed by returning to the betatron integration and repeating until all of the particles have been advanced one Δv. The outer DO loop carries the integration from $v = -u$ to $v = 1 - u$, then returns to the driver for the field advance.

Field Advance (FLDADV)

The information on particle currents necessary to carry out the field advance from $v = -u$ to $v = 1 - u$ has been stored in COMMON. As noted in Section II, it was found to be convenient to integrate the field equations in a form which has a z or v dependent phase term built in in order to facilitate the particle integration. As in the 1-D code LPULSE, the complex fields are calculated in the form of an amplitude times a $\sin \zeta'$ and $\cos \zeta'$ factor, but because of accuracy problems, a fully implicit, centered difference form of Equation (A23) was implemented.

The equations for a $\cos \zeta'$ and a $\sin \zeta'$ may be expressed in condensed form:

$$\frac{dx}{du} = Ax + By + S$$

$$\frac{dy}{du} = Cx + Dy + T \qquad \text{(A40)}$$

with

$$x = a\cos\zeta'$$

$$y = a\sin\zeta'$$

$$A = D = -\frac{z L_w}{z_o^2 (1 + z^2/z_o^2)}$$

$$B = -C = \frac{(2m+1) L_w}{z_o} \frac{1}{1 + z^2/z_o}$$

$$S = \eta h(u) \chi_m \quad \langle \sin\bar{\psi} \rangle$$

$$T = \eta h(u) \chi_m \quad \langle \cos\bar{\psi} \rangle$$

The difference equation used is

$$x^{n+1} - x^n = \frac{\Delta u}{2} A \left(x^{n+1} + x^n\right) + \frac{\Delta u}{2} B\left(y^{n+1} + y^n\right) + \Delta u S$$

$$y^{n+1} - y^n = \frac{\Delta u}{2} C \left(x^{n+1} + x^n\right) + \frac{\Delta u}{2} D\left(y^{n+1} + y^n\right) + \Delta u T$$

The function of subroutine NXT, the last step in the main u loop, is to shift the updated field arrays from the scratch arrays i which they were placed in FLDADV. This is done for all but the last Δu step.

After $(-u_F/\Delta u)$ steps in u integration, all the electrons in the extended pulse have been pushed through the wiggler and their interactions calculated, all of the photons have been moved from the $u + v = 0$, $u = -u_F$ locus in the u,v plane to $u = 0$, $u + v = 1$. In order to prepare for the next

pass through the wiggler, the effects of pulse propagation in the vacuum from the exit end of the wiggler to the exit mirror of the optical cavity, reflection and energy extraction, desynchronization with the succeeding electron pulse, and frequency discrimination must be simulated. These are the major tasks of subroutine NXTPLS.

The job is accomplished in three steps. A linear transformation of the code field components achieves the pass-to-pass phase shift and expresses the actual amplitudes along the line $u + v = 0$. Here the desynchronization algorithm and energy extraction are applied, and optical energy diagnostics are calculated. Finally, the amplitudes are again transformed into the code variables and propagate to the line $u + v = 0$, $0 > u > u_F$ and $u = u_F$.

The remaining subroutine in the main loop is DIAGNOS (entry DIAGE) which completes the particle and field energy bookkeeping.

The diagnostics for the code are in a preliminary state of development. Future improvements include modification of the current diagnostics output to produce physical units or more meaningful normalized quantities. It will be important to produce better information about the radial structure of the ponderomotive well.

Applications of the simulation code to several experimental FEL oscillators will be presented in the following section.

IV. SIMULATION RESULTS

The numerical code described in Section III is a powerful tool which can be used to investigate the effects introduced by transverse spatial variations of the EM pulse and wiggler. It includes the effects of diffraction of the EM pulse and transverse betatron motion of the electrons. These effects influence not only the growth of sideband instabilities, but also the efficiency of electron trapping.

The 2-D simulation code has been compared with the 1-D simulation code previously described in I-ARA-82-U-89, "Annual Technical Report for Theoretical Studies on Free Electron Lasers," M. N. Rosenbluth, H. Vernon Wong and B. N. Moore. In the limit where the lowest Gaussian mode (n = 0) is the only mode allowed to evolve and the Rayleigh length $z_R \to \infty$, the 2-D and 1-D simulation codes agree as they should. Intrinsic 2-D effects manifest themselves when the higher order Gaussian modes grow to an appreciable fraction of the lowest order mode amplitude or when the amplitude of the electron betatron motion is finite. The number of Gaussian modes which can be allowed to grow in the simulations is limited by computer time constraints. In practice, a series of simulations are carried out with a successively larger number of allowed Gaussian modes, and the series is terminated when the highest order

Gaussian mode never exceeds a few percent of the lowest order mode amplitude at saturation.

At the beginning of each pass, the electrons of each micropulse are injected into the wiggler with the initial phase $\bar{\psi}_o$, symmetrically and uniformly distributed over the range $-\pi$ to π, and the betatron phases q_x, q_y, sampled from a random uniform distribution. The distribution of betatron amplitudes among the electrons is exponential in $\hat{\alpha}_x^2$ and $\hat{\alpha}_y^2$, $\exp(-\hat{\alpha}_x^2 - \hat{\alpha}_y^2)$. The resulting radial density profile is Gaussian, $\exp(-r^2/r_b^2)$, with the parameter r_b determined by the emittance ε of the electron micropulse:

$$r_b^2 = \frac{\varepsilon}{\pi k_\beta} \tag{A41}$$

The distribution of $\hat{\gamma}_o$ is determined by the electron energy distribution. However, in all the simulation runs discussed in this section, the distribution of $\hat{\gamma}_o$ is taken to be a delta-function, $\delta(\bar{\gamma}_o - \sigma_o)$, where

$$\sigma_o = -\int_0^\infty d\hat{\alpha}_x^2 \int_0^\infty d\hat{\alpha}_y^2 \exp(-\hat{\alpha}_x^2 - \hat{\alpha}_y^2)$$

$$\frac{L_w k_s k_\beta^2 r_b^2 (\hat{\alpha}_x^2 + \alpha_y^2)}{2}$$

$$= -k_s L_w k_\beta^2 r_b^2 \tag{A42}$$

With this value of σ_o, the initial magnitude of $\partial\bar{\psi}/\partial v$ averaged over the electron distribution function is zero; most of the electrons are then close to being in resonance at the beginning of the wiggler.

At the end of each pass of the EM pulse and electrons through the wiggler, energy conservation is monitored to check the accuracy of the integration routines. The equation for energy conservation in the wiggler can be written in the following form:

$$\left[\frac{1}{2}\int dv \sum_n \hat{a}_n^2 (v,u)\right]_{u=-u_o}^{u=0}$$

$$- \eta \int du\, h(u) \left\langle \int_{-u}^{1-u} \Gamma\, dv - \left[\hat{\gamma}\right]_{v=-u}^{v=1-u} \right\rangle$$

$$= 0$$

The first term is proportional to the increase in the EM pulse energy and the second term to the energy extracted from the electrons. The step-lengths in u and v are adjusted so that energy is conserved to within a few percent.

If all of the electrons are trapped at the beginning of the wiggler and remain trapped all the way through the wiggler so that

$$\left\langle \left[\hat{\gamma}\right]_{-u}^{1-u} \right\rangle = 0$$

then the energy extraction is proportional to

$$\eta \int du\, h(u) \int_{-u}^{1-u} \Gamma\, du$$

Thus, the effective electron trapping fraction f may conveniently be defined to be:

$$f = \frac{\int du\, h(u) \left\langle \int_{-u}^{1-u} \Gamma\, dv - \left[\hat{\gamma}\right]_{-u}^{1-u} \right\rangle}{\int du\, h(u) \int_{-u}^{1-u} \Gamma\, du}$$

It should be noted that the pulse amplitude is arbitrarily set to zero for $u \leq V_{min}$ to reduce storage requirements. In the event that the pulse is passed through a band-pass filter of finite width to suppress the growth of sideband instabilities, V_{min} must be sufficiently far away from the interaction region so that the pulse amplitude near V_{min} is negligibly small. However, in the absence of frequency discrimination, it is sufficient that $V_{min} < 0$, since the pulse evolution due to interaction with electrons inside the wiggler is not affected.

The numerical code has been used to simulate the FEL oscillator experiments of TRW and LANL.

In these simulations, the growth of the EM pulse is started from low "noise" levels. The pulse amplitude grows

exponentially in the initial linear phase until it becomes large enough to trap electrons in the ponderomotive potential well. In the later nonlinear phase, energy is extracted from the trapped electrons as the resonant energy of the ponderomotive potential decreases down the wiggler and is transferred to the EM pulse. Growth continues until a limit cycle is reached when the energy extracted per pass is balanced by the energy losses per pass. Ideally, a large fraction of electrons should be trapped at the front of the wiggler and remain trapped all the way through the wiggler, and a smooth large amplitude EM pulse obtained at saturation. This idealized picture of FEL operation is not always realized, however, as will be seen from the results of the simulations.

There are two effects which can adversely affect the FEL oscillator efficiency. They are (1) the unstable growth of sideband modes; (2) the resonant coupling of the electron bounce motion to the betatron motion.

The growth of unstable sideband modes to large amplitudes can lead to a "break-up" of the EM pulse with consequent detrapping of electrons. This "break-up" of the pulse has previously been observed in 1-D simulations, and is again present in the 2-D simulations. However, this pulse "break-up" can be avoided by passing the pulse after each pass through a band-pass filter to suppress sideband growth and thus ensure stable propagation of a large amplitude EM pulse. In the case of 1-D FEL oscillators, the following inequality was

established for the width of the band pass filter necessary for stable large amplitude pulse propagation:

$$\frac{1}{\nu^2}\left[\frac{\Gamma\eta}{u_o(1-r)^3}\right]^{\frac{1}{2}} \gtrsim 50$$

with $\beta = \frac{1}{\nu}$.

A similar inequality has not yet been established for 2-D FEL oscillators and must await a more extensive survey of parameter space than has been possible to date.

Resonance coupling of the electron bounce motion and betatron motion occurs when the pulse amplitude is such that the bounce frequency is twice the betatron frequency, and this can also lead to electron detrapping. The magnitude of this coupling is determined by the curvature of the wave front, as well as by the geometry of the focusing magnetic wiggler fields. In the present simulation code, the coupling is due only to wave front curvature; the focusing fields of the wiggler configuration modeled by Equation (2) introduces no additional coupling. The conditions for resonant detrapping were satisfied in the simulations of the LANL. However, the simulation results have not yet been analyzed in sufficient detail to assess the importance of this detrapping mechanism.

It should be mentioned that quadrupole focusing fields produce a very strong resonant coupling between the bounce and betatron motion. Such focusing fields are not included in the present simulation code, although their inclusion requires but

a minor modification. The influence of such fields will be the subject of later investigations.

Simulation of the TRW Experiment

The physical parameters of the TRW experiment and the simulation parameters are listed in Table A2.

The wiggler configuration used in the simulation consists of a constant parameter section of length 15 λ_w followed by a variable parameter section with a uniform 1% taper of length 90 λ_w. This does not reproduce exactly the experimental configuration since additional drift and constant parameter sections present in the experiment are omitted. These additional sections are assumed to influence primarily the linear gain phase and only weakly the nonlinear saturated phase.

The electron micropulse is ~7 slippage distances long, which implies $u_o = 7$. In the simulations, $u_o = 3$ is used, and the electron density is assumed to be constant throughout the micropulse length. It will be noted from Figure A2 that the only part of the pulse which interacts with electrons all the way through the wiggler lies in the range $u_o > v > 1$. Thus, the larger the magnitude of u_o, the greater is the separation of the effects due to the "head" and the "tail" of the electron micropulse. Previous theoretical investigations and simulations of 1-D FELs suggest that the linear gain phase of long electron micropulses is adequately simulated when $\Gamma^{\frac{1}{2}} u_o >> 1$

TABLE A2

TRW FEL PARAMETERS

	Physical	Simulation
ELECTRON BEAM		
Energy	66 MeV	66 MeV
Current (Peak)	2.5 amps	2.5 amps
Microbunch Length	4 psecs	1.7 psecs
Emittance	0.15 mm mrad	0.15 mm mrad
Energy Spread	0.03%	0.0%
WIGGLER		
Wavelength λ_w	3.56 cm	3.56 cm
Length	3.74 m	3.74 m
B-field	2.9 KG	2.9 KG
Constant Parameters Section	0.534 m	0.534 m
Taper	1.0%	0.86%
OPTICAL		
Optical Wavelength	1.57 μ	1.57 μ
Rayleigh Range	2.71 m	2.71 m
Cavity Length	12.68 m	12.68 m
Mirror Relfectivity	0.9984	0.9987
Radius of Curvature	7.5 m	7.5 m

and that the nonlinear saturated state is not significantly affected if u_o is doubled from 3 to 6. At the present time, we have done no simulations with $u_o > 3$ because of computer time constraints. The simulation of longer electron micropulses with $u_o > 3$ will be taken up at a later date.

With a beam emittance of 0.15π mm mrad, and the betatron "frequency" $k_\beta = a_w k_w/(2)^{\frac{1}{2}} \gamma_r$, the root mean square beam radius r_b calculated from Equation (A41) is $r_b = 0.04$ cm. The parameter r_b is a measure of the amplitude of the transverse betatron motion. The effective energy spread $\Delta\gamma_\beta$ introduced by the betatron motion is:

$$\frac{\Delta\gamma_\beta}{\gamma_R} = \frac{k_s k_\beta^2 r_p^2}{(2)^{3/2} k_w} = 0.0008$$

$\Delta\gamma_\beta/\gamma_R$ is larger than 0.0003, the real energy spread, and hence the electron energy distribution function $F_o(\hat{\gamma}_o)$ can be approximated by a delta-function.

The EM pulse, initially smooth with amplitude and phase constant, is grown from low noise levels. In Figure A3, the average pulse power $\langle P \rangle$ is plotted as a function of pass number, where

$$\langle P \rangle = 0.543 \times 10^9 \frac{r_p^2 \gamma_R^4}{k_w^2 L_w^4 a_w^2 u_o} \sum_n \int_{V_{min}}^{V_{max}} \hat{a}_n^2 \, dv \quad \text{watts}$$

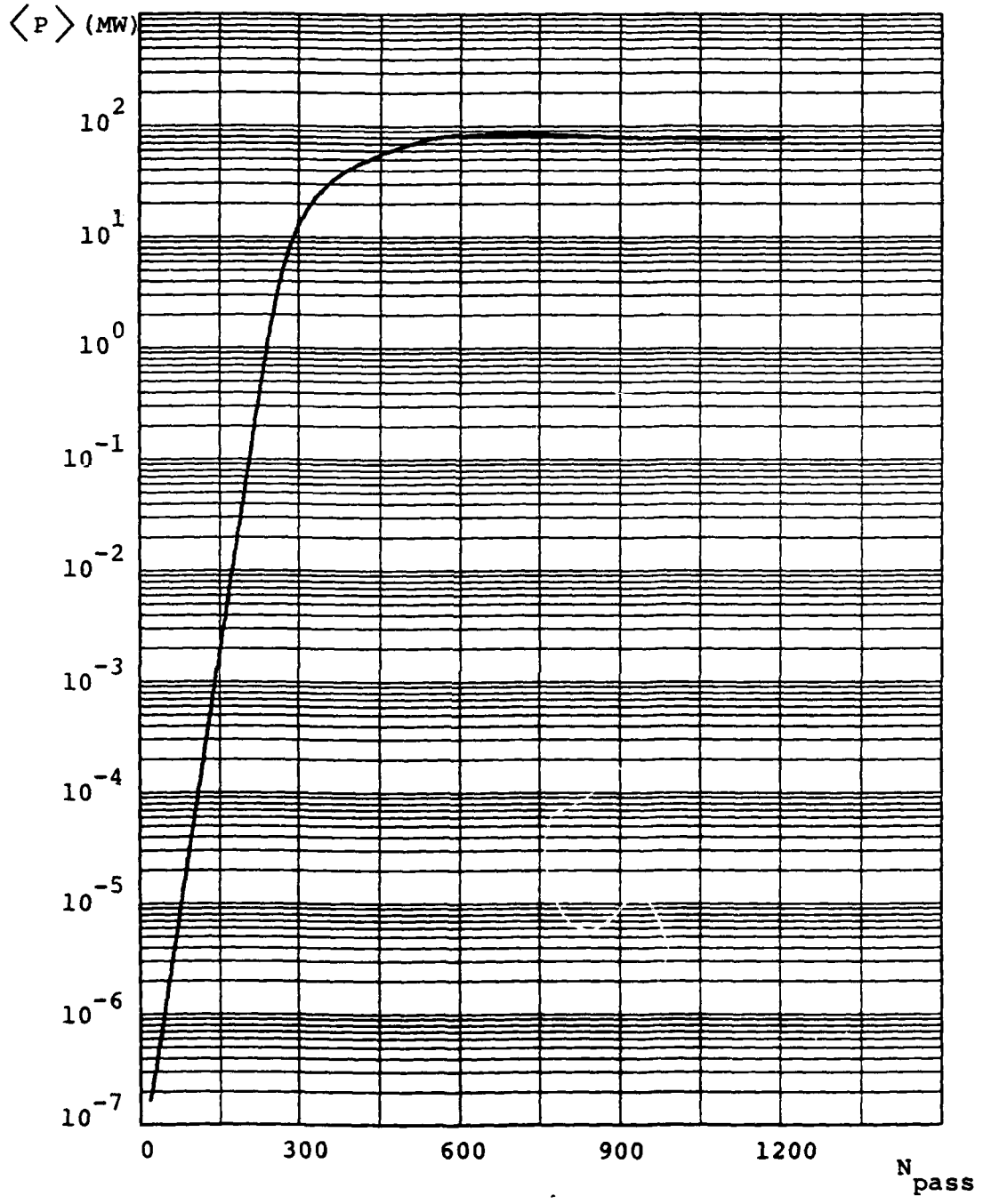

Figure A3. Average Circulating Power vs. Pass Number TRW Parameters, 1% taper.

The average pulse power $\langle P \rangle$ increases exponentially during the linear phase when the amplitude is small. Eventually, the amplitude becomes large enough for electrons to be trapped by the ponderomotive potential well. Growth continues until the energy extracted from the electrons is balanced by the energy losses.

The effective fraction of electrons trapped is $f \sim 33\%$. The average output power is

$$\left\langle P_{output} \right\rangle \sim 0.511 \; f \, \bar{I}(\text{amps}) \; \Delta\gamma_R \text{ megawatts (MW)}$$
$$\sim 0.47 \text{ MW}$$

The pulse shape at saturation of the lowest Gaussian mode (n=0) is shown in Figure A4, and it has a single maximum. The amplitude $|\hat{a}_{n=0}|$ is plotted as a function of v at $u = 0$ (see Figure A2). The only part of the pulse which interacts with the electrons inside the wiggler during a given pass lies in the range $1 + u_o > v > 0$. With positive $\beta > 0$, the pulse is shifted to the left on each successive pass. The front part of the pulse ($v < 0$) does not "see" electrons inside the wiggler and is damped by reflection energy losses at the mirrors. The Fourier transform a_κ of the pulse amplitude

$$a_\kappa = \sum_n \int_1^{u_o} dv \; \hat{a}_n(u+v=1, v) \; \exp\left[i\kappa v - i(2n+1) \tan^{-1} \frac{L_w}{2z_R} \right]$$

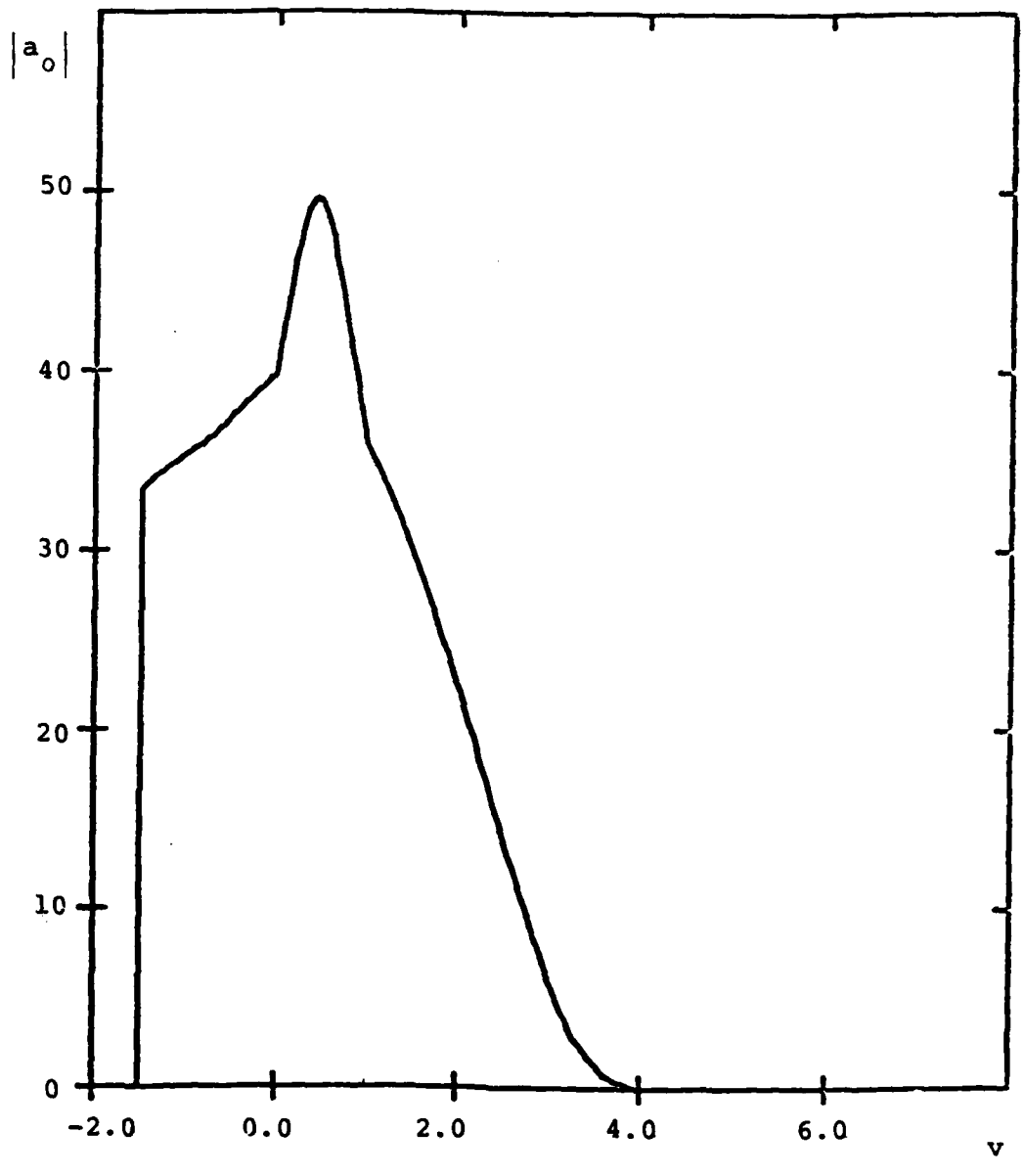

Figure A4. Modulus of Amplitude vs. v (n = 0).
TRW Parameters, 1% taper.

is plotted as a function of κ in Figure A5. For a particular value of κ, the corresponding frequency ω in the laboratory frame is:

$$\frac{\omega}{\omega_s} = 1 + \frac{\kappa}{k_w L_w} \tag{A43}$$

There is no evidence of sideband activity during the pass-to-pass evolution of the pulse, even though there was no frequency discrimination of the pulse. The spectral width at half maximum $\Delta\omega$ is $\Delta\omega/\omega_s \approx 0.005$ at saturation.

The results of the simulation are in qualitative agreement with the experimental observations. These results were obtained for simulations in which the wiggler taper is ~1% and only the lowest order Gaussian mode is allowed to grow. They remained essentially the same when the allowed modes were $n = 0$ and $n = 1$; the $n = 1$ mode amplitude was never larger than 1% of the $n = 0$ mode amplitude.

Further simulations were done with no wiggler taper and with a 2% wiggler taper. The spectrum of the EM pulse amplitude is again sharply peaked. The output power at saturation for these simulations are tabulated in Table A3.

Energy conservation for these simulations was satisfied to within 1.5%.

Simulation of the LANL Experiment

The physical and simulation parameters of the LANL experiment are listed in Table A4.

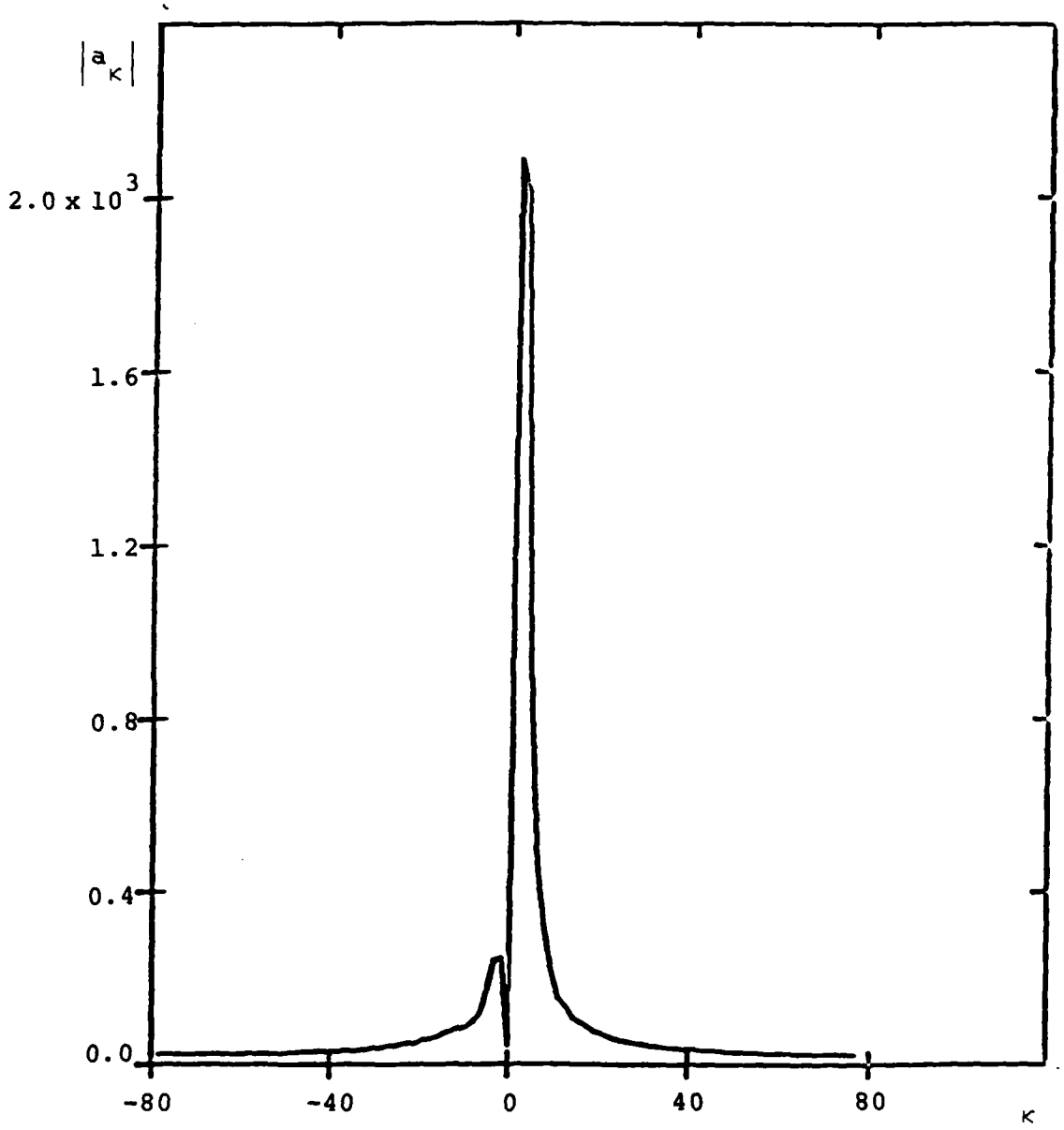

Figure A5. Modulus of Fourier Transform vs. κ
TRW Parameters, 1% taper.

TABLE A3

TRW SIMULATION RESULTS

RUN NUMBER	β	Γ	GAIN	$\langle P \rangle$	TRAPPING FRACTION AT SATURATION
TR2D060	0.005	26.4	0.0107 @ 100 0.0113 @ 200 0.0116 @ 350 0.0 @ 1793	250 MW	32.0%
TR2D062 1 Mode	0.01	13.2	0.0339 @ 100 0.0376 @ 200 0.0112 @ 300 0.0 @ 586	81.3 MW	27.0%
TR2D058	0.01	26.4	0.0105 @ 100 0.0103 @ 200 0.0100 @ 300	Was not run to saturation	
TR2D064 2 Modes	0.01	13.2	0.0279 @ 100 0.0335 @ 200 0.010 @ 300 0.0 @ 651	84.6 MW	27.0%

TABLE A4

LANL FEL PARAMETERS

	Physical Parameter	Simulation Parameter
ELECTRON BEAM		
Energy	21 MeV	22.3 MeV
Current (Peak)	25 - 80 A	25 - 80 A
Microbunch Length	30 psecs	3.66 psecs
Emittance	2-4 mm-mrad	1.9 mm-mrad
Energy Spread	1-3%	0%
WIGGLER		
Wavelength λ_w	2.73 - 2.42 cm	2.73 cm
Length	100 cm	100 cm
B-field	3 KG	3.1 KG
Constant Parameter Section	0	0
Taper-Energy	7.35%	6.0%
OPTICAL		
Optical Wavelength	10.6 - 10.8 μ	10 μ
Rayleigh Range	63.2 cm	61.58 cm
Cavity Length	6.92 m	6.92 m
Mirror Reflectivity	0.9834	0.9834
Mirror Curvature	3.56 m	3.57 m

The wiggler is a simple variable parameter wiggler 100 cm long with a uniform taper of 6%. The electron micropulse is ~20 slippage distances; however, $u_o = 3$ is used in the simulations. The parameter r_b for a beam emittance of 2π mm mrad is [Equation (A41)] $r_b = 0.08$ cm. The effective energy spread $\Delta\gamma_\beta$ due to the betatron motion is $\Delta\gamma_\beta/\gamma_r \approx 0.0006$. $\Delta\gamma_\beta$ is somewhat less than the real energy spread of 1 to 2%. However, the electron energy distribution function was taken to be a delta-function [Equation (A42)] in order to reduce the number of particles in the simulations and hence the run time.

More realistic electron energy distributions as well as longer electron micropulse lengths ($u_o > 3$) and larger electron beam emittances are planned for later investigations.

The EM pulse is grown from low noise levels and followed all the way to saturation. The linear gain is negligibly small when the electron current is 25 amps ($\eta/u_o = 5.23$) and ~5% when the electron current is 80 amps ($\eta/u_o = 16.75$).

In Figure A6, the average pulse power $\langle P \rangle$ is plotted as a function of pass number for a representative run with the detuning parameter $\beta = 0.01$.

Figures A7 through A16 display the EM pulse shape and spectrum at the end of several pass numbers in the run. The pulse amplitude $|\hat{a}_n|$ is plotted as a function of v at $u = 0$. The pulse is initially smooth with amplitude and phase constant in the range $5.5 > v > -1.5$. The pulse is shifted

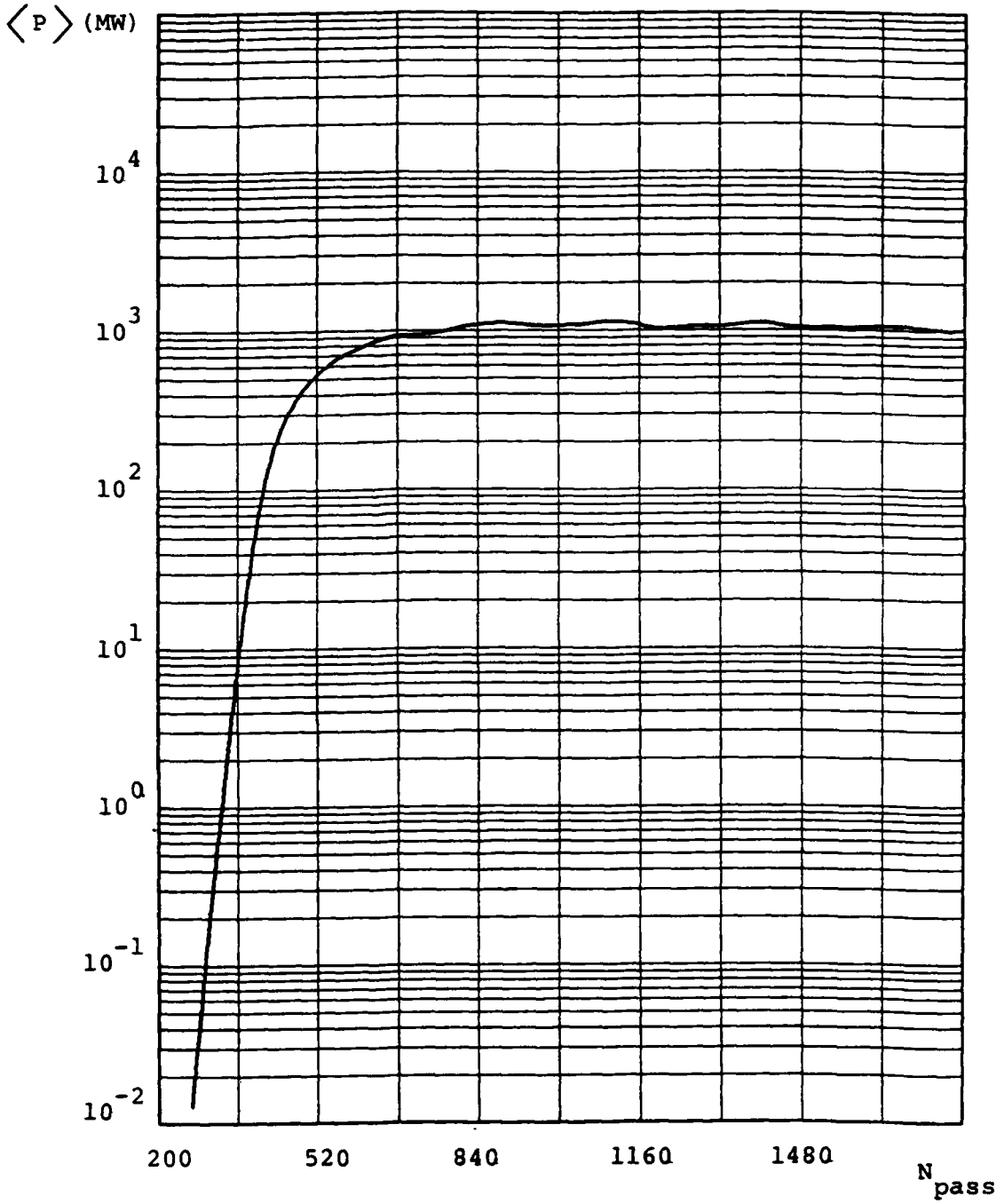

Figure A6. Amplitude of Circulating Power vs. Pass Number.
LANL Parameters, 80 amps.

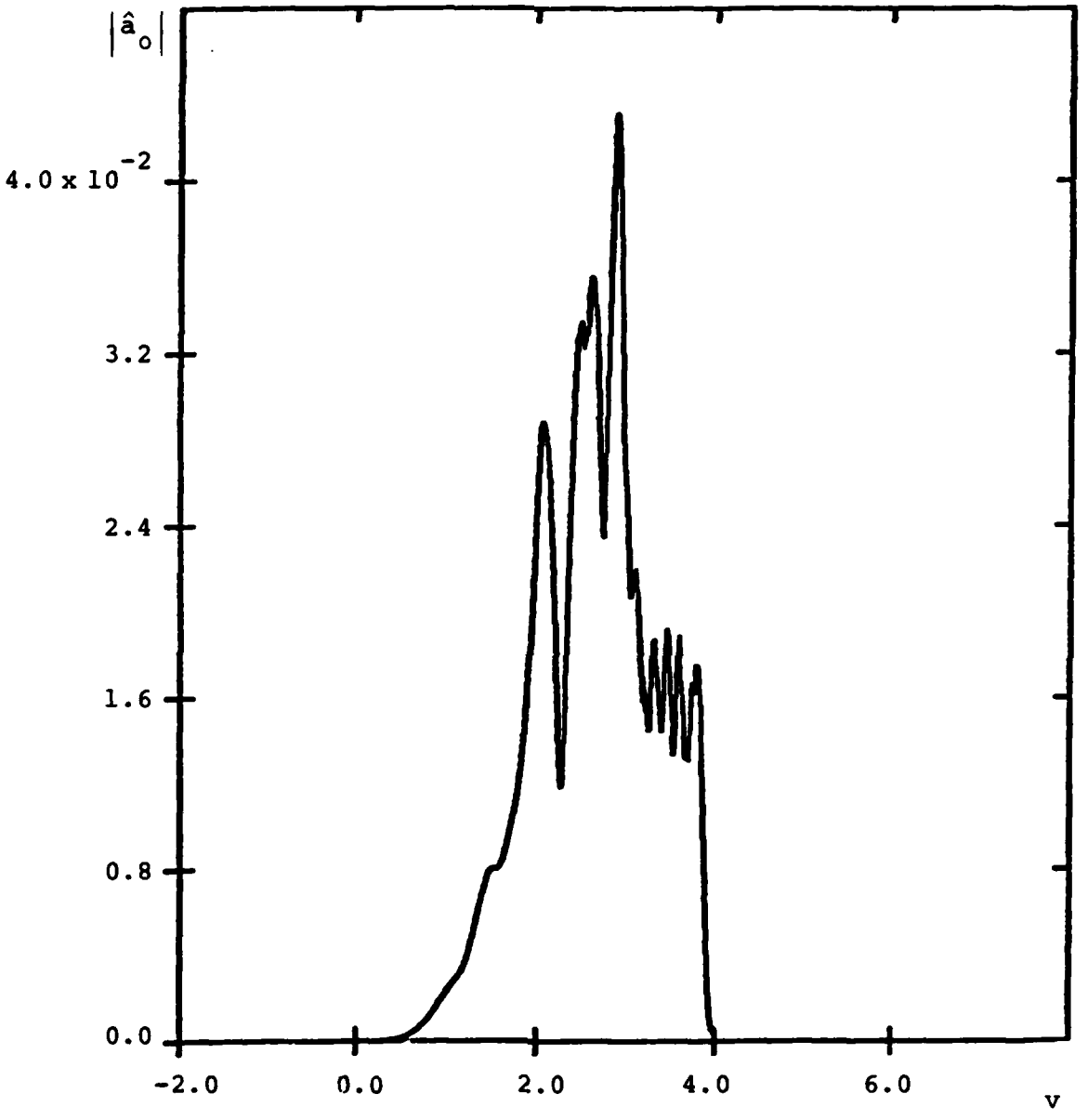

Figure A7. Modulus of Amplitude vs. v
at Pass Number 201.
LANL Parameters, 80 amps.

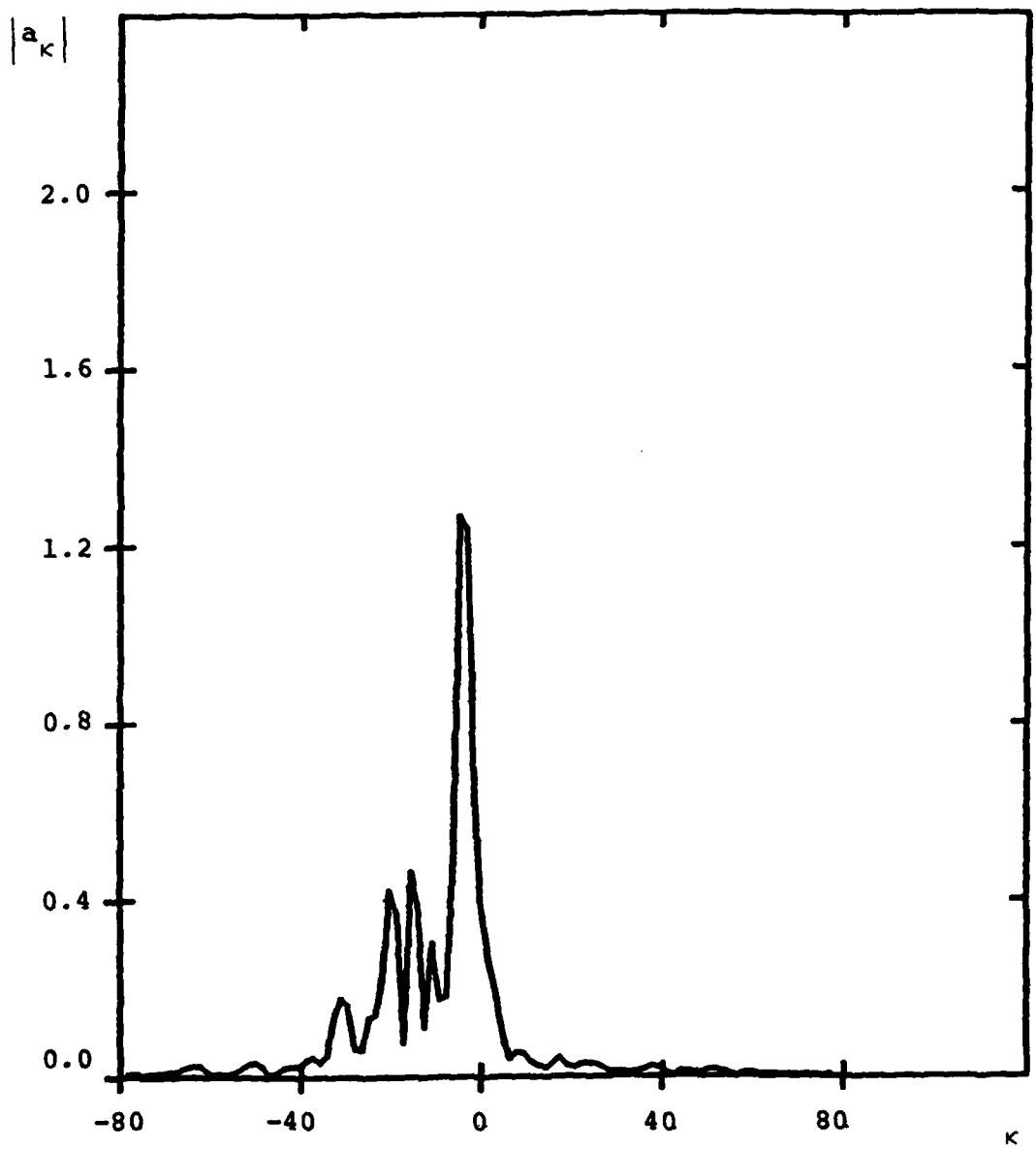

Figure A8. Modulus of Fourier Transform vs. κ at Pass Number 201. LANL Parameters, 80 amps.

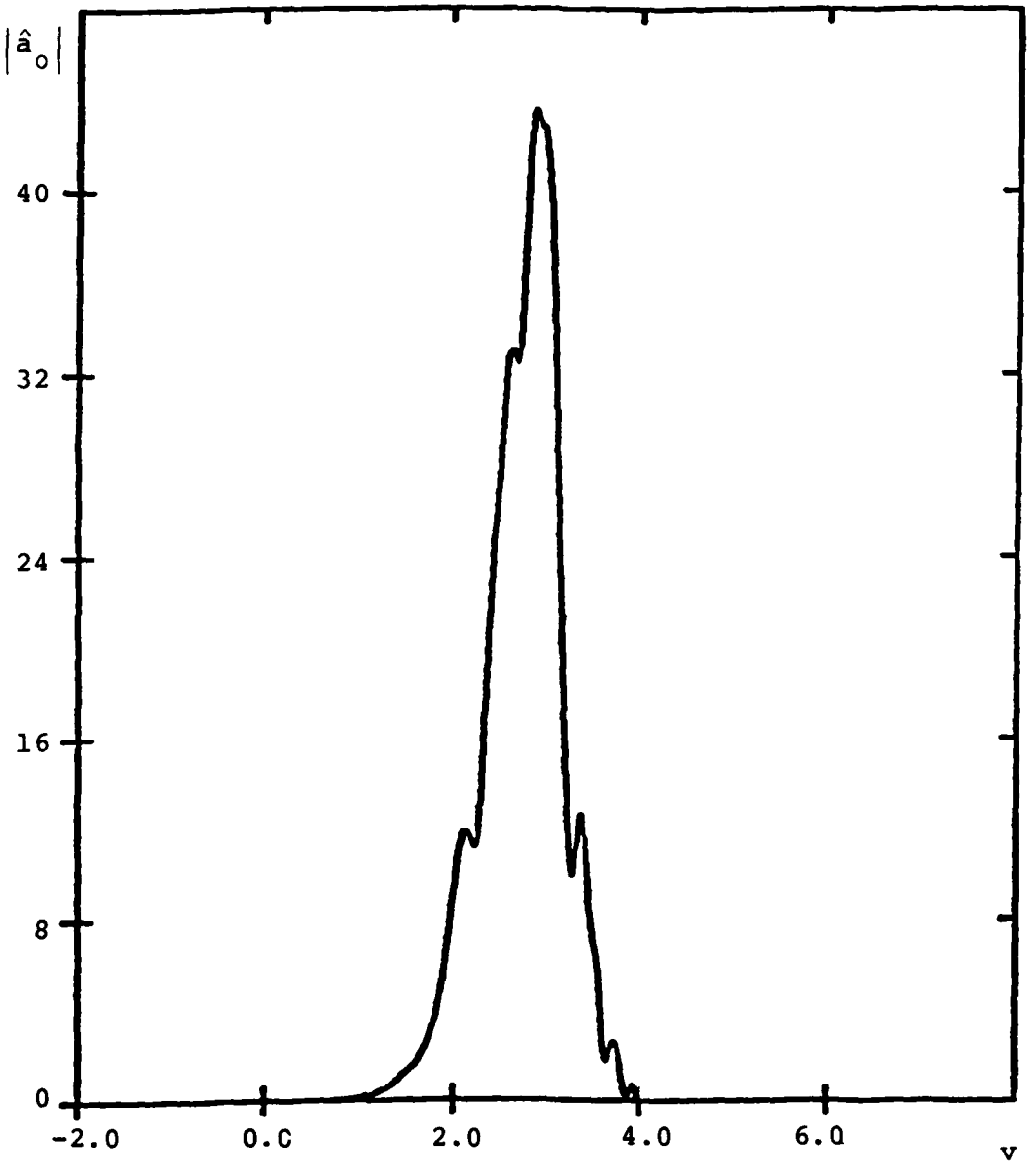

Figure A9. Modulus of Amplitude vs. v
at Pass Number 401.
LANL Parameters, 80 amps.

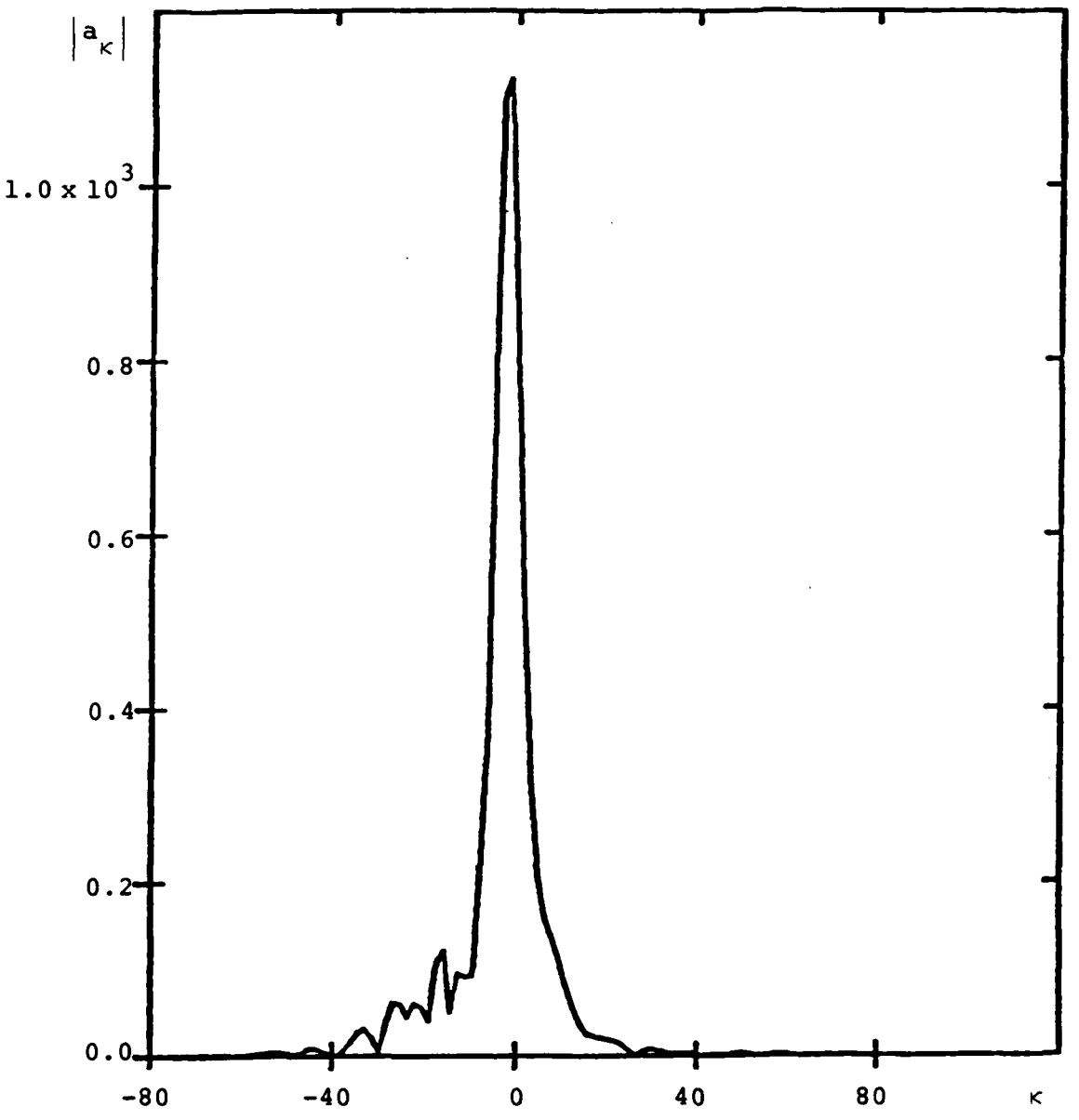

Figure A10. Modulus of Fourier Transform vs. κ at Pass Number 401. LANL Parameters, 80 amps.

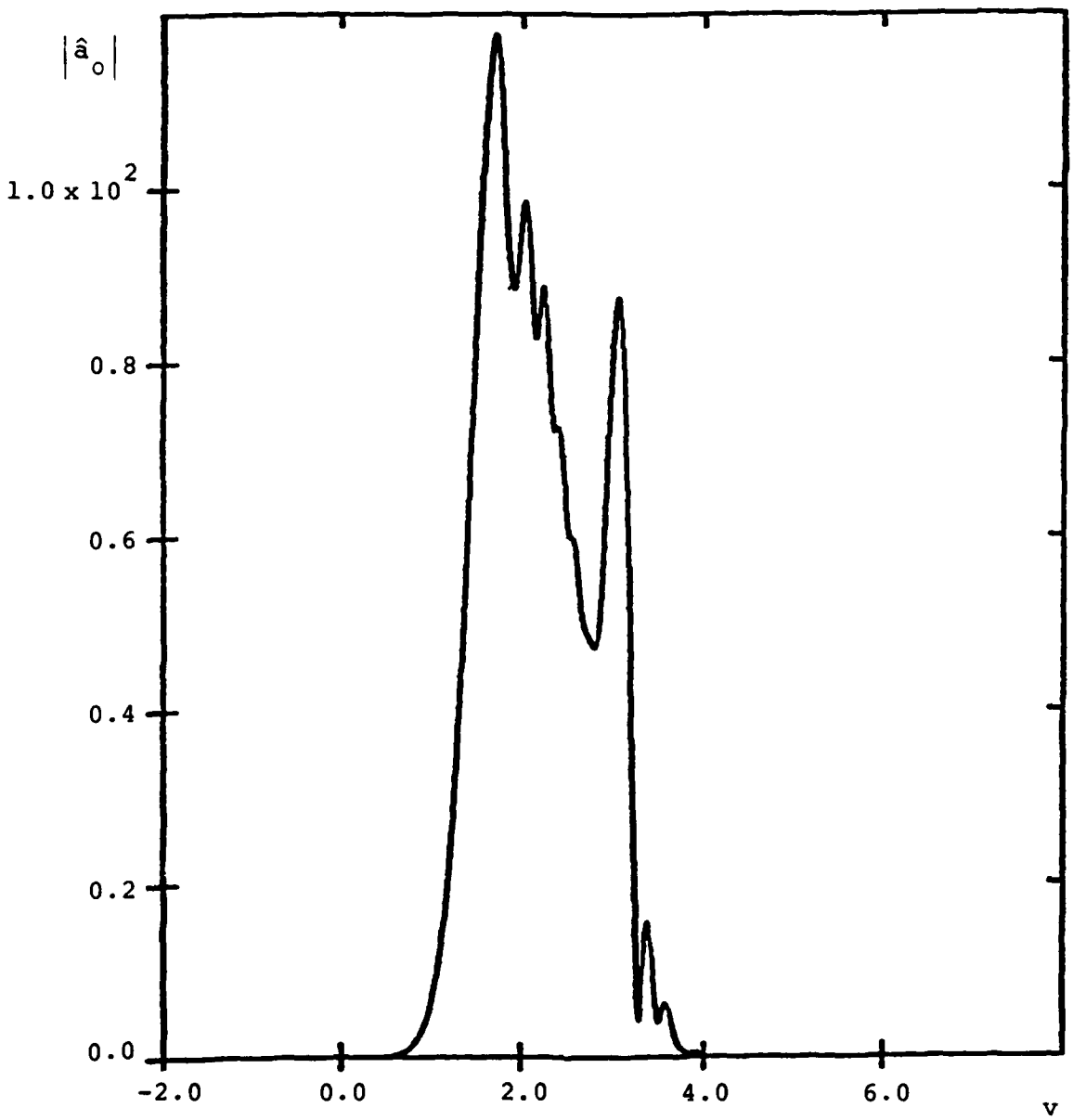

Figure A11. Modulus of Amplitude vs. v
at Pass Number 601.
LANL Parameters, 80 amps.

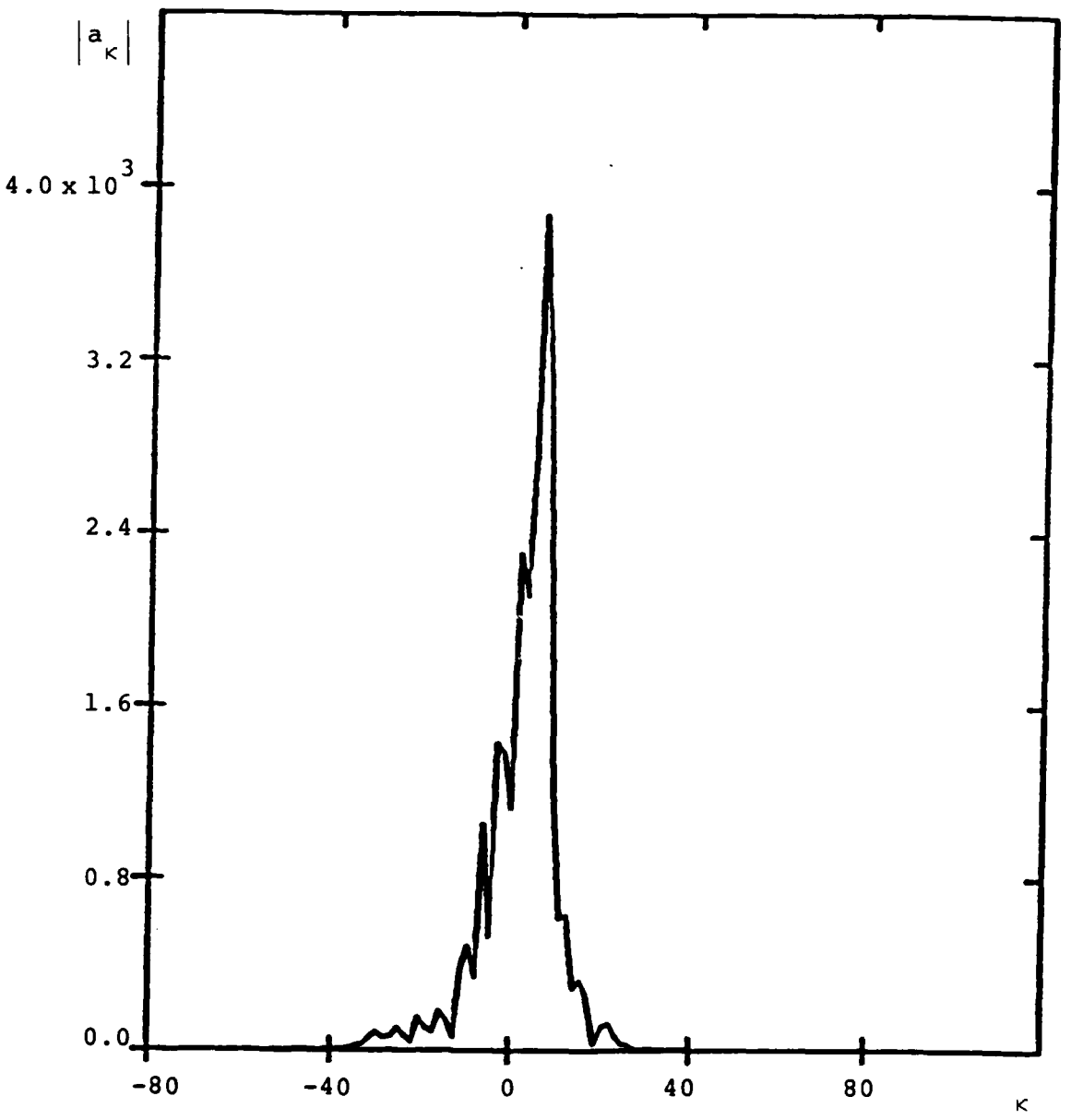

Figure A12. Modulus of Fourier Transform vs. κ at Pass Number 601. LANL Parameters, 80 amps.

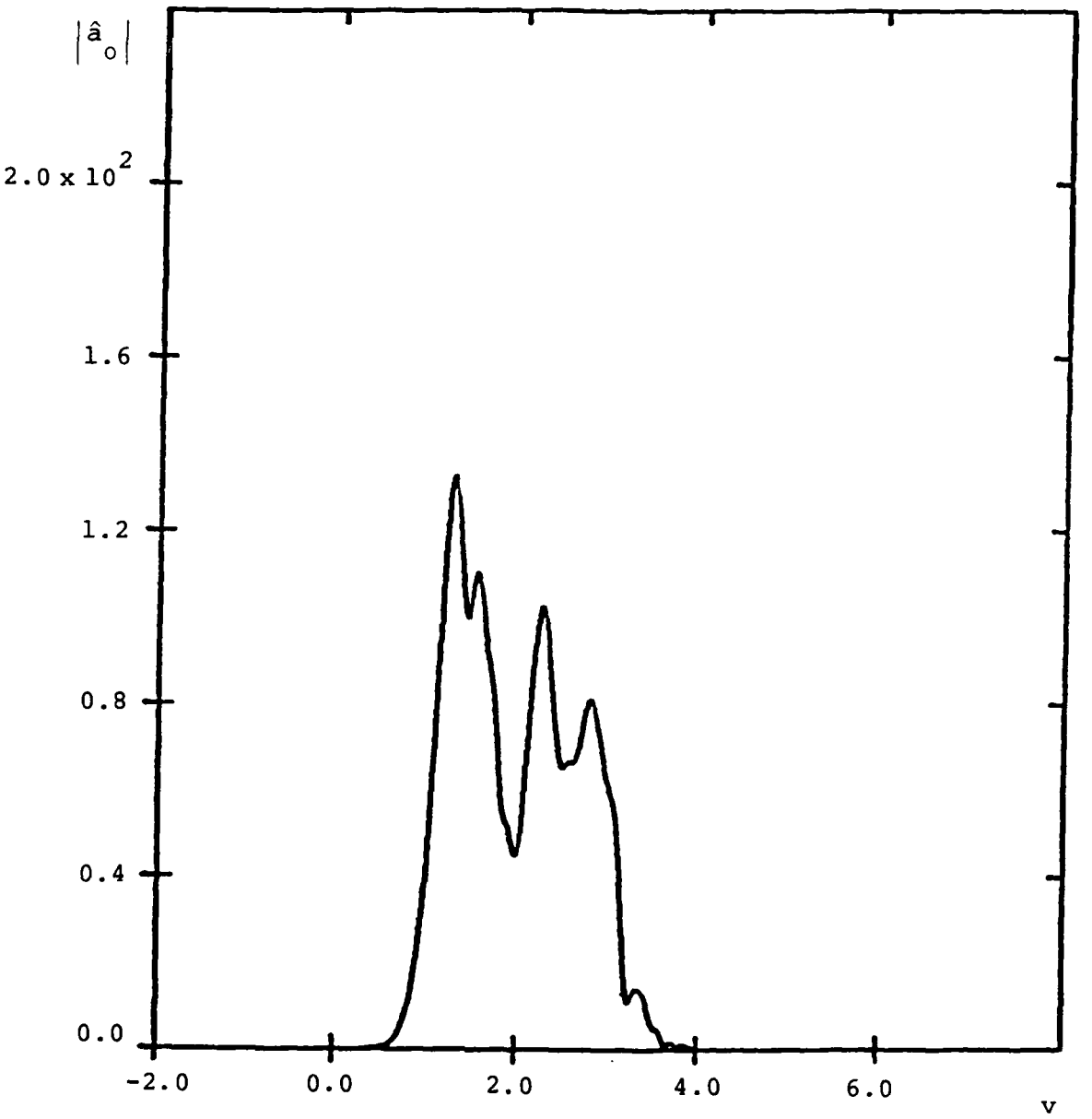

Figure A13. Modulus of Amplitude vs. v
at Pass Number 701.
LANL Parameters, 80 amps.

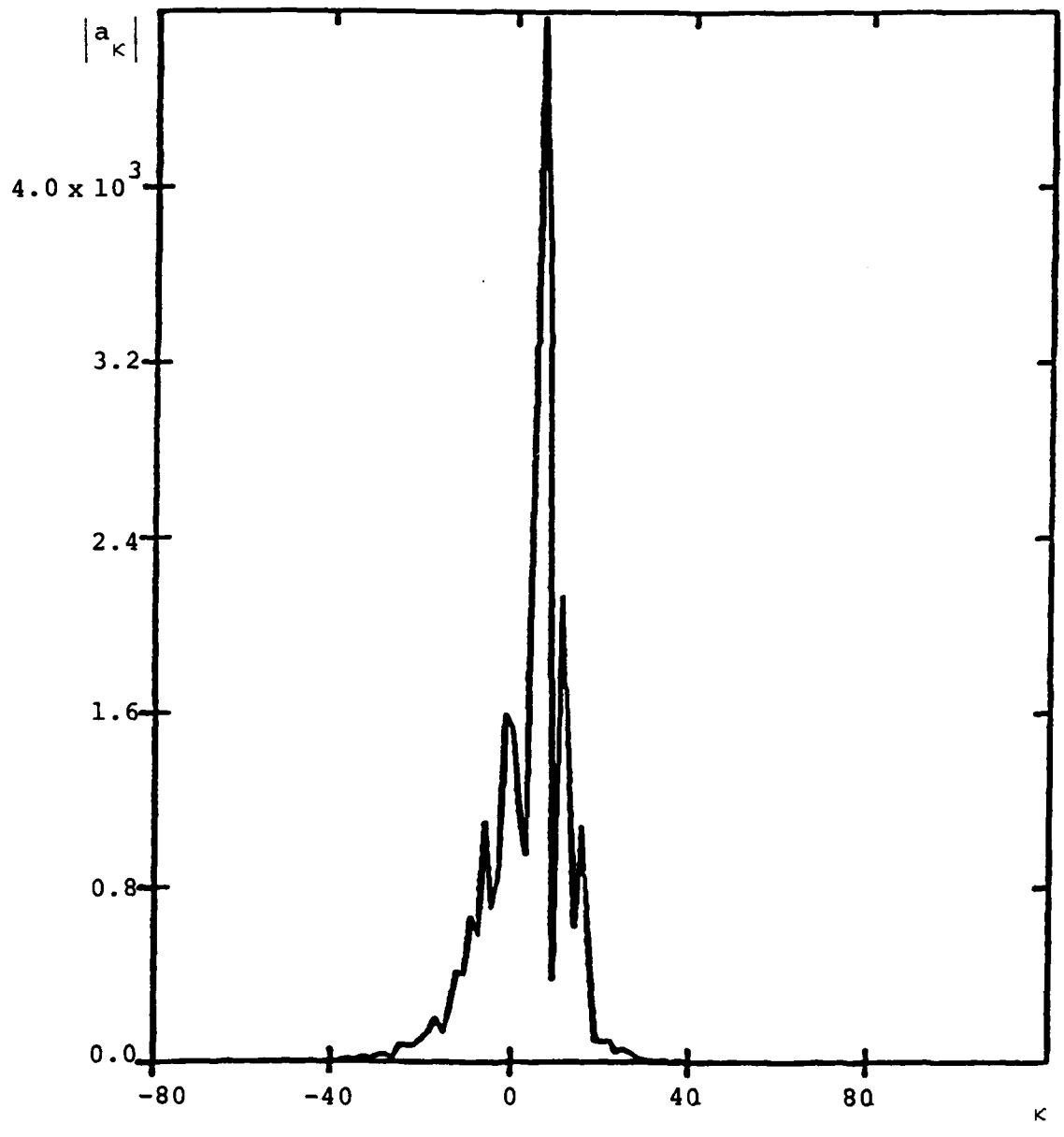

Figure A14. Modulus of Fourier Transform vs. κ at Pass Number 701. LANL Parameters, 80 amps.

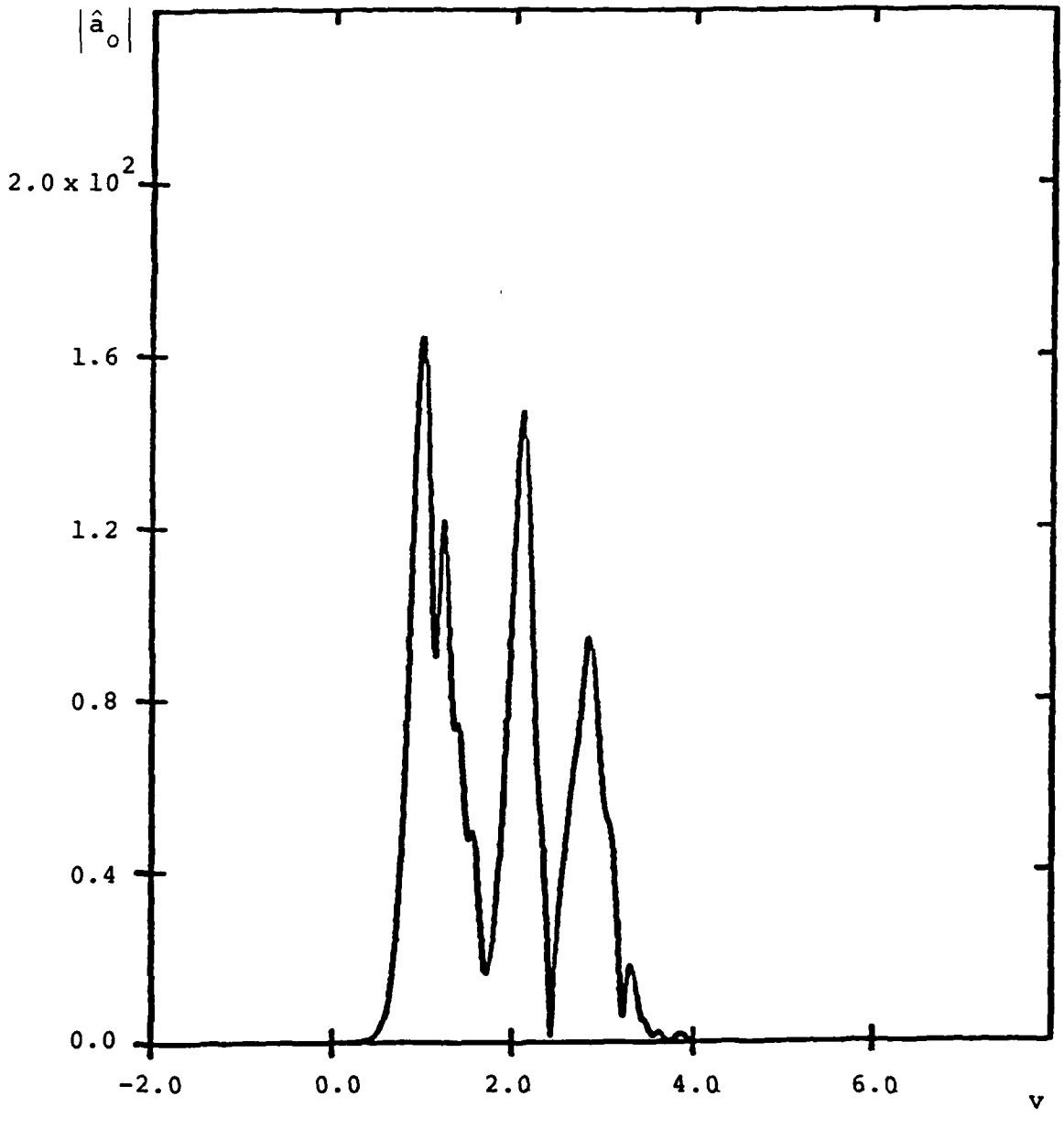

Figure A15. Modulus of Amplitude vs. v
at Pass Number 801.
LANL Parameters, 80 amps.

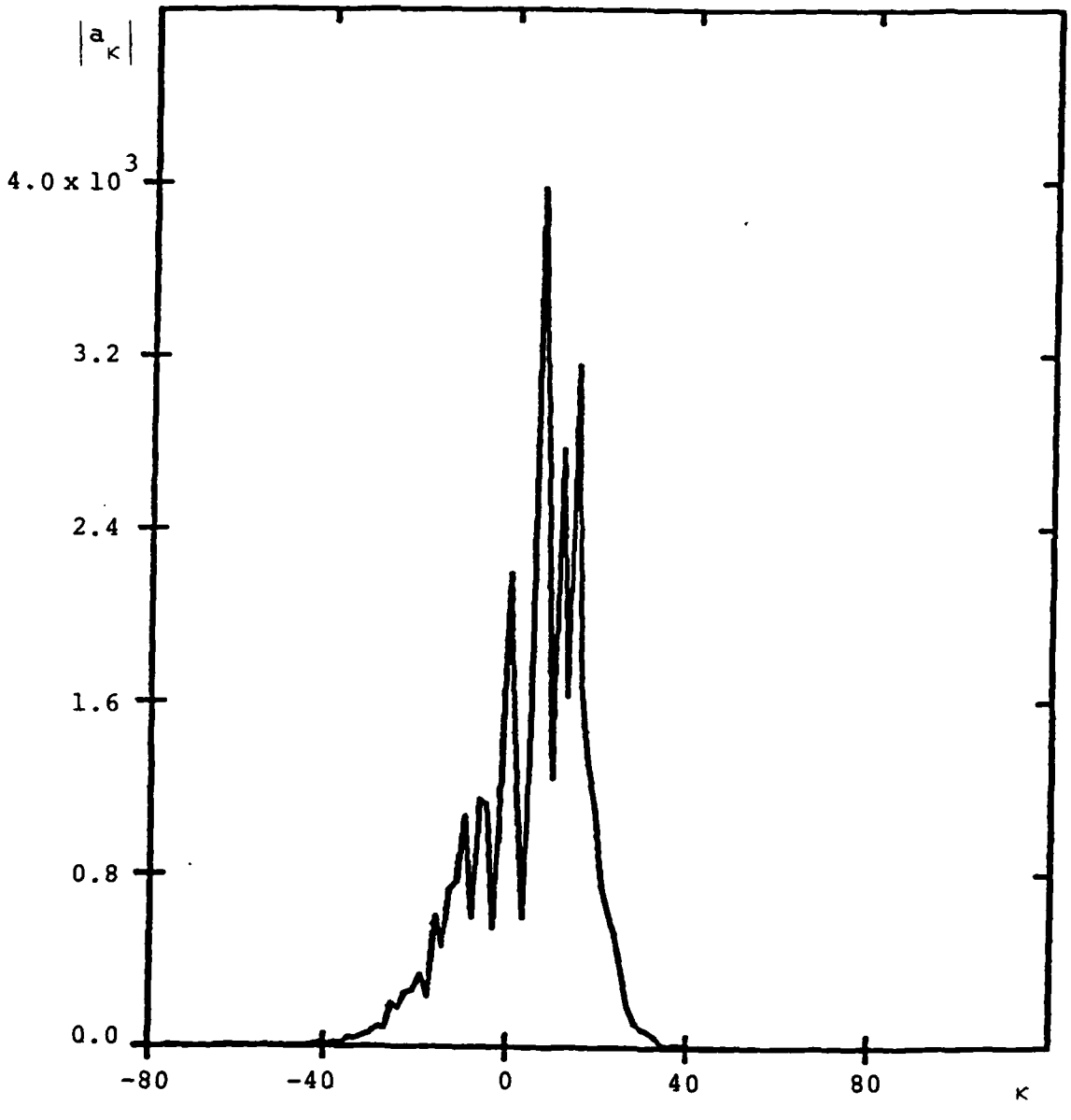

Figure A16. Modulus of Fourier Transform vs. κ at Pass Number 801. LANL Parameters, 80 amps.

to the left by an amount $\Delta v = \beta = 0.01$ on each successive pass. The only part of the pulse which interacts with electrons inside the wiggler during a given pass lies in the range $4 > v > 0$. The pulse spectrum is plotted as a function of κ (see Equation (A43). Electron trapping begins at about pass number 400 and reaches a maximum at pass number 800. During this interval, along with the growth in pulse energy, the pulse shape evolves from a relatively smooth profile to one with several maxima and minima. At the same time, the pulse spectrum exhibits significant growth of sideband frequencies. This pulse distortion is due to the growth of unstable sideband modes and has previously been investigated in 1-D FEL simulations.

The growth of sideband modes can be suppressed by passing the pulse through a band-pass filter at the end of each pass. 2-D simulations with frequency discrimination have not yet been done, although they are planned for future investigations.

Despite the pulse distortion due to the presence of sideband modes, the effective electron trapping fraction is still appreciable $f \sim 40\%$ at saturation. The output power is

$$P_{output} \sim 21.4 \text{ MW} \quad .$$

The bounce frequency (in computer units) of an electron in the ponderomotive potential is $\sim \hat{a}_o^{\frac{1}{2}} \approx 8$ and the betatron

frequency is $k_\beta L_w \approx 3.0$. The condition for resonant coupling of the bounce motion and the betatron motion, that is $\hat{a}_o^{\frac{1}{2}} = 2k_\beta L_w$, is satisfied at some stage of the evolution. However, the simulations have not yet been analyzed in sufficient detail to assess whether any significant detrapping was produced by this resonance coupling.

Further simulations were done at different values of the detuning parameter β. In all the runs, there is pulse distortion and sideband activity, with the distortion becoming more severe at smaller values of β. The results for the effective electron trapping fraction and the output power are summarized in Table A5.

The power ratio of the $n = 1$ Gaussian mode to the lowest order Gaussian mode $n = 0$ never exceeded 0.1%. Energy conservation was typically of the order of 5%.

TABLE A5

LASL SIMULATIONS

β	GAIN	$\langle P \rangle$	PEAK TRAPPING FRACTION
0.01	0.051 @ 100 0.051 @ 200 0.052 @ 300 0.0 @ 480	656 MW @ 574	39.5%
0.0025	0.056 @ 100 0.060 @ 200 0.025 @ 300	647 MW @ 701	38.9%

REFERENCE

1. W. B. Colson and S. K. Ride, "The Free Electron Laser: Maxwell's Equations Driven by Single Particle Currents," Free Electron Generators of Coherent Radiation, Physics of Quantum Electronics, Vol. 7 (Addison-Wesley, 1980), p. 377.

   J. C. Goldstein, "Evolution of Long Pulses in a Tapered Wiggler Free Electron Laser," Free Electron Generators of Coherent Radiation, SPIE, Vol. 453 (June 1983), p. 2.

   M. N. Rosenbluth, H. V. Wong and B. N. Moore, "Free Electron Laser (Oscillator) - Linear Gain and Stable Pulse Propagation," Free Electron Generators of Coherent Radiation, SPIE, Vol. 453 (June 1983), p. 11.

   M. N. Rosenbluth, H. Vernon Wong and B. N. Moore, "Annual Technical Report for Theoretical Studies on Free Electron Lasers," ARA Report No. I-ARA-82-U-89 (NTIS No. AD-A121673), August 1982.

   M. N. Rosenbluth, H. Vernon Wong and B. N. Moore, "Final Technical Report for Theoretical Studies on Free Electron Lasers," ARA Report No. I-ARA-83-U-62 (NTIS No. AD-136333), November 1983.

2. M. N. Rosenbluth, "Two-Dimensional Effects in Free Electron Lasers," Journal of Quantum Electronics (to be published in 1985), Appendix E, ARA Report No. I-ARA-83-U-62 (NTIS No. AD-136333), November 1983.

3. W. M. Fawley, D. Prosnitz and E. T. Schorlemann, submitted to Phys. Rev. A (1985), Lawrence Livermore National Laboratory Report UCRL-90838 (1984).

A P P E N D I X B

SIMULATION OF MSNW EXPERIMENT

The difference equations discussed in Appendix A were not sufficiently accurate to be used to simulate the FEL experiment proposed by MSNW. Energy conservation better than 10% was never achieved for the smallest practical steplengths which could be chosen.

The difference equations were therefore modified to be correct to second order in the steplengths by using the centered difference approximation and to conserve energy exactly through the wiggler. The details of this improved numerical algorithm will be reported elsewhere.

Two additional versions of the 2-D FEL simulation code were written:

1. A "renormalized" code in which the EM pulse energy at the beginning of each pass was fixed at a low "noise" level. This enabled the linear eigenmode with the largest linear gain to be determined by repeatedly passing the pulse through the wiggler until the initial transients have decayed away and a stationary state was reached. Once the linear eigenmode was formed, it could then be allowed to evolve and grow into the nonlinear regime.

2. A "steady state" code in which the FEL variables were constrained to be a function of one independent variable (instead of two, u and v), namely $u + v - \frac{1}{2} = z/L_w$. This was used to simulate the idealized limit of a long electron micropulse interacting with a long EM pulse, the FEL variables changing only with z through the wiggler.

The physical parameters of the proposed MSNW experiment and the simulation parameters are listed in Table B1.

The simulations were done both without and with frequency discrimination. In the absence of frequency discrimination, the EM pulse shape at saturation was highly irregular and characterized by random peaks due to the onset of sideband instabilities. When frequency discrimination was present to suppress the growth of sideband modes, a smooth saturated pulse shape and a significantly larger saturated pulse energy was obtained.

A. No Frequency Discrimination

Two Gaussian modes, $n = 0$ and $n = 1$, are allowed to evolve in the simulation. The micropulse length corresponds to $u_o = 2$. the desynchronization parameter is taken to be $\beta = 0.01$.

The EM pulse is grown from low noise levels and followed into the nonlinear regime all the way to saturation when the energy extracted from the electrons is balanced by the energy losses at the mirrors.

TABLE B1

MATH SCIENCES FEL PARAMETERS

ELECTRON BEAM	EXPERIMENTAL	SIMULATION
Energy	120 MeV	120 MeV
Current	0.2 kA	0.2 kA
Microbunch Length	25 ps	0.826 ps
Beam Radius	0.033 cm	0.033 cm
Energy Spread	1%	0
WIGGLER		
Wavelength	2.018 cm	2.018 cm
Length	5 m	5 m
B-field	9.96 kG	9.96 kG
Constant Parameter Section	50 cm	50 cm
Taper	12.5%	12.5%
OPTICAL CAVITY		
Optical Wavelength	0.5 m	0.5 m
Rayleigh Range	2.4 m	2.4 m
Cavity Length	60 m	60 m
Mirror Reflectivity	0.95	0.95
Radius of Curvature	30.192	30.192

In Figure B1, the average pulse power $\langle P \rangle$ is plotted as a function of pass number, where

$$\langle P \rangle = 0.543 \times 10^{9} \frac{r_p^2 \gamma_R^4}{k_w^2 L_w^4 a_w^2 u_o} \sum_n \int \hat{a}_n^2 \, dv \quad \text{watts}$$

Figure B2 displays the pulse shape and spectrum in the intermediate stage of the nonlinear evolution, and Figure B3 displays the saturated pulse shape and spectrum. The part of the pulse which interacts with electrons throughout the wiggler lies in the range $2 > v > 1$ (see Figure A2, Appendix A). In the intermediate stage, the front of the pulse is amplified to a large amplitude, while the back of the pulse remains at a low amplitude. This behavior is reminiscent of that seen in the 1-D simulations described in Report No. I-ARA-82-U-89 (ARA-467). In that report, it was concluded that any tendency of the EM pulse to broaden towards the back is hindered by the growth of sideband modes destabilized by the "bounce" motion of the electrons trapped in the ponderomotive potential well. The growth of sidebands leads to a loss of coherence and the electrons are not effectively trapped throughout the length of the wiggler. By the time the final saturated state is reached, the pulse shape "breaks up" into a succession of irregular peaks, and the pulse energy fluctuates in a limit cycle.

The effective fraction of electrons trapped in the saturated state fluctuates in the range

$$f \sim 10\% \text{ to } 17\%$$

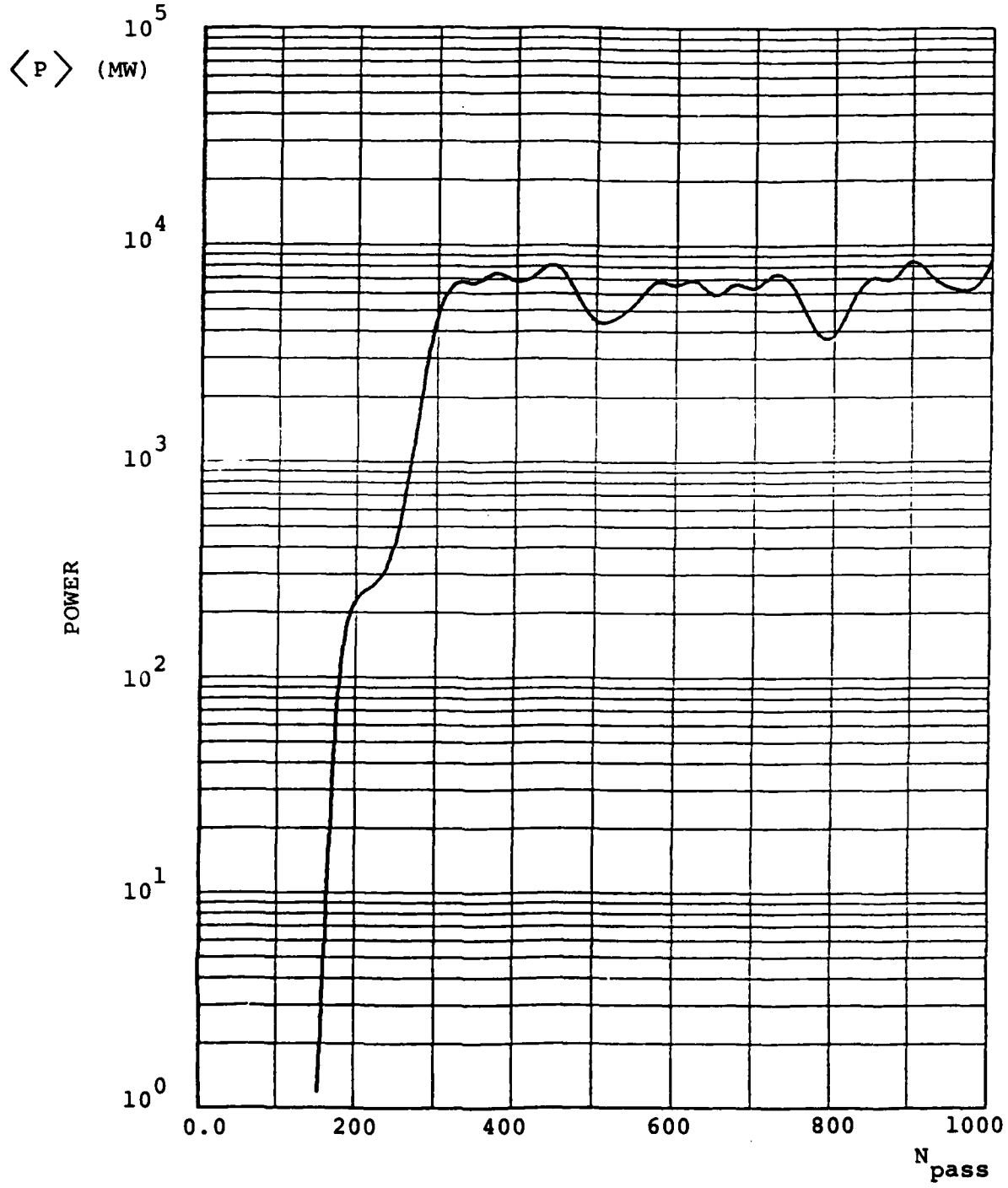

Figure B1. Power vs. Pass Number
MSNW Parameters, no frequency discrimination.

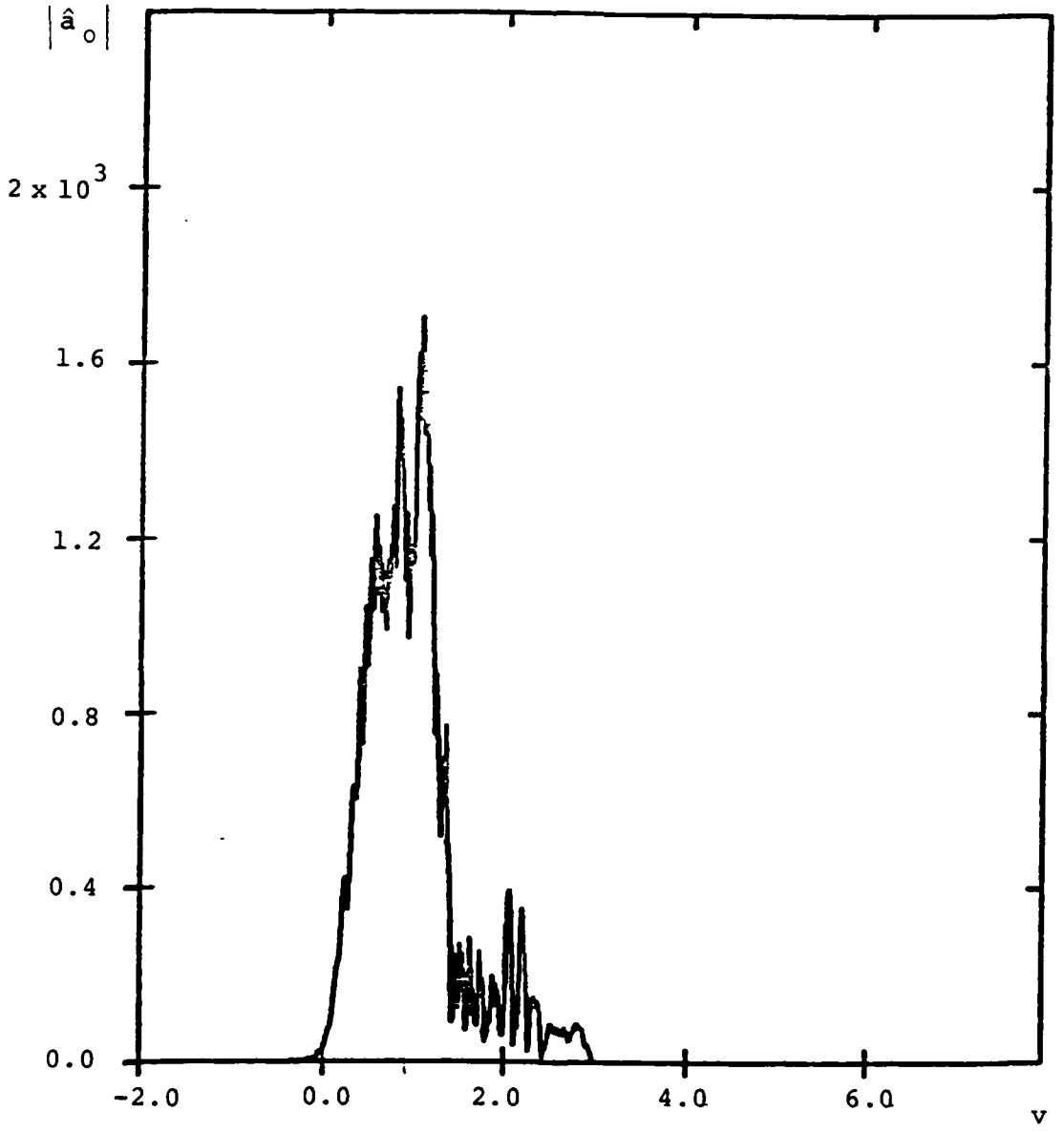

Figure B2(a). Amplitude vs. v at Pass 300
for Mode n = 0.
MSNW Parameters, no frequency discrimination.

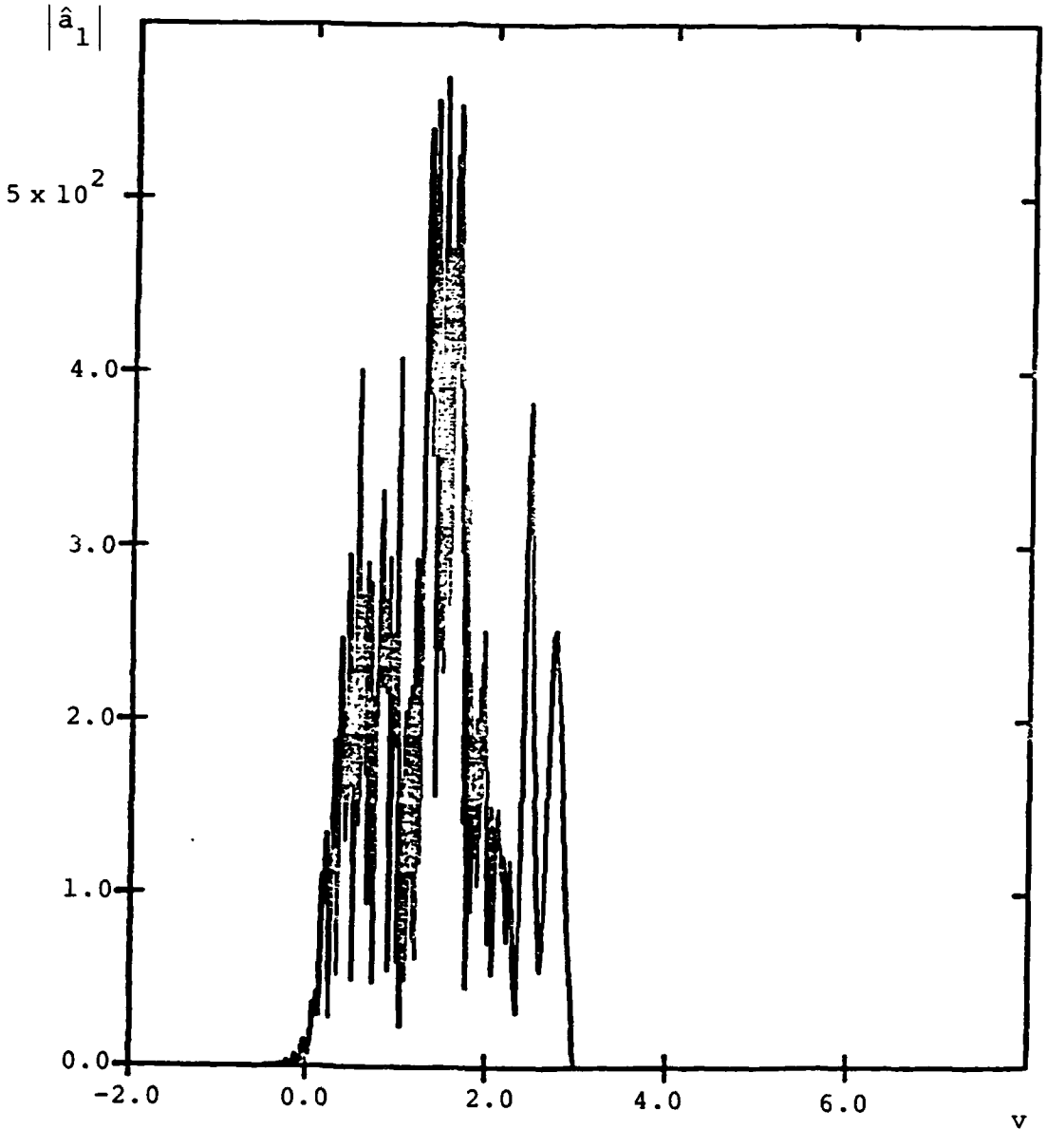

Figure B2(b). Amplitude vs. v at Pass 300
for Mode n = 1.
MSNW Parameters, no frequency discrimination.

AD-A158 229 THEORETICAL STUDIES OF TWO-DIMENSIONAL EFFECTS IN FREE ELECTRON LASERS(U) AUSTIN RESEARCH ASSOCIATES INC TX M N ROSENBLUTH ET AL. DEC 84 I-ARA-84-U-121

UNCLASSIFIED AFOSR-TR-85-0493 F/G 20/5 NL

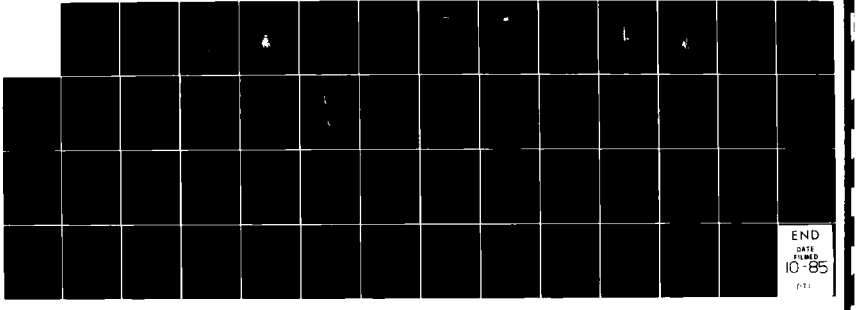

END
DATE FILMED
10-85
DTIC

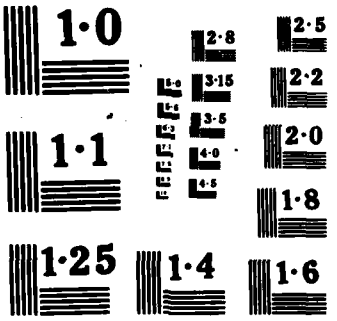
1·0
1·1
1·25
1·4
1·6
1·8
2·0
2·2
2·5
2·8
3·15
3·5
4·0
4·5

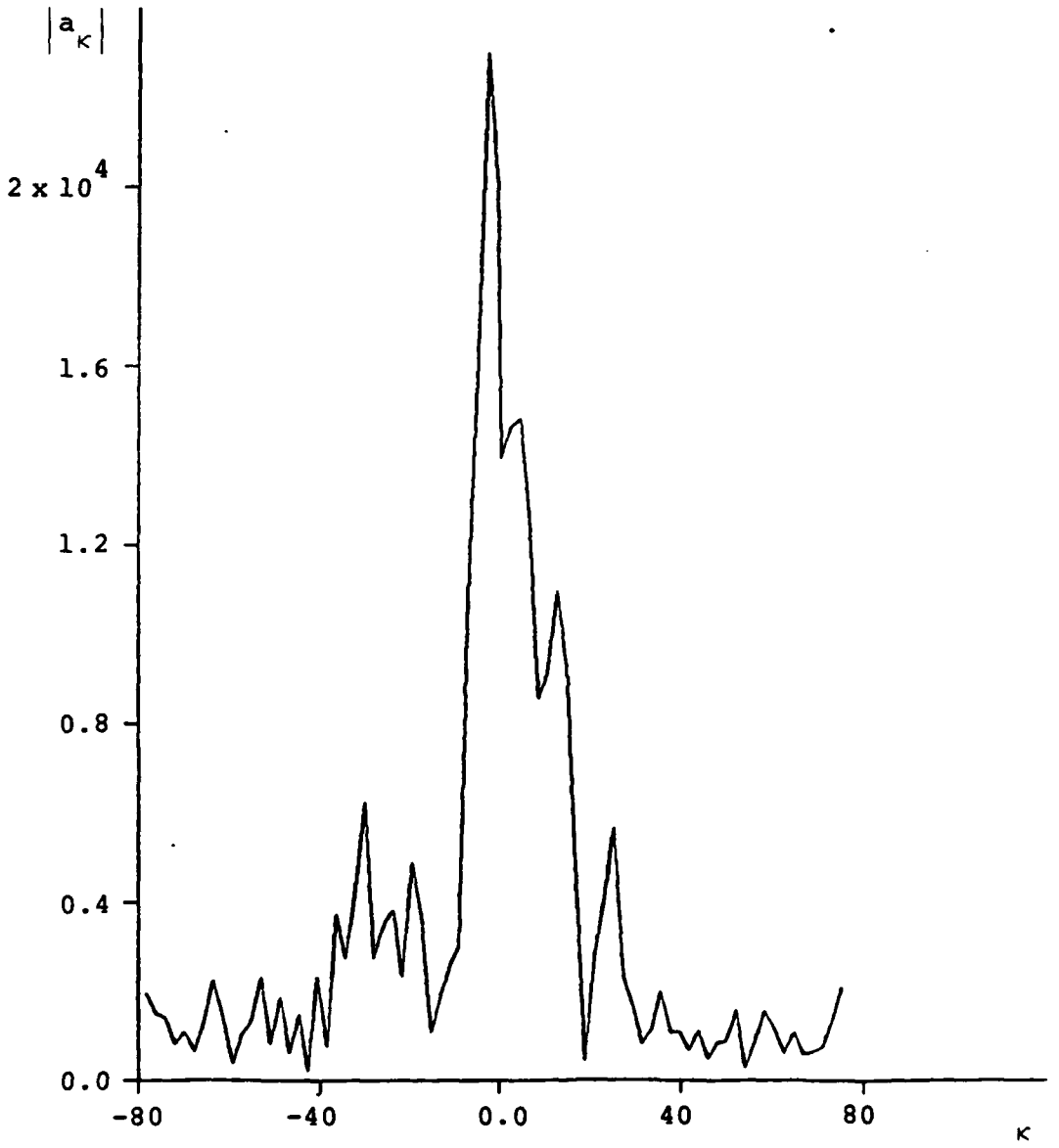

Figure B2(c). Modulus of Fourier Transform of Pulse at Pass 300.
MSNW Parameters, no frequency discrimination.

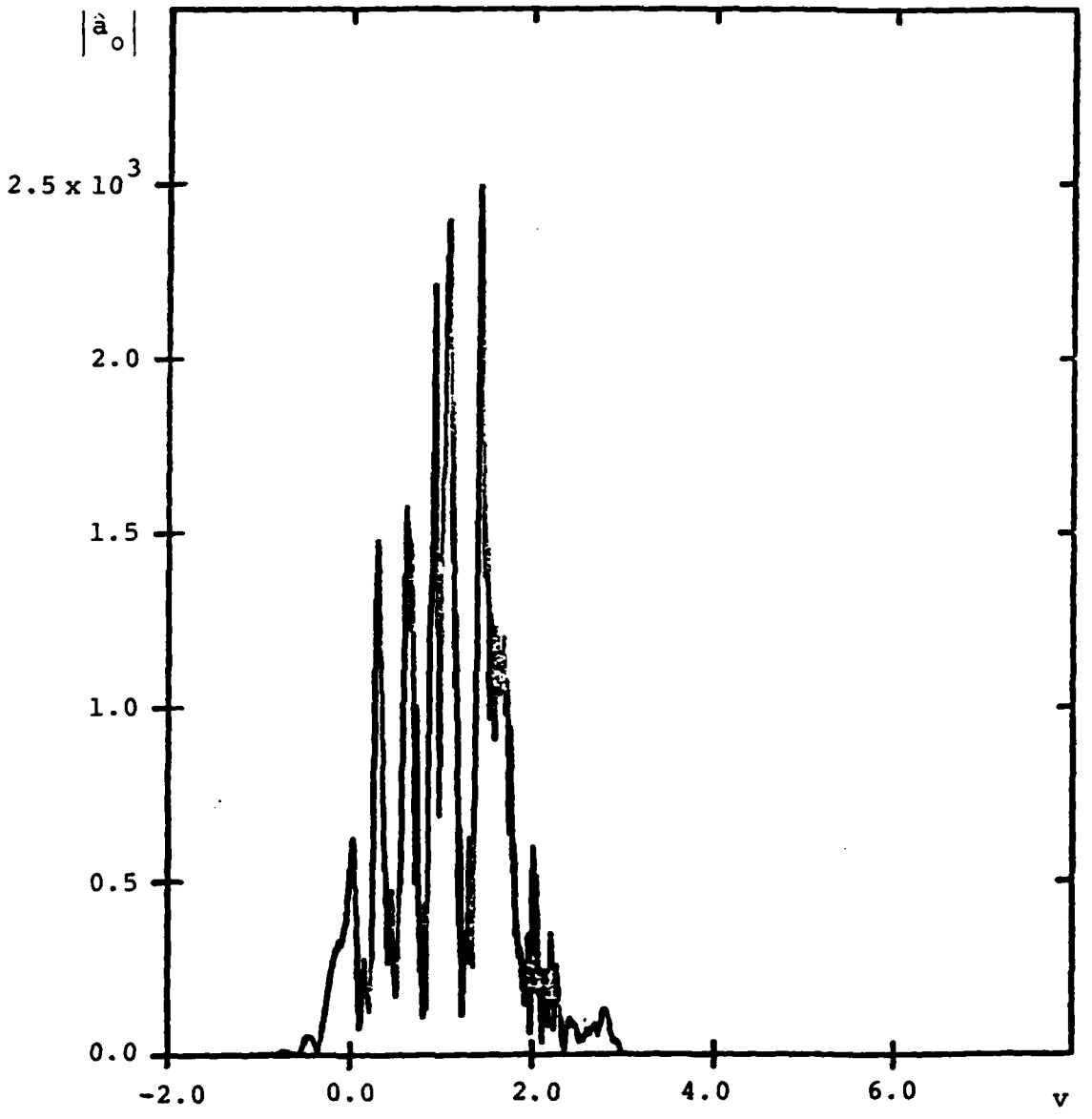

Figure B3(a). Amplitude vs. v at Pass 600
for Mode n = 0.
MSNW Parameters, no frequency discrimination.

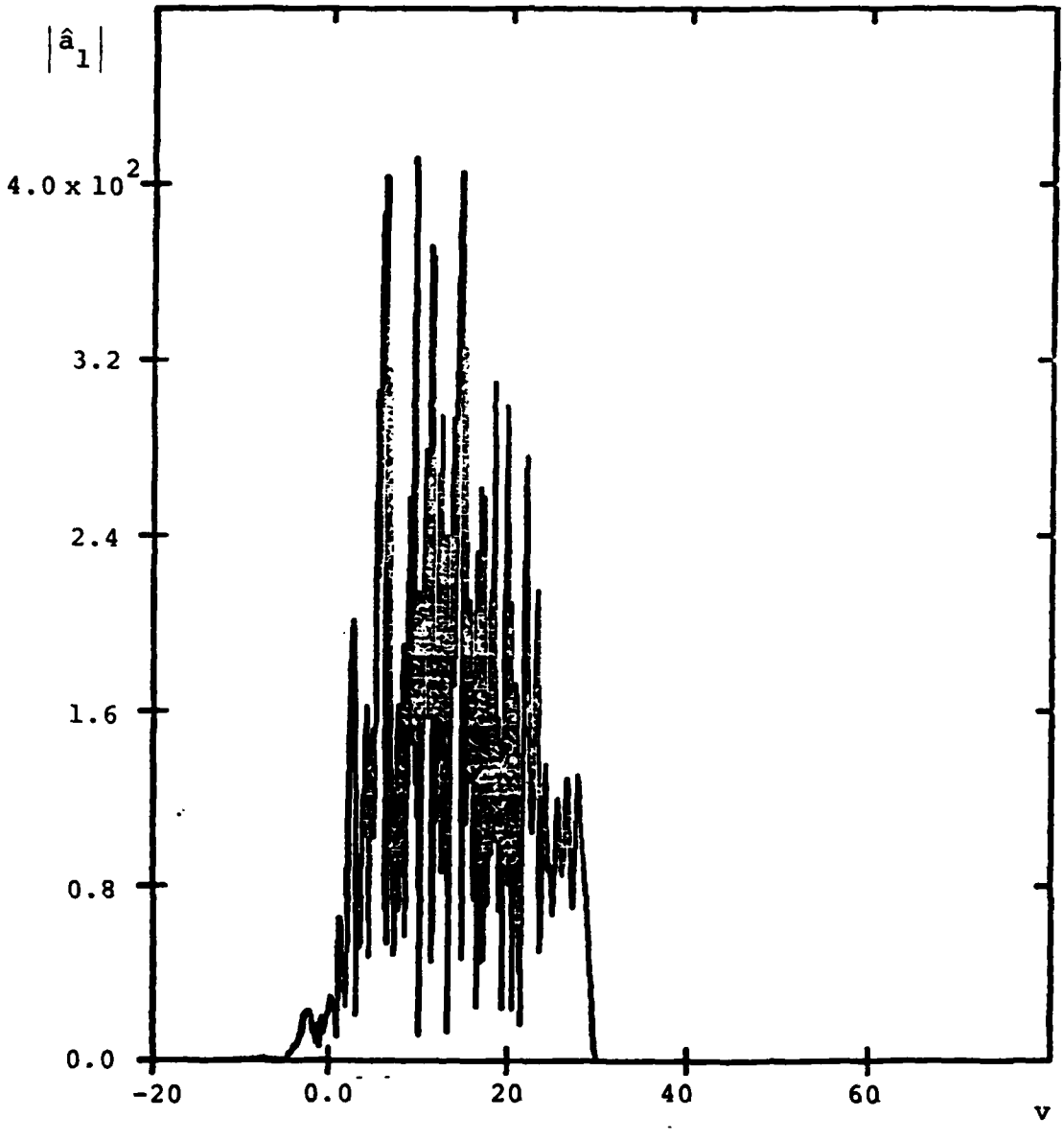

Figure B3(b). Amplitude vs. v at Pass 600
for Mode n = 1.
MSNW Parameters,
no frequency discrimination.

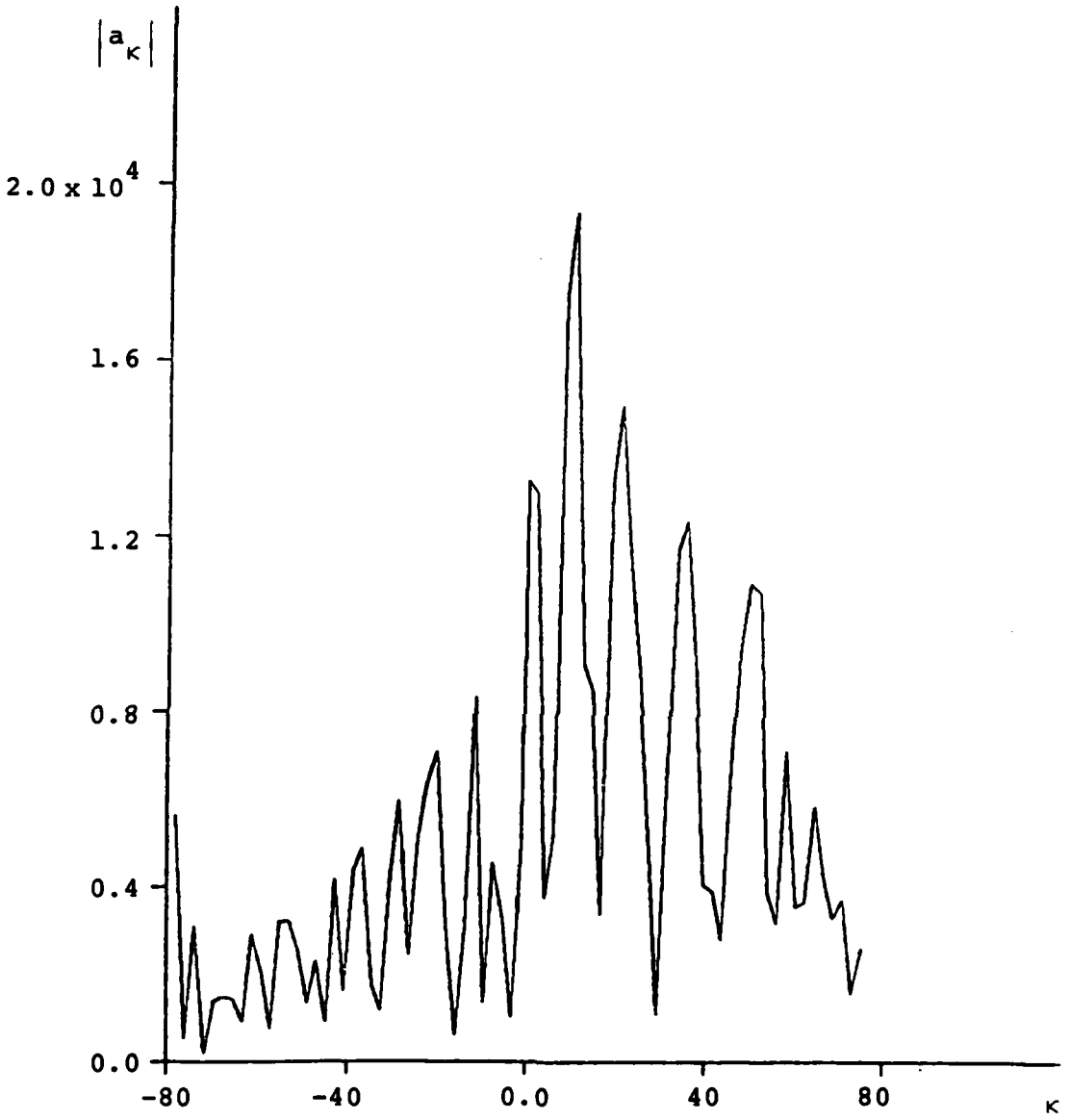

Figure B3(c). Modulus of Fourier Transfor of Pulse at Pass 600.
MSNW Parameters,
no frequency discrimination.

and the average output power fluctuates between

$$\left\langle P_{output} \right\rangle \sim 300 \text{ to } 500 \text{ megawatts.}$$

The pulse energy in the $n = 1$ mode was about 4% of the energy in the $n = 0$ mode at saturation.

The same final state is obtained by starting the simulation run with a square wave pulse of finite amplitude large enough to trap electrons. Figures B4 and B5 exhibit the deterioration of the pulse shape into highly irregular peaks as unstable sideband frequencies of the order of the "bounce" frequency $|\hat{a}_0|^{\frac{1}{2}} \sim 50$ grow in amplitude.

As will be seen in the next section, the suppression of sideband modes by frequency discrimination results in a considerable improvement in the pulse shape and the total pulse energy at saturation.

B. Frequency Discrimination

Two Gaussian modes, $n = 0$ and $n = 1$, were allowed to evolve in the simulation. The micropulse length corresponds to $u_0 = 2$. With frequency discrimination by a band pass filter, it is appropriate to set $\beta = 1/\nu$ for reasons previously discussed in Reference 1: The pulse advance produced by a positive value of β then compensates for the effective pulse delay (proportional to $1/\nu$) introduced by the frequency

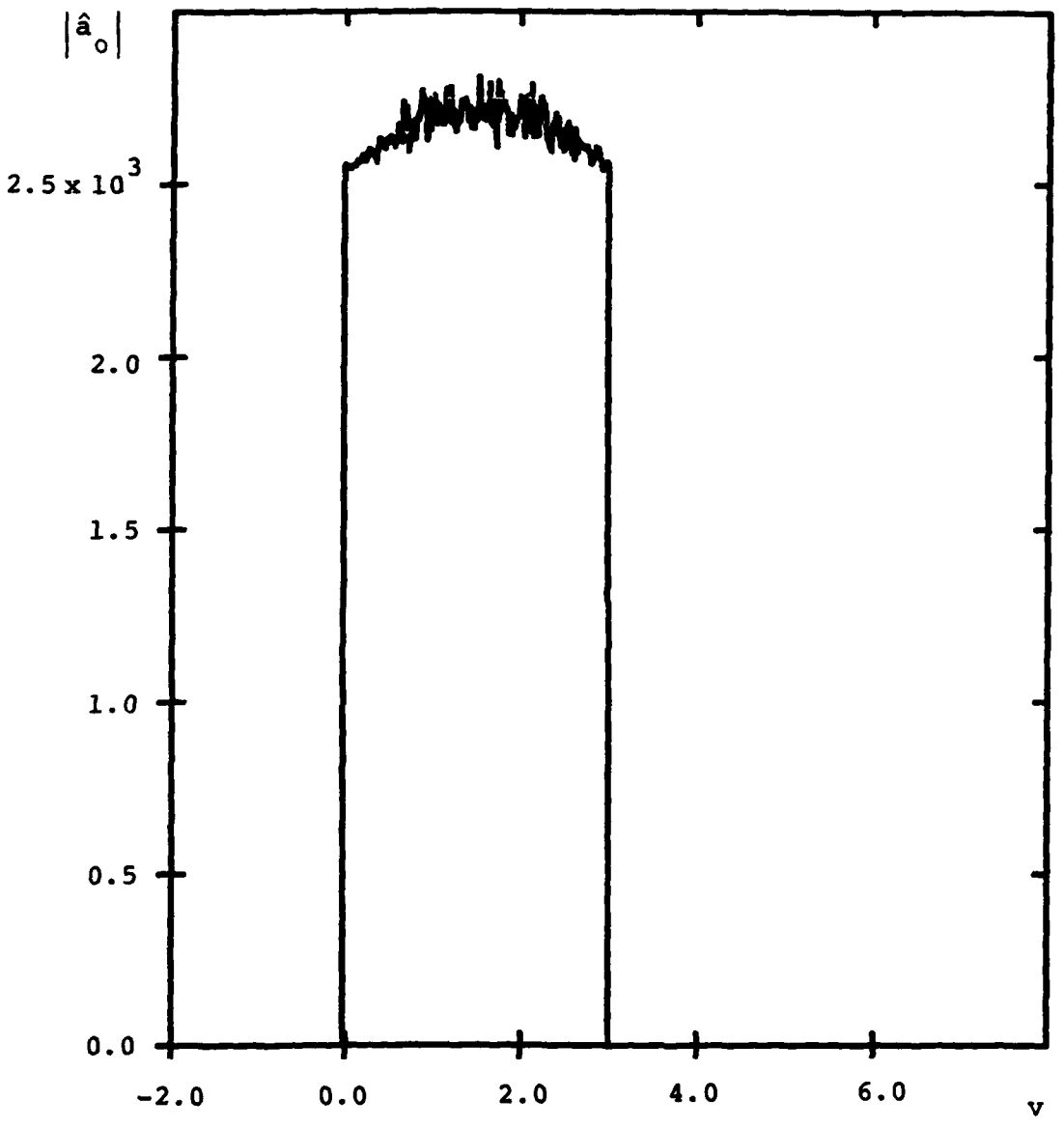

Figure B4(a). Amplitude vs. v for
Pass 2 (n = 0).
MSNW Parameters, large initial
amplitude, no frequency discrimination.

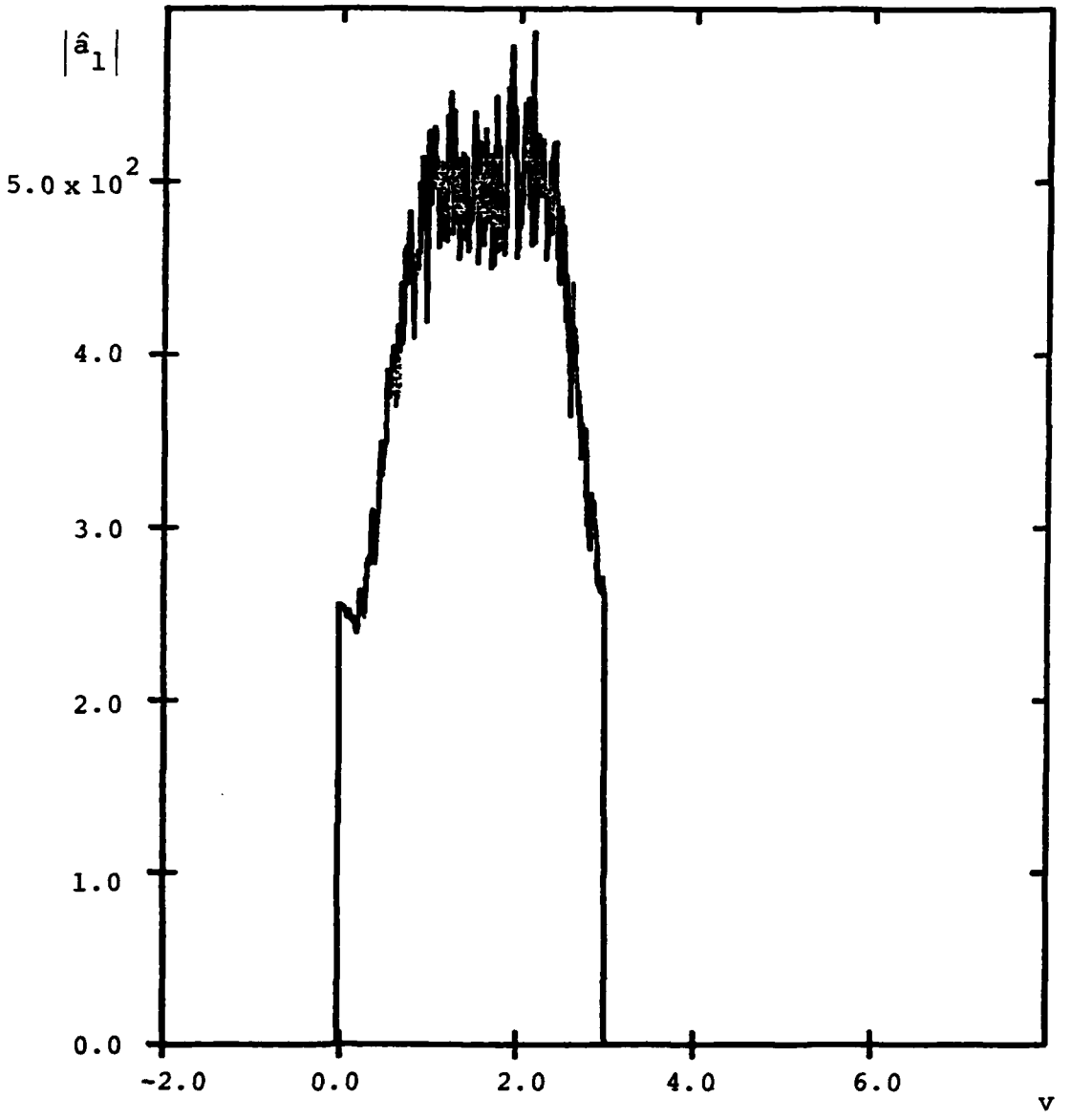

Figure B4(b). Amplitude vs. v for
Pass 2 (n = 1).
MSNW Parameters, large initial
amplitude, no frequency discrimination.

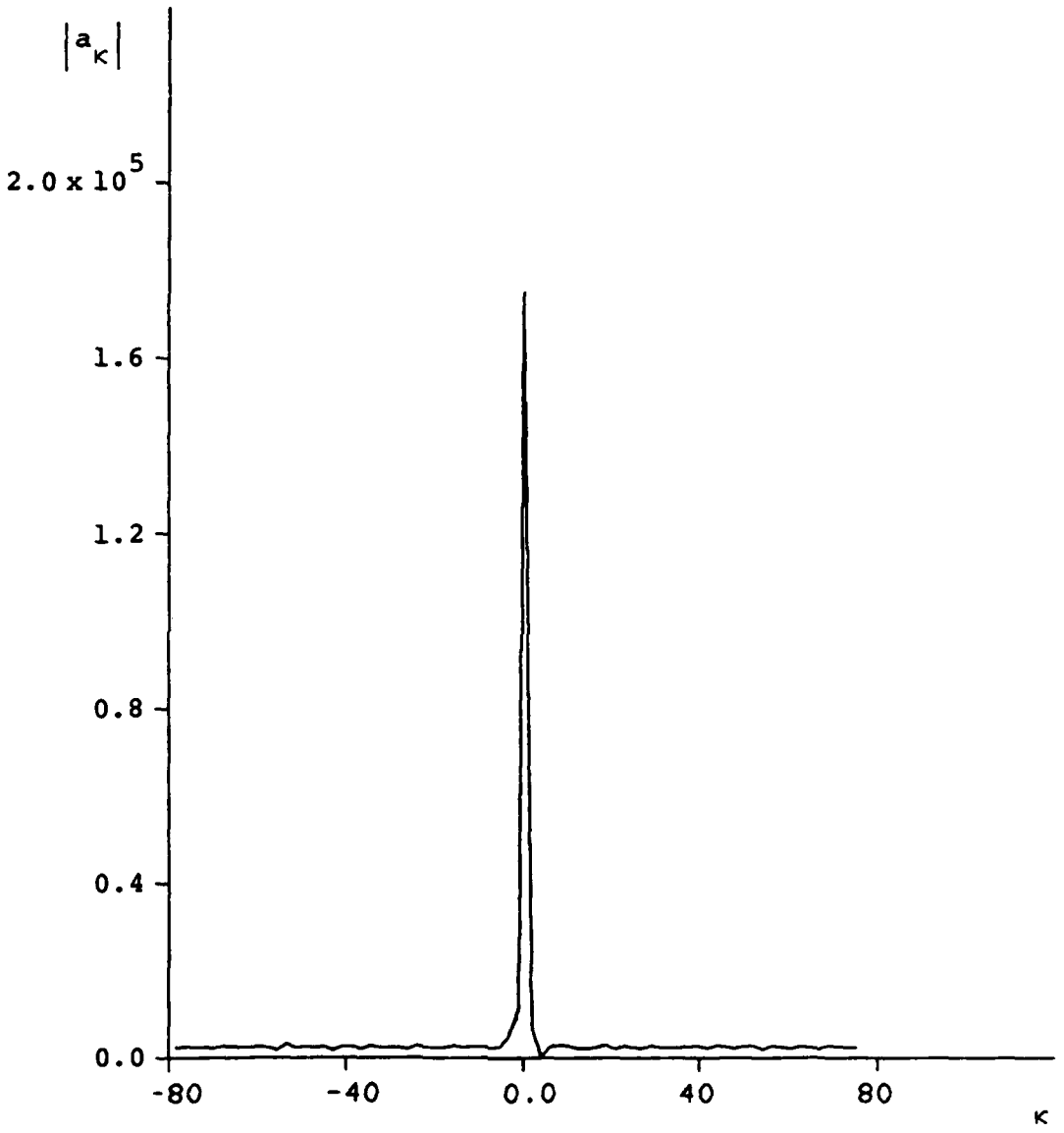

Figure B4(c). Modulus of Fourier Transform for Pulse at Pass 2.

MSNW Parameters, large initial amplitude, no frequency discrimination.

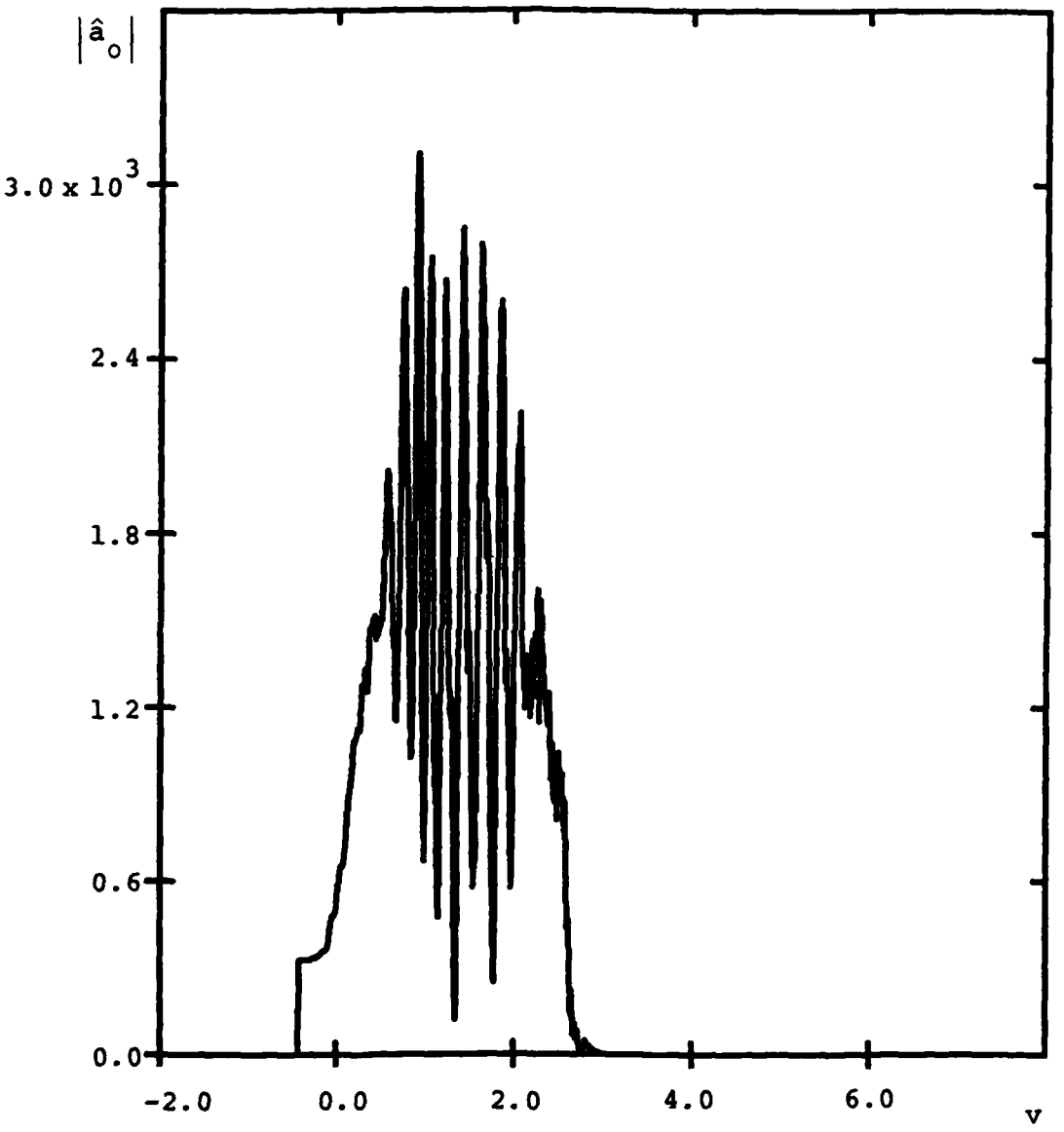

Figure B5(a). Amplitude vs. v at Pass 40 (n = 0). MSNW Parameters, large initial amplitude, no frequency discrimination.

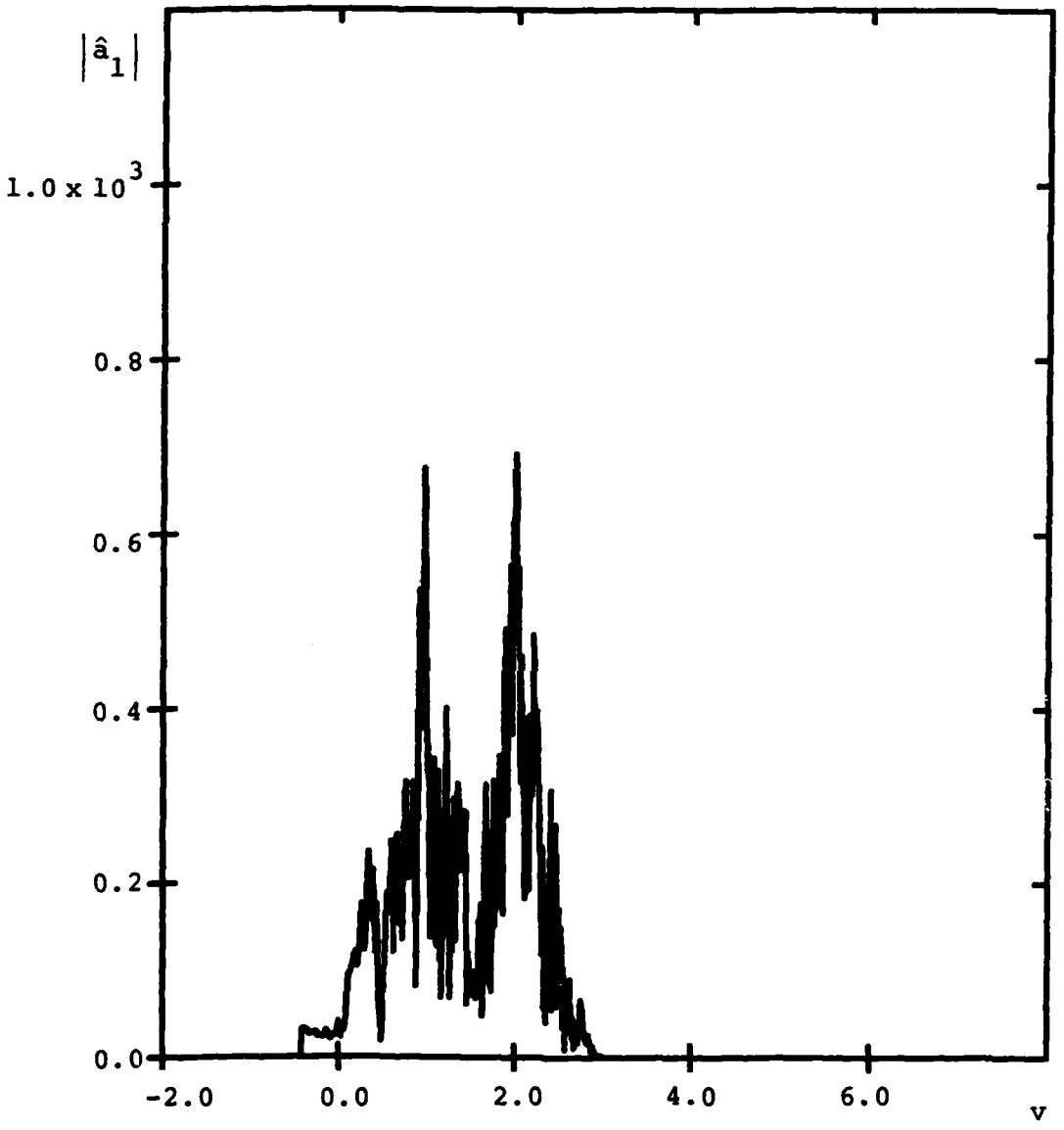

Figure B5(b). Amplitude vs. v at Pass 40 (n = 1).
MSNW Parameters, large initial amplitude, no frequency discrimination.

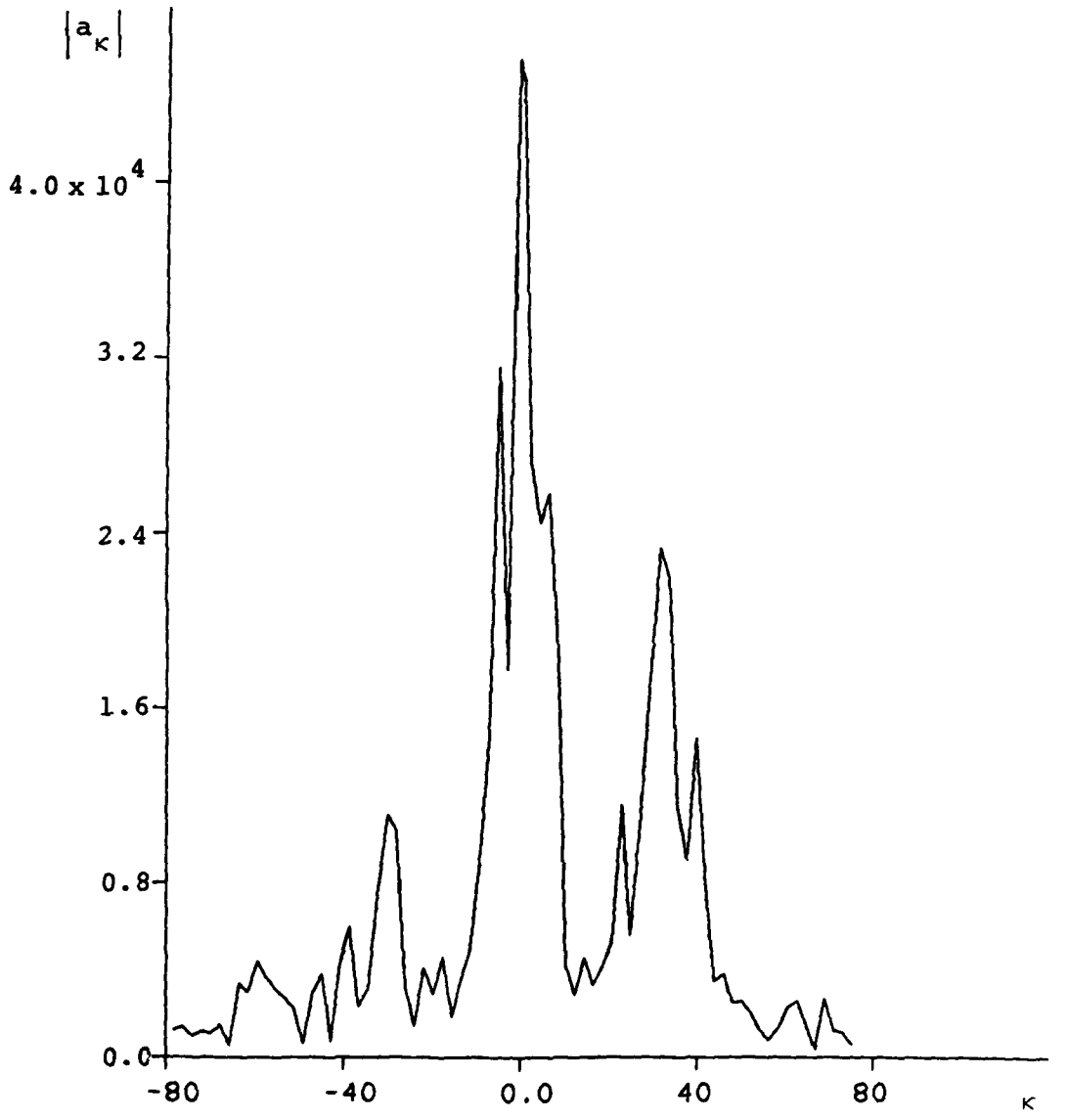

Figure B5(c). Modulus of Fourier Transform at Pass 40.
MSNW Parameters, large initial amplitude, no frequency discrimination.

discrimination. On the basis of Equation (A43) of Appendix A, it is estimated to be necessary that

$$\beta = \frac{1}{\nu} > 0.027 \qquad \text{(B1)}$$

in order to suppress the growth of sideband modes.

For these simulations, $\beta = 0.1$ so that Equation (B1) is well satisfied.

The linear gain in the absence of mirror losses, as determined by the "renormalization" code, is 8.5% per pass.

In Figure B6, the average pulse power $\langle P \rangle$ is plotted as a function of pass number.

The pulse shape and spectrum of the linear eigenmode are displayed in Figure B7.

Figures B8 and B9 exhibit the pulse shape and spectrum at different stages of the growth of the pulse to saturation.

In contrast to the simulation without frequency discrimination, the pulse shape remains smooth and the spectrum consists of a single narrow peak. Sidebands have been suppressed, and the large amplitude saturated pulse propagates coherently. The effective electron trapping fraction is

$$f \sim 22\%$$

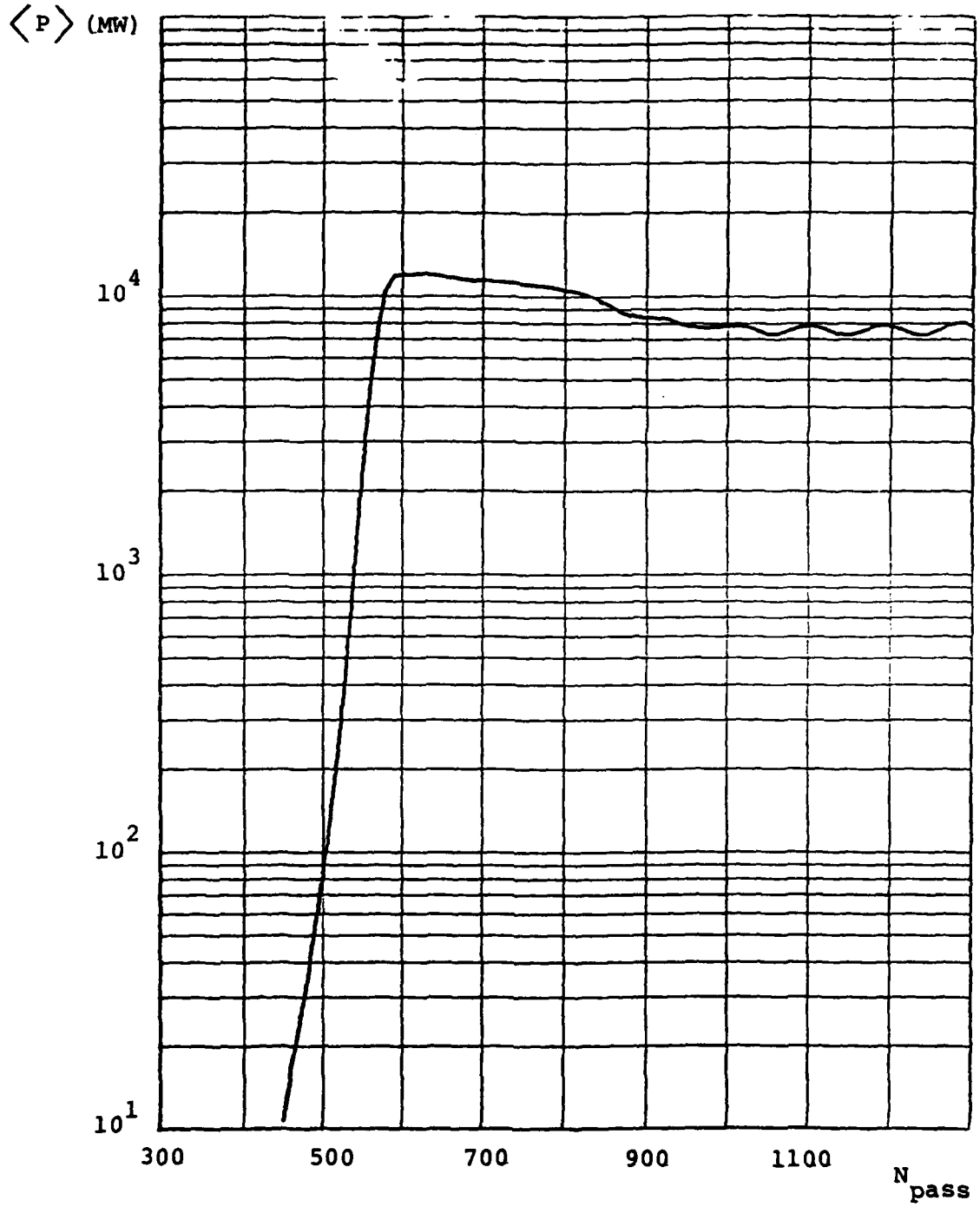

Figure B6. Power vs. Pass Number
MSNW Parameters, frequency discrimination.

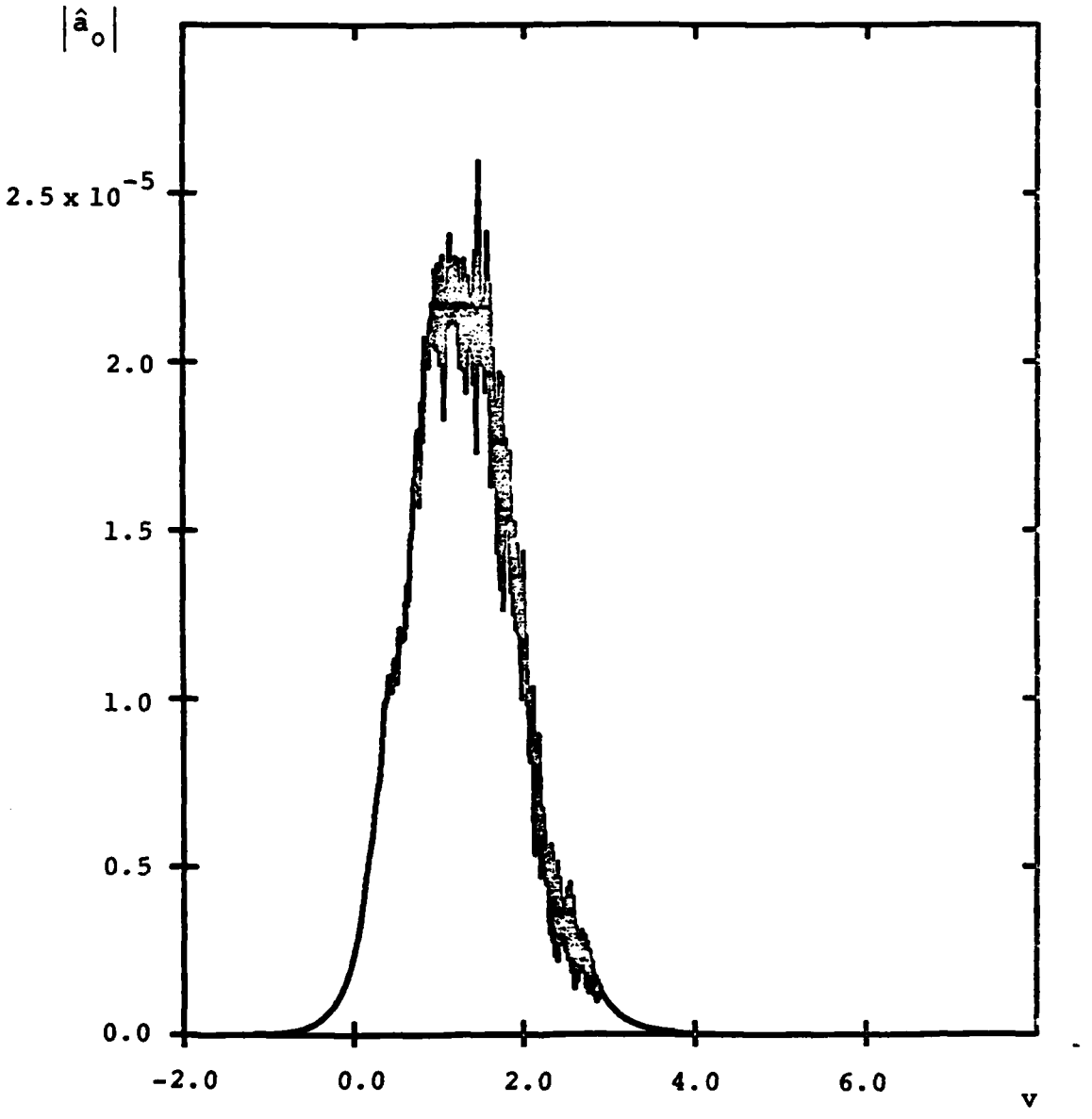

Figure B7(a). Amplitude vs. v for
Linear Eigenmode (n = 0).
MSNW Parameters, frequency discrimination.

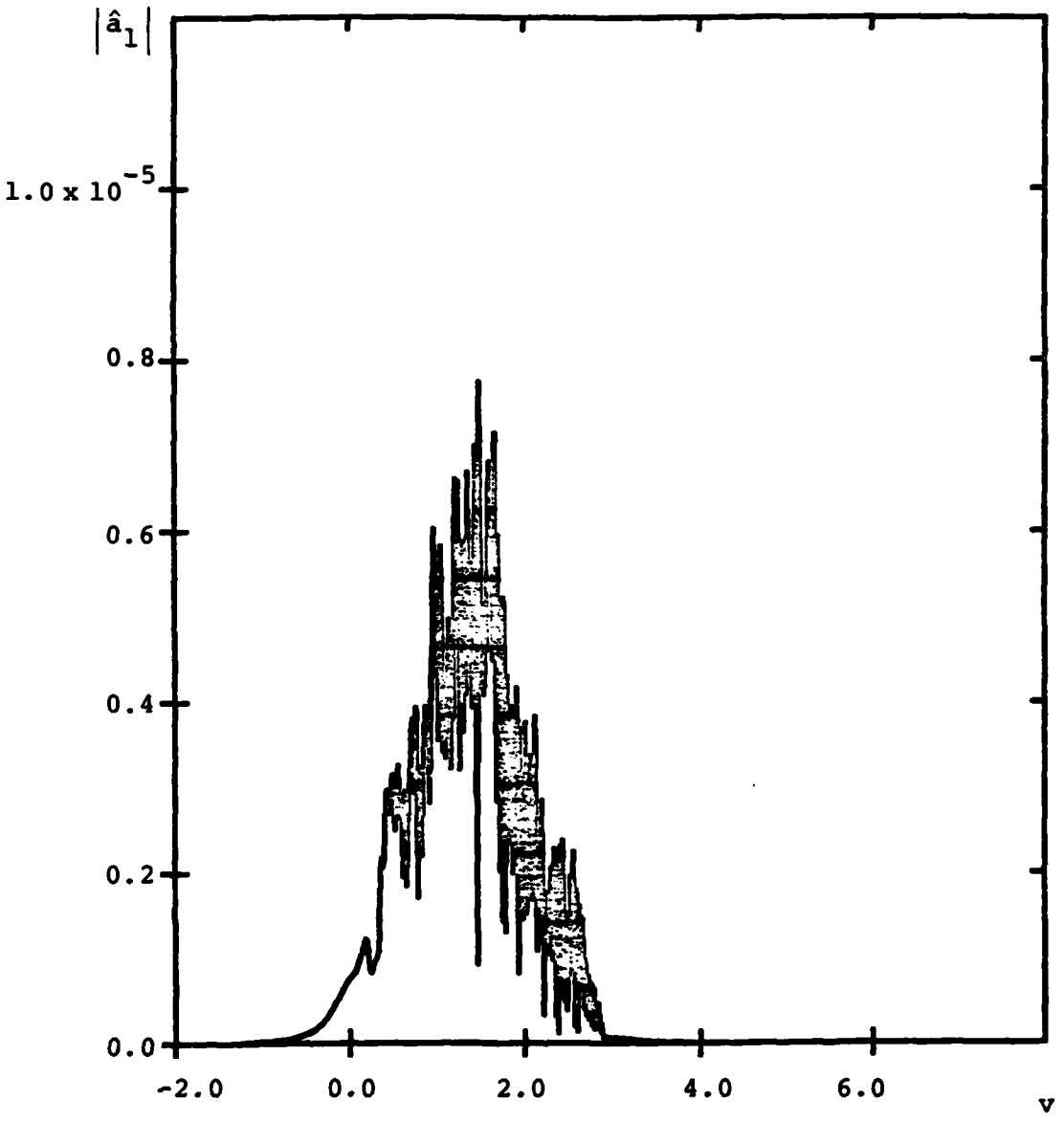

Figure B7(b). Amplitude vs. v for
Linear Eigenmode (n = 1).
MSNW Parameters, frequency discrimination.

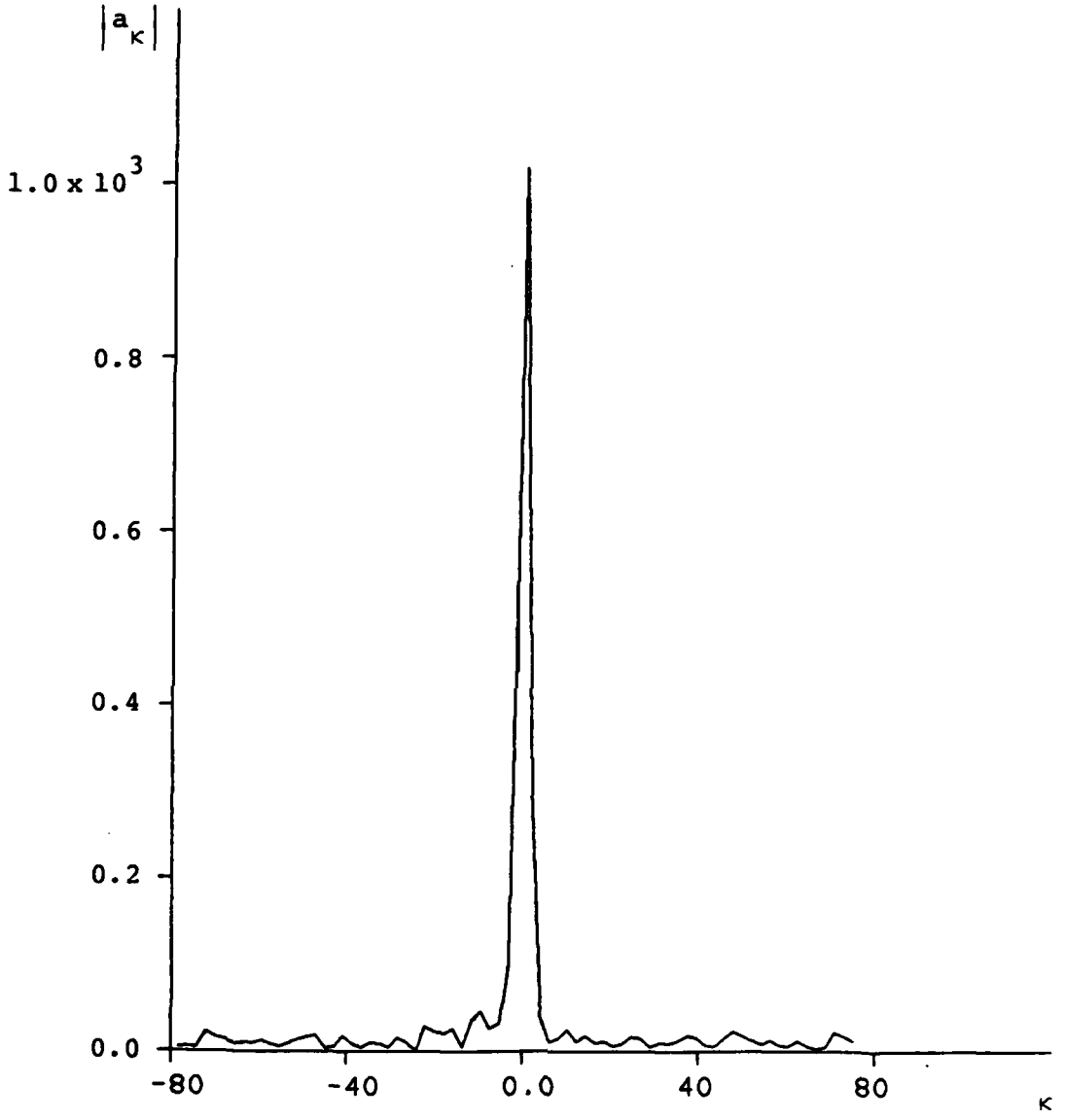

Figure B7(c). Modulus of Fourier Transform for Linear Eigenmode.
MSNW Parameters, frequency discrimination.

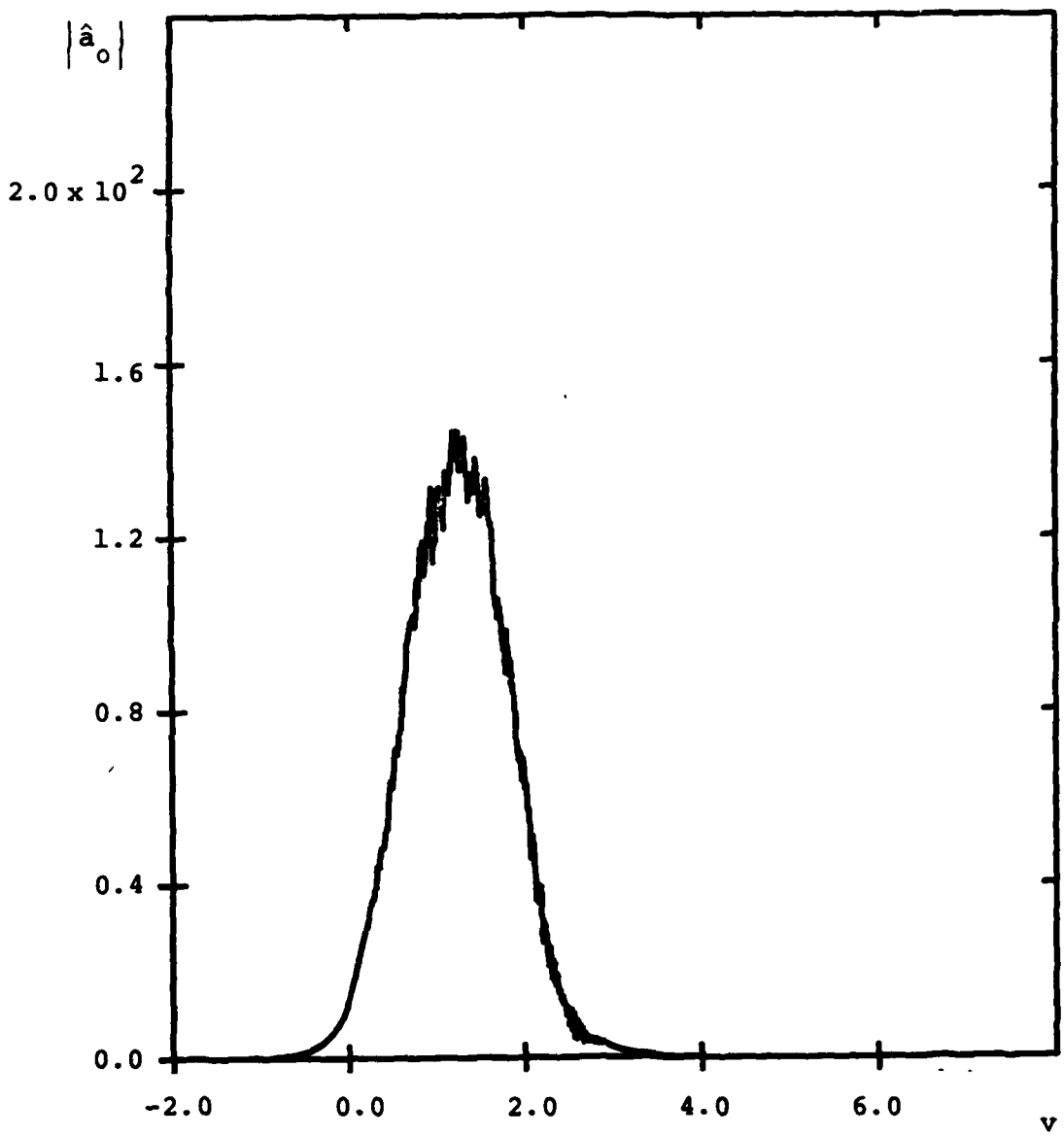

Figure B8(a). Amplitude vs. v for
Pass Number 500 (n = 0).
MSNW Parameters, frequency discrimination.

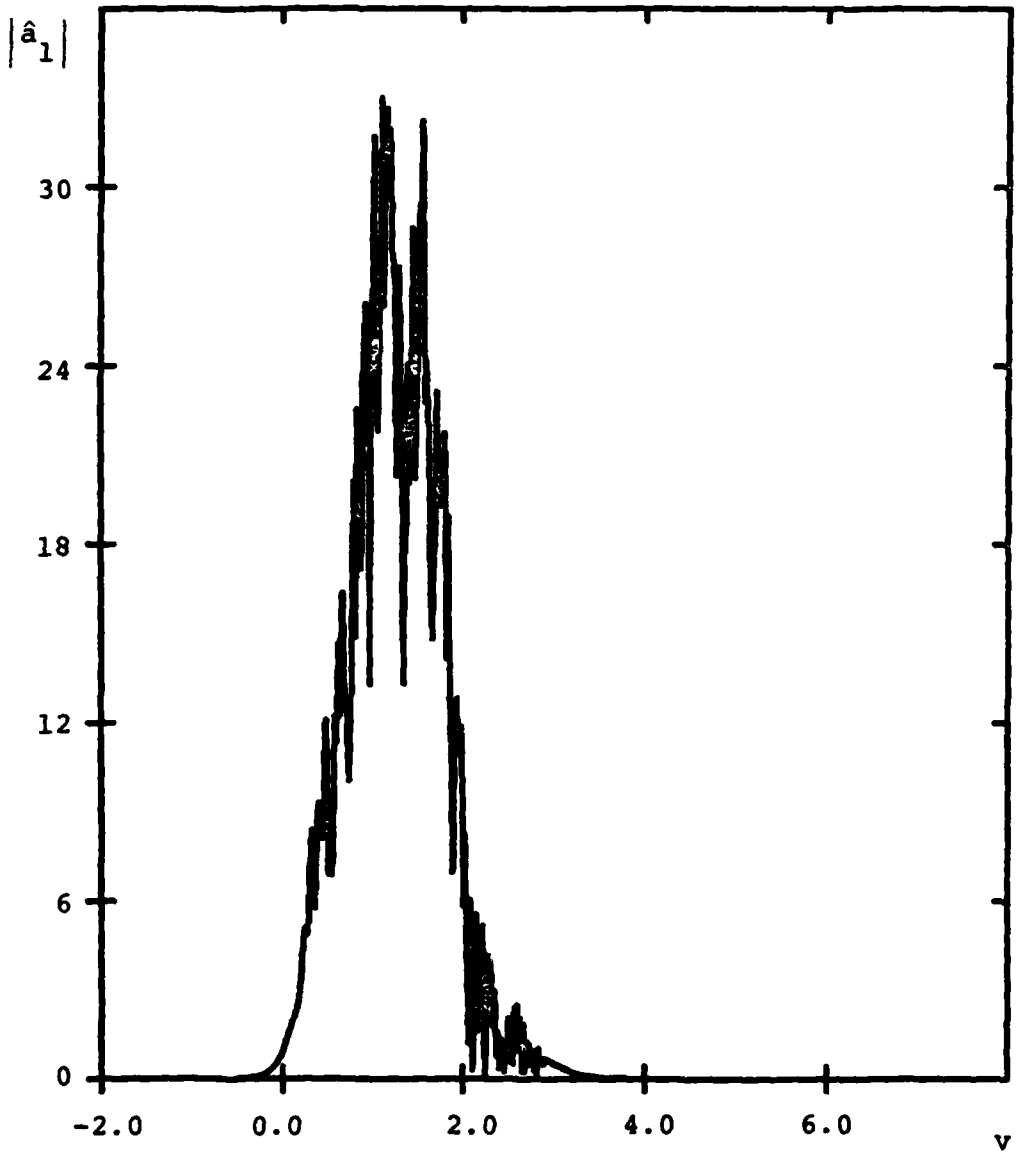

Figure B8(b). Amplitude vs. v for
Pass Number 500 (n = 1).
MSNW Parameters, frequency discrimination.

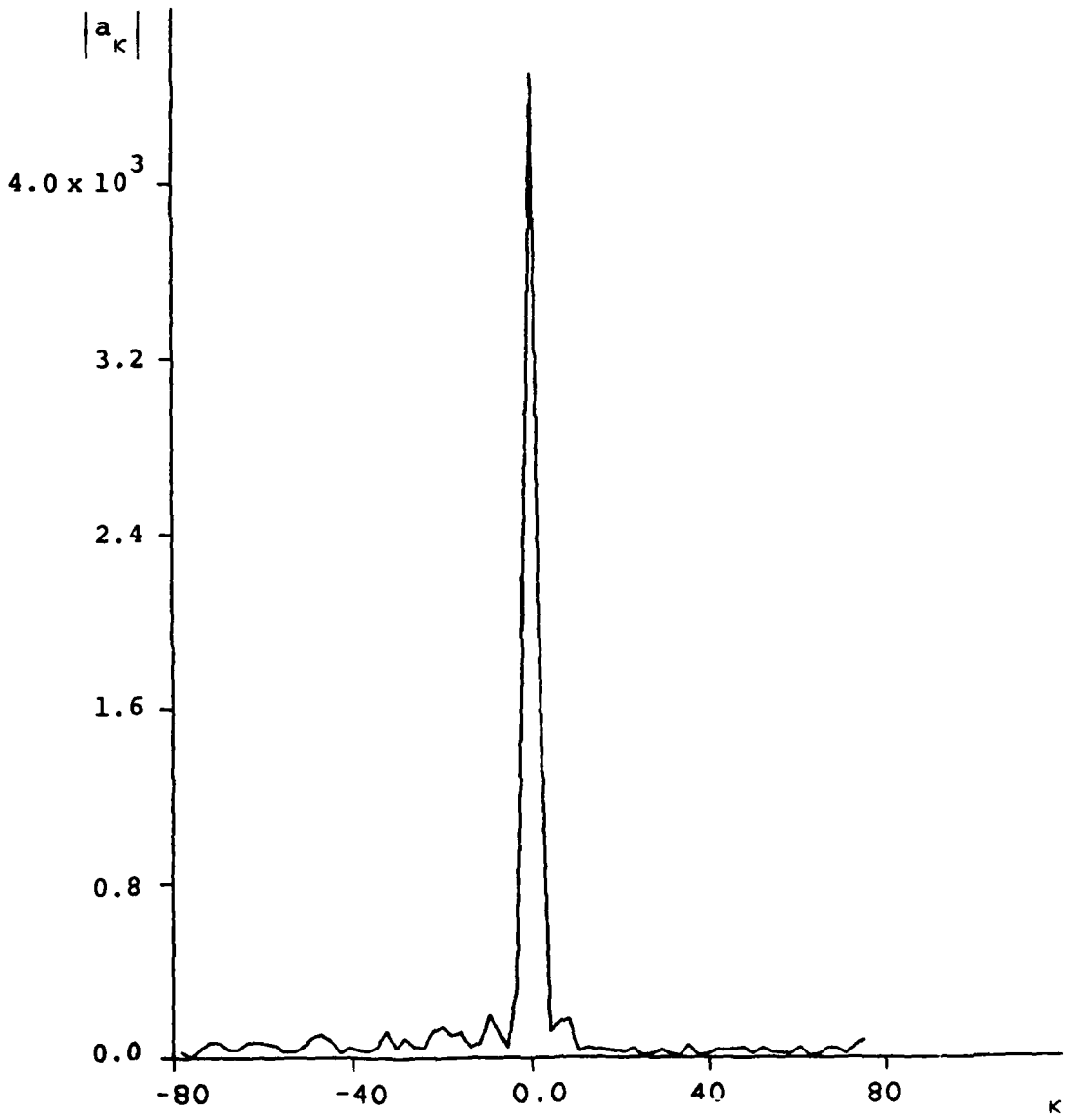

Figure B8(c). Modulus of Fourier Transform
at Pass Number 500.
MSNW Parameters, frequency discrimination.

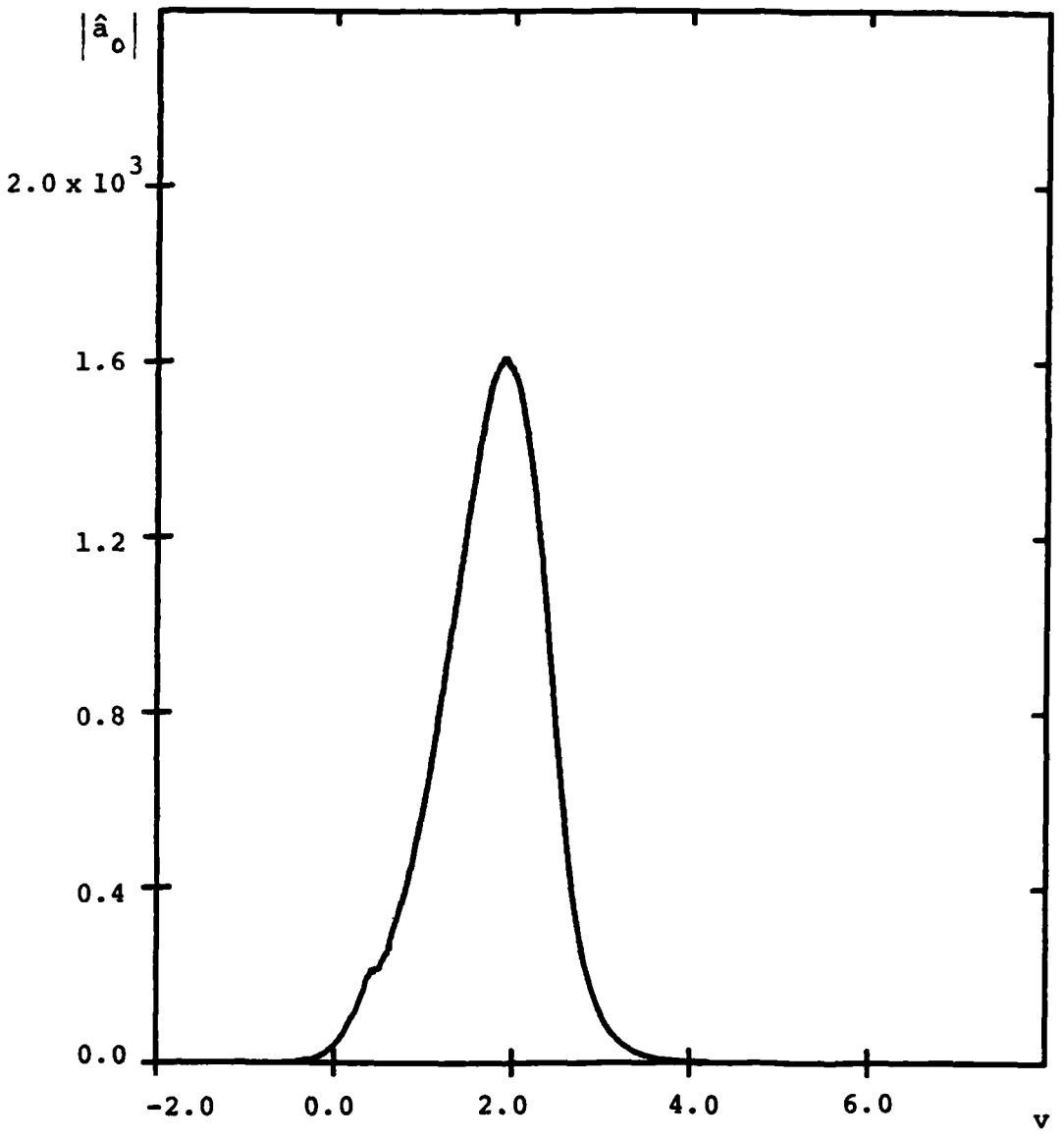

Figure B9(a). Amplitude vs. v at
Pass Number 1100 (n = 0).
MSNW Parameters,
frequency discrimination.

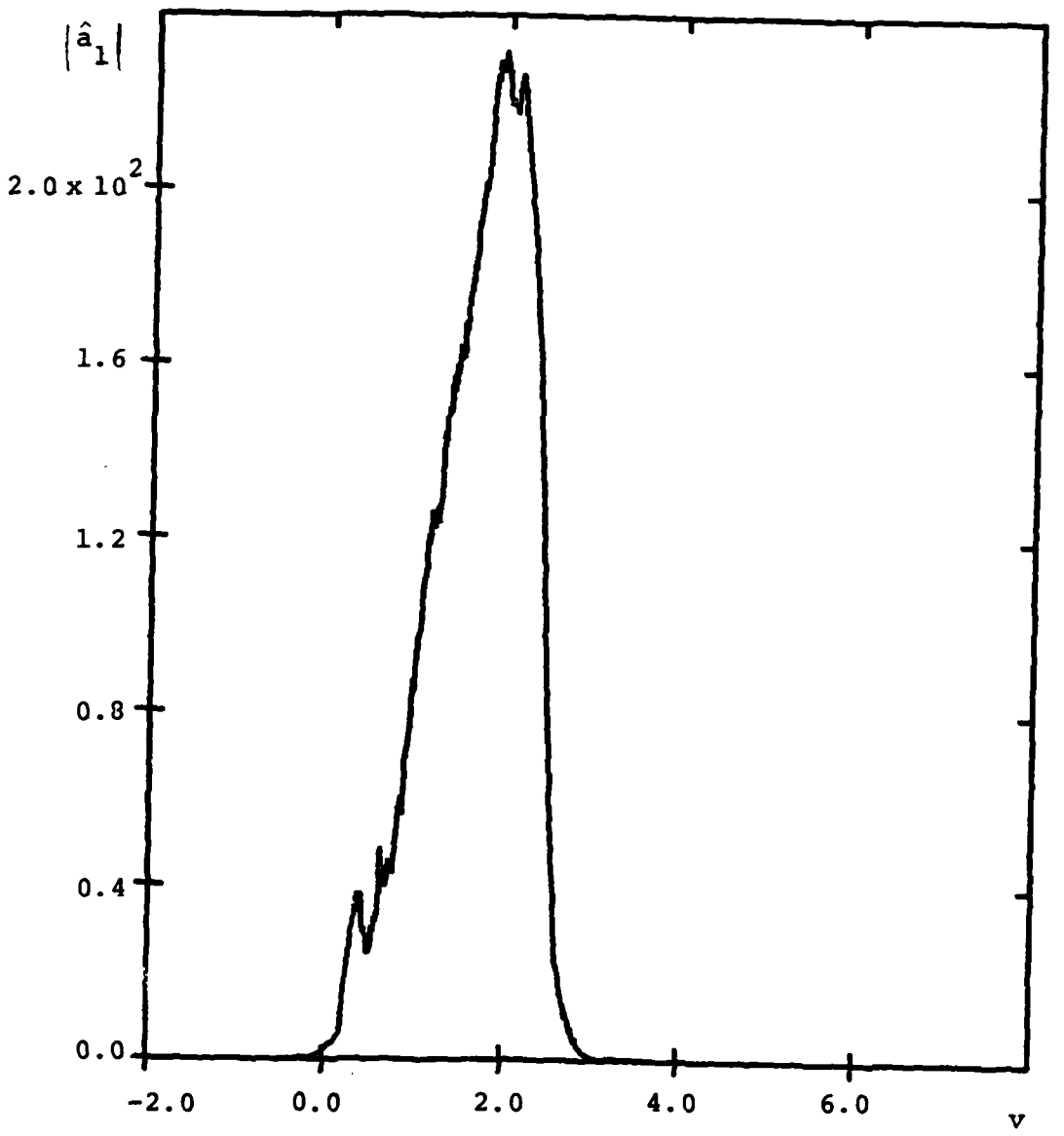

Figure B9(b). Amplitude vs. v at
Pass Number 1100 (n = 1).
MSNW Parameters,
frequency discrimination.

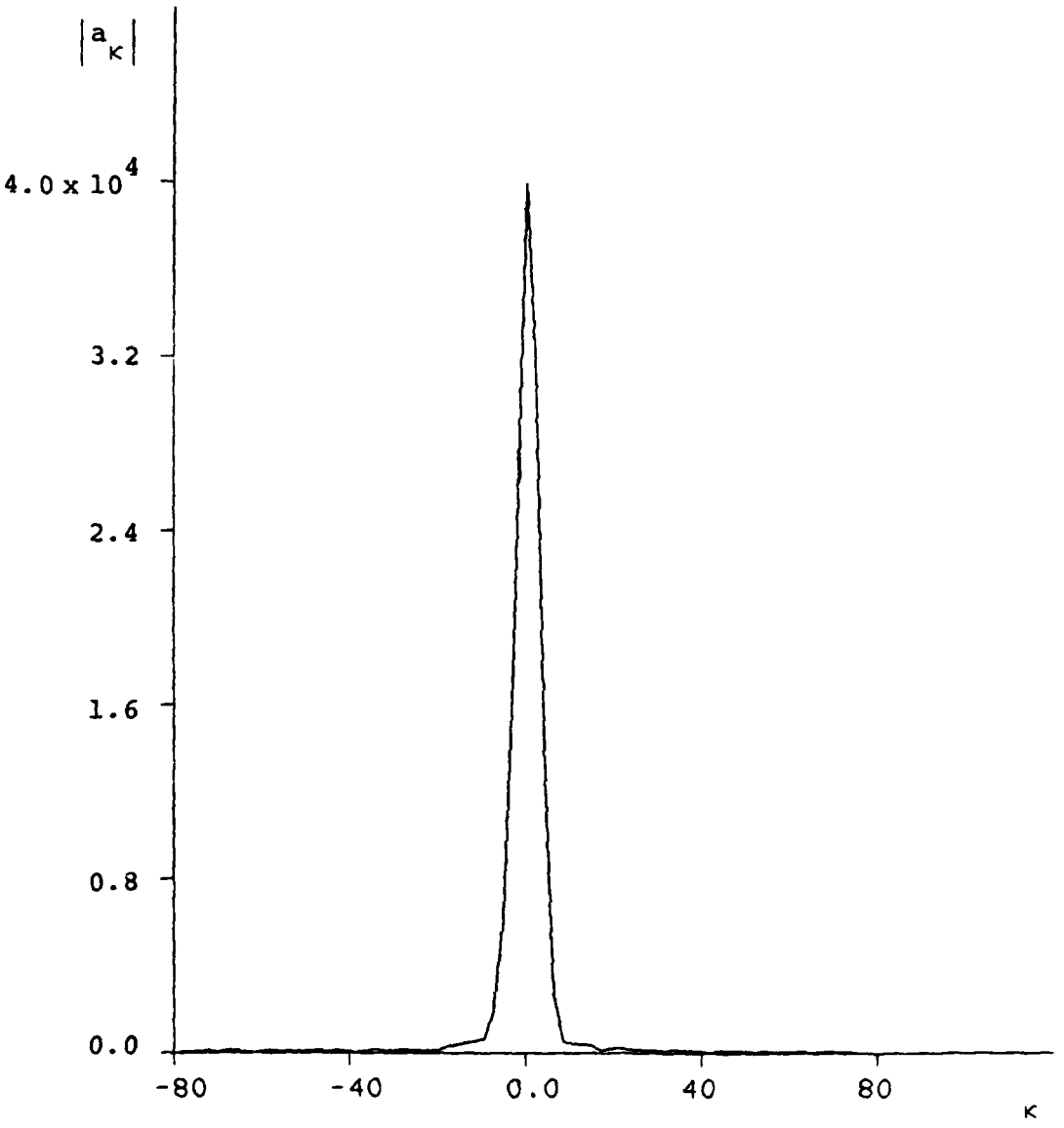

Figure B9(c). Modulus of Fourier Transform at Pass Number 1100. MSNW Parameters, frequency discrimination.

and the average output power is

$$\left\langle P_{output} \right\rangle \sim 660 \text{ megawatts.}$$

The pulse energy in the $n = 1$ mode was about 2% of the energy in the $n = 0$ mode at saturation.

Frequency discrimination is effective not only in producing a smooth pulse shape, but also in enhancing the FEL efficiency.

More recent simulations with frequency discrimination indicate that larger effective electron trapping fractions approaching $f \sim 40\%$ are obtained with longer electron pulse lengths, $u_o \sim 8$.

With the steady state version of the code where no sideband instabilities are allowed to grow, a trapping fraction of $f \sim 55\%$ is obtained.

The general trends exhibited by these simulations are similar to those of the MSNW 1-D simulations. In both, frequency discrimination improves the trapping efficiency and produces a smooth EM pulse.

REFERENCES

1. M. N. Rosenbluth, H. Vernon Wong and B. N. Moore, "Annual Technical Report for Theoretical Studies on Free Electron Lasers," ARA Report No. I-ARA-82-U-89 (NTIS No. AD-A121673), August 1982.

   M. N. Rosenbluth, H. Vernon Wong and B. N. Moore, "Final Technical Report for Theoretical Studies on Free Electron Lasers," ARA Report No. I-ARA-83-U-62 (NTIS No. AD-136333), November 1983.

2. J. Slater, W. Grossman, D. Quimby, A. Vetter and J. Wilcoxon, "Final Report for the MSNW Tapered Wiggler Free Electron Laser Oscillator Program," Report No. C.11.198.01, Mathematical Sciences Northwest, Inc., May 1984.

A P P E N D I X C

PHASE AREA DISPLACEMENT WIGGLER IN STORAGE RING

The phase area displacement wiggler[1] has two features which are attractive with respect to operating a variable parameter Free Electron Laser (FEL) in conjunction with a storage ring: (1) The energy extracted is insensitive to the beam energy spread; (2) The ratio of the energy extracted to the increase in the root mean square energy spread can be made large.

In the deceleration of relativistic beam electrons by phase area displacement, the beam electrons are injected into a variable parameter wiggler in which the resonant energy of the wiggler γ_r increases from the front to the back, $\gamma_r(L) > \gamma_r(0)$. The initial beam energy is such as to produce a resonant interaction of the beam electrons with the ponderomotive potential well or "bucket" [produced by the combined fields of the wiggler and electromagnetic (EM) pulse] near the center of the wiggler $\gamma_i = \gamma_r(z)$, $z \sim L/2$. The interaction may be viewed in terms of an acceleration of the bucket through the phase area (γ,ψ) of the beam electrons, where ψ is the relative phase of the electrons in the EM pulse. The result is

where

$$\Gamma = 2k_w L \frac{\Delta\gamma_r}{\gamma_r} \tag{C5}$$

These formulas were derived in the limit:

$$a >> \Gamma$$

$$\Gamma > 4a^{\frac{1}{2}} \tag{C6}$$

The first inequality is required for the formation of a bucket and should be well satisfied for adiabaticity. The second inequality ensures that the bucket moves in phase space a distance greater than the total width of the bucket. These inequalities imply that

$$a^{\frac{1}{2}} >> 4 \tag{C7}$$

and for a given set of FEL parameters, Equation (C7) imposes a lower limit on the EM pulse power.

In order to operate a phase area displacement wiggler in steady state, the increase in the beam energy spread produced on each passage through the wiggler must be balanced by a corresponding decrease due to incoherent synchrotron radiation ($\Delta\gamma_{syn}$) in the storage ring, and the beam energy boosted to compensate for the losses in the wiggler and storage ring.

a downward displacement in energy of the phase area occupied by the beam electrons by an amount:

$$\frac{\Delta\gamma}{\gamma} \approx -\frac{1}{2k_w L}\ \frac{8}{\pi}\ (a)^{\frac{1}{2}} \tag{C1}$$

where

$$a \equiv 1.36\ \frac{(k_w L)^{3/2}}{\gamma_r}\left(\frac{2a_w^2}{1+a_w^2}\right)^{\frac{1}{2}}\left(\frac{L}{k_s r_p^2}\right)^{\frac{1}{2}}\ P^{\frac{1}{2}}(GW) \tag{C2}$$

$$\gamma_r^2 \equiv \frac{k_s}{2k_w}\ (1 + a_w^2) \tag{C3}$$

k_w is the wiggler wave number, $a_w = eA_w/mc^2$ the dimensionless wiggler amplitude, L the wiggler length, k_s the wave number of the EM pulse, πr_p^2 the pulse area, and P(GW) the pulse power in gigawatts. The wiggler and EM pulse are taken to be circularly polarized.

If the bucket acceleration is adiabatic and no electrons are trapped in the bucket during the interaction, the increase in the root mean square energy spread is

$$\left(\Delta\gamma_{rms}\right)_{wiggler} \approx \frac{\Gamma}{a}\ |\Delta\gamma| \tag{C4}$$

where

$$\Gamma = 2k_w L \frac{\Delta\gamma_r}{\gamma_r} \tag{C5}$$

These formulas were derived in the limit:

$$a >> \Gamma$$

$$\Gamma > 4a^{\frac{1}{2}} \tag{C6}$$

The first inequality is required for the formation of a bucket and should be well satisfied for adiabaticity. The second inequality ensures that the bucket moves in phase space a distance greater than the total width of the bucket. These inequalities imply that

$$a^{\frac{1}{2}} >> 4 \tag{C7}$$

and for a given set of FEL parameters, imposes a lower limit on the EM pulse power.

In order to operate a phase area displacement wiggler in steady state, the increase in the beam energy spread produced on each passage through the wiggler must be balanced by a corresponding decrease due to incoherent synchrotron radiation ($\Delta\gamma_{syn}$) in the storage ring, and the beam energy boosted to compensate for the losses in the wiggler and storage ring.

An approximate theoretical criterion[2] for steady state operation imposes the following lower limit on $\Delta\gamma_{syn}$

$$\left|\frac{\Delta\gamma_{syn}}{\gamma_r}\right| > 73.6\left(\frac{k_w L}{\Gamma}\frac{\Delta\gamma_{rms}}{\gamma_r}\right)^2$$

$$\approx 119/a \qquad \text{(C8)}$$

The Stanford storage ring under construction has been designed for an electron energy of 1 GeV and peak currents of 270 amperes. The stored electron beams will each be 1.0 cm in length and ~0.05 cm in radius. The synchrotron energy loss is less than 0.1% per round trip. The space available to accommodate FEL wigglers is ~20 meters long.

A reasonable set of FEL parameters which would produce an optical pulse with wavelength equal to 0.5 microns is

$a_w = 6.245$

$\lambda_w = 2\pi/k_w = 10$ cm

$\gamma_r = 2000$

$L = 2000$ cm

$r_p = 0.05$ cm
Em pulse radius

These parameters have been chosen for the purpose of illustrating the discussion which follows. However, it should be mentioned that somewhat more favorable operating conditions are possible if λ_w can be reduced, thereby increasing the number of periods inside the wiggler.

For these parameters, the dimensionless parameter 'a' is

$$a = 106.7\ P^{\frac{1}{2}}(GW) \qquad (C9)$$

If an optimistic estimate of $\Delta\gamma_{syn}/\gamma_r \sim 0.001$ per round trip is assumed for this discussion, it is readily seen from Equation (C8) that steady state operation requires very high EM pulse power levels, exceeding by many orders of magnitude the limit $P >> 0.0225$ GW set by Equation (C7).

These very high steady state power levels can be reduced if the effective cooling by incoherent synchrotron radiation can be increased. A simple way to accomplish this would be to adjust the relative round trip times of the EM pulse and the electron beams so that interaction (overlap) occurs, for example, once every 100 electron round trips. Then $\Delta\gamma_{syn}/\gamma_r \sim 0.1$ and steady state peak circulating power levels would be $P \sim 100$ GW. Thus

$$a \sim 10^3$$

and to satisfy Equation (C6), Γ can have the value $\Gamma \sim 250$.

It is unlikely that EM radiation sources with power levels above 10 GW can be procured, in which case steady state will have to be reached by growing the EM pulse, at least in part, in the FEL. This growth to steady state must take place before appreciable energy spreading occurs.

A major concern in growing the EM pulse from lower levels and also in steady state is the avoidance of electron trapping. The variations induced in the ponderomotive potential must be adiabatic. Such variations can be minimized by a careful wiggler design. However, an additional requirement will be a smooth, long EM pulse with negligible amplitude fluctuations occurring in an electron traversal time across a bucket. Thus frequency discrimination will be necessary to have a smooth pulse, and long electron beams to produce a long pulse. An approximate qualitative criterion on the allowable pulse amplitude A_s variation is:[2]

$$\frac{L}{A_s}\frac{dA_s}{dz} < \frac{\tau (2a)^{\frac{1}{2}} \lambda_w}{\lambda_s 10} \sim 89 \qquad \text{(C10)}$$

where $\tau \sim 10^{-4}$ is the fractional number of trapped particles permissible. Hence electron beam lengths of the order of 100 cm are required if trapping is to be kept very small.

Can steady state power levels of 100 GW be sustained by the available beam currents?

The power transferred ΔP from the electrons to the EM pulse is:

$$\Delta P = |\Delta\gamma| \frac{mc^2}{e} I(\text{amps})$$

$$\approx 270 \left|\frac{\Delta\gamma}{\gamma_r}\right| \text{GW} \qquad \text{(C11)}$$

Let the power loss at the mirrors in the interval between interactions of the beam electrons and the EM pulse be $(1-\mathcal{R})P$ where P is the circulating power and $\mathcal{R} \lesssim 1$ is the effective "power reflectivity" of the mirrors. In steady state:

$$P \approx \frac{270}{(1-\mathcal{R})} \left|\frac{\Delta\gamma}{\gamma_r}\right| \qquad \text{(C12)}$$

Substituting Equations (C1) and (C9) for $\left|\frac{\Delta\gamma}{\gamma_r}\right|$:

$$(1-\mathcal{R}) = \frac{2.83}{P^{3/4}} \qquad \text{(C13)}$$

For $P = 100$,

$\mathcal{R} = 0.911$.

If the effective fractional power loss of $(1 - \mathcal{R})$ occurs in 100 round trips of the EM pulse, the fractional power loss per pass is

$$(1 - r) \approx 0.00093 \quad .$$

Hence "power reflectivities" of $r \sim 0.999$ are required to maintain steady state operation.

The fractional beam energy change in one interaction with the EM pulse is

$$\left| \frac{\Delta\gamma}{\gamma} \right| \approx 0.033$$

which is at the limit of the designed storage ring aperture of 3%, although, of course, this is just the energy loss at wiggler exit and may thus be allowable.

The feasibility of operating an FEL oscillator with a phase area displacement wiggler 20 meters long in conjunction with the proposed Stanford storage ring appears to be impossible unless the wiggler performance can be appreciably enhanced.

An interesting modification in this direction suggested by Deacon is to "phase bunch" the electrons in a "pre-buncher" prior to entry into the wiggler. With careful "phase bunching," it may be possible to optimize the electron interaction with the bucket inside the wiggler in order to reduce considerably the accompanying energy spreading. A modest amount of phase bunching may be adequate to reduce the energy

spreading by an order of magnitude. This reduction is, of course, advantageous only if it exceeds the increase produced during phase bunching. If this procedure proves to be practicable, steady state operation should be possible at lower pulse power levels.

The success of this scheme would seem to depend critically on maintaining through the wiggler the phase correlation established between the beam electrons and the EM pulse in the pre-buncher. The slippage S in the wiggler is

$$S \approx \frac{\lambda_s}{\lambda_w} L = 200 \lambda_s$$

and thus fluctuations, for example, in the wavelength of the pulse over this distance S must be small: < 0.1. The effect of the beam dielectric on pulse propagation could become significant and may have to be included in the analysis. And the importance of frequency discrimination (with band width of 0.1%) to produce a smooth coherent pulse is again manifest. A further consideration concerns the pulse length; this must be long enough so that bucket changes are adiabatic. With phase bunching, the probability of particle trapping is reduced so that $\tau \sim 1$ in Equation (C10), and 1.0 cm long electron beams would not be a limitation.

The startup scenario in which the EM pulse evolves from low noise levels to steady state is complex and remains to be elucidated. For the above FEL parameters, the linear gain for a cold beam is ~10%, but oscillates strongly with the beam

energy so that even for storage ring parameters this high gain does not apply. The linear gain is significantly modified by a finite energy spread.

Even if linear gain is adequate, it is not known how the pulse behaves in the transition phase from the linear to the nonlinear regime. This uncertainty may be bypassed by initiating growth in the nonlinear regime, the minimum power level necessary for bucket formation ($a > \Gamma$) being $P > 5.5$ GW for our parameters.

In summary, without pre-bunching in the Stanford storage ring, steady state operation appears to be impossible even if an extremely smooth pulse can be obtained because:

1. Very good "power reflectivities" > 0.999 per pass are required since the electron beam and optical pulse can only be allowed to interact infrequently to avoid excessive spread,
2. Long electron beams of the order of 100 cm are required to keep trapping below 10^{-4},
3. At steady state power levels of 100 GW, there is the added complication of having to grow the pulse from lower levels.
4. An exceedingly smooth EM pulse with no sidebands would be required to avoid trapping.

Probably a 1-10 GW seed laser would be required. Phase bunching could help considerably in relaxing the operating conditions stated in (1) and (2) and could lead to an attractive experiment. However, this scheme is yet to be analyzed in detail, and success will certainly require long steady optical pulses.

Finally, a less ambitious non-steady state experiment to test the ideas of phase area displacement might be possible, but this has not been explored.

We are also beginning to look at an alternative scheme for storage rings, a tapered wiggler with adiabatic trapping and detrapping. It appears somewhat more favorable than phase area displacement, although many of the same problems arise, in particular the need for a very smooth optical pulse (see Appendix D).

REFERENCES

1. M. N. Rosenbluth, H. Vernon Wong and B. N. Moore, "Final Technical Report for Theoretical Studies on Free Electron Lasers," ARA Report No. I-ARA-83-U-62 (NTIS No. AD-136333), November 1983.

A P P E N D I X D

STORAGE RING FEL WITH CONVENTIONAL VARIABLE PARAMETER WIGGLER

In designing an FEL wiggler for use in a storage ring, it is desirable to reduce as much as possible the ratio of the increase in the root mean square energy spread to the energy extracted. For phase area displacement wigglers, this ratio decreases if the number of wiggler periods or the optical power level is increased. Typically, the wigglers have to be very long and very high power levels are required in order to reduce this ratio to acceptable values (see Appendix C).

An alternative possibility which is discussed in this appendix is to use a conventionally tapered wiggler with adiabatic trapping of electrons at the front of the wiggler, adiabatic decrease of the wiggler resonant energy to extract energy from the trapped electrons, and adiabatic detrapping of electrons at the back of the wiggler. In this scheme, negligible increase in the electron energy spread is produced during the adiabatic deceleration of the trapped electrons. Thus, no significant increase in the energy spread occurs while energy is being extracted. The critical task is then to minimize the increase in the energy spread during trapping and detrapping.

This separation of energy extraction from energy spreading introduces a degree of flexibility which can be exploited to reduce the ratio of energy spreading to energy extraction to desirable levels.

Ratio of Increase in Energy Spread To be Extracted

The electron equations of motion are derivable from the Hamiltonian $H(\hat{\gamma},\psi,\tau)$

$$H(\hat{\gamma},\psi,\tau) = \frac{\hat{\gamma}^2}{2} + V(\psi,\tau) \qquad (D1)$$

where the ponderomotive potential $V(\psi,\tau)$ is

$$V(\psi,\tau) = -\Gamma(\tau)\,\psi - a(\tau)\cos(\psi+\zeta) \qquad (D2)$$

The variable $\hat{\gamma}$ is proportional to the derivation of the electron γ from the resonant energy γ_r of the wiggler:

$$\hat{\gamma} = \frac{2k_w L_w}{\gamma_R}(\gamma - \gamma_R)$$

$$\gamma_R^2 = \frac{k_s}{2k_w}(1 + a_w^2)$$

$k_s \equiv$ optical wave number

$k_w \equiv$ wiggler wave number

$a_w \equiv \frac{eA_w}{mc^2}$ dimensionless wiggler amplitude

$L_w \equiv$ wiggler length

$\gamma \equiv$ electron energy parameter.

ψ is the electron phase relative to the optical pulse. The depth "a" of the ponderomotive potential depends on the magnitude of the wiggler and optical amplitudes:

$$a = 1.36 \frac{(k_w L_w)^{3/2}}{\gamma_R} \left(\frac{2a_w^2}{1+a_w^2}\right)^{\frac{1}{2}} \left(\frac{L_w}{k_s r_p^2}\right)^{\frac{1}{2}} P^{\frac{1}{2}}(GW)$$

ζ is the optical phase. Γ determines the wiggler taper and hence the change in the resonant energy $\Delta\gamma_R$ through the wiggler:

$$\Gamma = 2k_w L_w \frac{\Delta\gamma_R}{\gamma_R}$$

The independent variable is the dimensionless variable τ which measures distance along the wiggler:

$$\tau = \frac{z}{L_w}$$

At the beginning of the wiggler, Γ is zero and $a(\tau)$ is adiabatically increased from zero until the electrons are trapped in the ponderomotive potential well. Electrons become trapped when the trapping parameter $\kappa^2 < 1$ where

$$\kappa^2 = \frac{H + a}{2a}$$

When the electrons are deeply trapped, Γ is increased from zero to a finite value. The electrons are decelerated and energy transferred to the optical pulse. At the end of the wiggler, the electrons are detrapped by adiabatic decrease of the ponderomotive potential well depth.

In order to estimate the energy spread due to trapping or detrapping, it is convenient to use the adiabatic invariant J to characterize the electron motion. The goal is to calculate the changes in J which occurs during trapping and detrapping when the motion is not adiabatic. This has previously been done by Timofeev[1] and by Cary, et. al.[2]

The adiabatic invariant can be written as a power series in the smallness parameter

$$\varepsilon = \frac{1}{a^{3/2}} \frac{da}{d\tau} << 1:$$

$$J = J_0 + J_1 + \ldots \qquad \text{(D3)}$$

where

$$J_o = \int_{-\psi_o}^{\psi_o} \left[2(H + a\cos\psi)\right]^{\frac{1}{2}} d\psi \qquad \text{(D4)}$$

$$J_1 = \frac{\partial a}{\partial \tau} \; T \int^{\psi} \frac{d\psi \left\{\cos\psi - \langle\cos\psi\rangle\right\}}{\left[2(H + a\cos\psi)\right]^{\frac{1}{2}}} \qquad \text{(D5)}$$

$$\frac{\partial J_o}{\partial H} = T \equiv \int_{-\psi_o}^{+\psi_o} \frac{d\psi}{\left[2(H + a\cos\psi)\right]^{\frac{1}{2}}}$$

$$\langle\cos\psi\rangle \equiv \frac{1}{T} \int_{-\psi_o}^{+\psi_o} \frac{d\psi\cos}{\left[2(H + a\cos\psi)\right]^{\frac{1}{2}}}$$

$\psi_o = \pi$ for untrapped trajectories and $\cos\psi_o = -\frac{H}{a}$ for trapped trajectories.

For electron motion along trajectories far from the separatrix (the boundary in phase space separating untrapped and trapped trajectories), the change in J is exponentially small.

For electron motion along trajectories close to the separatrix, the adiabaticity condition is no longer satisfied, and finite changes in J occur.

Let us consider the trapping cycle of the electron motion during which the electron crosses the separatrix from an untrapped to a trapped trajectory. Let $a = a_o + \dot{a}_o \tau$, where $\dot{a}_o \equiv \partial a_o / \partial \tau$, $\dot{a}_o \tau << a_o$. During this cycle, the solutions for the electron motion take the form:[1]

$$\psi_-(\tau) \approx -\pi + 4 \tan^{-1} \exp(u) - \frac{1}{4} (k_o^2 - 1 + \varepsilon_o) \exp(-u) \qquad \text{(D6)}$$

$$\psi_+(\tau) \approx \pi - 4 \tan^{-1} \exp(-u) + \frac{1}{4} (k_o^2 - 1 - \varepsilon_o) \exp(u) \qquad \text{(D7)}$$

$$u = a_o^{\frac{1}{2}} \tau$$

and the Hamiltonian H and trapping parameter κ^2 may be approximated by

$$H \approx H_o + \dot{a}_o \tau - \frac{2\dot{a}_o}{a_o^{\frac{1}{2}}} \text{th } u \qquad \text{(D8)}$$

$$\kappa^2 = \frac{H + a}{2a}$$

$$\approx k_o^2 - \varepsilon_o \text{th}\, u \qquad \text{(D9)}$$

where

$$k_o^2 \equiv \frac{H_o + a_o}{2a_o}$$

$$\varepsilon_o \equiv \frac{\dot{a}_o}{a_o^{3/2}}$$

$$|k_o^2 - 1| < \varepsilon_o << 1$$

ψ_- is valid near $\psi_- \sim -\pi$ and ψ_+ near $\psi_+ \sim \pi$. The electron phase is $\psi = -\pi$ when

$$\tau = \tau_-$$

$$\approx -\frac{1}{2a_o^{\frac{1}{2}}} \log \frac{16}{k_o^2 - 1 + \varepsilon_o} \qquad \text{(D10)}$$

and the electron is reflected $\left(\frac{\partial \psi_+}{\partial \tau} = 0\right)$ when

$$\tau = \tau_+$$

$$\approx \frac{1}{2a_o^{\frac{1}{2}}} \log \frac{16}{\varepsilon_o - k_o^2 + 1} \qquad \text{(D11)}$$

The interval $\Delta\tau$ for the trapping cycle is:

$$\Delta\tau = \tau_+ - \tau_- = \frac{1}{2a_o^{\frac{1}{2}}} \left\{ \log \frac{16}{\varepsilon_o - k_o^2 + 1} + \log \frac{16}{\varepsilon_o + k_o^2 - 1} \right\} \quad \text{(D12)}$$

In the neighborhood of the separatrix, the adiabatic invariant may be approximated by:

$$J_o(\tau) \approx 8\, a_o^{\frac{1}{2}} \left\{ 1 + \frac{(\kappa^2-1)}{4} \log \frac{16}{|\kappa^2-1|} + \frac{(\kappa^2-1)}{4} + \frac{1}{2} \frac{\dot{a}_o \tau}{a_o} \right\} \quad \text{(D13)}$$

Thus, the change in the adiabatic invariant during the trapping cycle ($\tau_+ > \tau > \tau_-$) is:

$$\begin{aligned} \Delta J^{(o)} &= J_o + \ldots \\ &= J_o(\tau_+) - J_o(\tau_-) + \ldots \\ &\approx 4a_o^{\frac{1}{2}} \left[\frac{(k_o^2 - 1)}{2} \log \left| \frac{k_o^2 - 1 + \varepsilon_o}{k_o - 1 + \varepsilon_o} \right| - \varepsilon_o \right] \end{aligned} \quad \text{(D14)}$$

J_1 is periodic to lowest order and does not contribute to $\Delta J^{(0)}$ to first order in ε.

More generally, if we denote the trapping cycle by $n = 0$, the trapping parameter κ^2 at the beginning of the n^{th} cycle is:

$$\kappa_n^2 = k_n^2 + \varepsilon_0$$

$$= k_0^2 - (2n-1)\,\varepsilon_0 \tag{D15}$$

and the interval $\Delta\tau_n$ of the n^{th} cycle is:

$$\Delta\tau_n = \frac{1}{2a_n^{\frac{1}{2}}} \left\{ \log \frac{16}{|\varepsilon_0 - k_n^2 + 1|} + \log \frac{16}{|\varepsilon_0 + k_n^2 - 1|} \right\} \tag{D16}$$

$n < 0$ labels untrapped trajectories and $n > 0$ trapped trajectories. κ^2 increases by $2\varepsilon_0$ during each cycle of the electron motion. We assume

$$\frac{\dot{a}_n}{a_n^{3/2}} = \varepsilon_0$$

to be independent of n.

The change in the adiabatic invariant during the n^{th} cycle is:

$$\Delta J^{(n)} \approx 4a_n^{\frac{1}{2}} \left[\frac{k_n^2 - 1}{2} \log \left| \frac{k_n^2 - 1 + \varepsilon_o}{k_n^2 - 1 - \varepsilon_o} \right| - \varepsilon_o \right]$$

$$\approx 4a_o^{\frac{1}{2}} \left[(\alpha_o - n\varepsilon_o) \log \left| \frac{2\alpha_o - 2n\varepsilon_o + \varepsilon_o}{2\alpha_o - 2n\varepsilon_o - \varepsilon_o} \right| - \varepsilon_o \right] \qquad \text{(D17)}$$

where $a_n^{\frac{1}{2}} \approx a_o^{\frac{1}{2}}$, and $2\alpha_o \equiv k_o^2 - 1$.

If we sum over all cycles, we obtain:

$$J = \sum_{n=-\infty}^{n=+\infty} J^{(n)}$$

$$= 2a_o^{\frac{1}{2}} \varepsilon_o \left\{ \beta \log \frac{(1+\beta)}{(1-\beta)} - 2 \right\}$$

$$+ 2a_o^{\frac{1}{2}} \varepsilon_o \sum_{n=1}^{\infty} \left\{ \beta \log \frac{4n^2 - (1+\beta)^2}{4n^2 - (1-\beta)^2} + 2n \log \frac{(2n+1)^2 - \beta^2}{(2n-1)^2 - \beta^2} - 4 \right\}$$

$$= 4a_o^{\frac{1}{2}} \varepsilon_o \operatorname*{Lt}_{N \to \infty} \log \frac{\left\{ (N+\frac{1}{2})^2 - \frac{\beta^2}{4} \right\}^N \pi}{e^{2N+1} \cos \frac{\pi\beta}{2} \, \Gamma\left(N + \frac{1}{2} - \frac{\beta}{2}\right) \Gamma\left(N + \frac{1}{2} + \frac{\beta}{2}\right)} \qquad \text{(D18)}$$

$$= -4a_o^{\frac{1}{2}} \varepsilon_o \log 2 \cos \frac{\pi\beta}{2}$$

where

$$\beta = \frac{2\alpha_o}{\varepsilon_o} \quad .$$

The parameter α_o may be related to the electron phase ψ_s where the electron trajectory crosses the separatrix during the trapping cycle:

$$2\alpha_o = k_o^2 - 1 = \varepsilon_o \sin \frac{\psi_s}{2} \tag{D19}$$

The electrons trapped during this cycle are characterized by $\varepsilon_o/2 > \alpha_o - \varepsilon_o/2$, and the change in J for these electrons is determined by Equation (D18).

Let us assume that the electrons are uniformly distributed in α_o. The mean value of ΔJ is:

$$\langle \Delta J \rangle = \int_{-\frac{\varepsilon_o}{2}}^{\frac{\varepsilon_o}{2}} d\alpha_o \, \Delta J \Big/ \int_{-\frac{\varepsilon_o}{2}}^{\frac{\varepsilon_o}{2}} d\alpha_o = 0 \tag{D20}$$

and the mean square value of $(\Delta J)^2$ is:

$$\left\langle (\Delta J)^2 \right\rangle = \left(\frac{4\dot{a}_o}{a}\right)^2 \frac{1}{\varepsilon_o} \int_{-\frac{\varepsilon_o}{2}}^{\frac{\varepsilon_o}{2}} d\alpha_o \left\{ \log 2 \cos \frac{\pi \alpha_o}{\varepsilon_o} \right\}^2$$

$$= \frac{4\pi^2}{3} \left(\frac{\dot{a}_o}{a_o}\right)^2 \qquad \text{(D21)}$$

If we further assume that a similar increase in the mean square value of ΔJ occurs when the electrons are detrapped, and we note that $\Delta J \approx 2\pi\Delta\hat{\gamma}$ outside the wiggler, we obtain the following estimate for the increase in the root mean square energy spread $\Delta\gamma_{rms}$

$$\Delta\gamma_{rms} \approx \frac{\gamma_r}{2k_w L_w} \sqrt{\frac{2}{3}} \frac{\dot{a}_o}{a_o} \qquad \text{(D22)}$$

Thus the ratio of the increase in the energy spread to the energy extracted per pass through the wiggler is

$$\frac{\Delta\gamma_{rms}}{\Delta\gamma} = \left(\frac{2}{3}\right)^{\frac{1}{2}} \frac{\dot{a}_o}{a_o} \frac{1}{\Gamma} \qquad \text{(D23)}$$

For a given value of $\dot{a}_o/a_o$, $\Delta\gamma_{rms}/\Delta\gamma$ decreases with increasing Γ. However, $\Gamma < a_o$ is required to form a bucket. If we set $\Gamma = fa_o$, where $f < 1$,

$$\frac{\Delta\gamma_{rms}}{\Delta\gamma} = \left(\frac{2}{3}\right)^{\frac{1}{2}} \frac{\dot{a}_o}{a_o} \frac{1}{fa_o} \tag{D24}$$

and $\Delta\gamma_{rms}/\Delta\gamma$ decreases with increasing a_o.

Comparison with Phase Area Displacement Wiggler

The ratio

$$\left(\frac{\Delta\gamma_{rms}}{\Delta\gamma}\right)_{PAD}$$

for a phase area displacement wiggler [see Equation (C4), Appendix C] is

$$\left(\frac{\Delta\gamma_{rms}}{\Delta\gamma}\right)_{PAD} \approx \frac{\Gamma}{a_o} \tag{D25}$$

where $a_o >> \Gamma > 4a_o^{\frac{1}{2}}$. In order to minimize this ratio, it is appropriate to scale Γ with $a_o^{\frac{1}{2}}$, $\Gamma = ga_o^{\frac{1}{2}}$, with $a_o^{\frac{1}{2}} > g > 4$. This implies that

$$\left(\frac{\Delta\gamma_{rms}}{\Delta\gamma}\right)_{PAD} = \frac{g}{a_o^{\frac{1}{2}}} \tag{D26}$$

and this ratio is inversely proportional to $a_o^{\frac{1}{2}}$.

However, the ratio

$$\left(\frac{\Delta\gamma_{rms}}{\Delta\gamma}\right)_{CON}$$

for a conventionally tapered wiggler with adiabatic trapping and detrapping, as determined by Equation (D24), is inversely proportional to a_o. This suggests that it would be advantageous to use a conventionally tapered wiggler when the dimensionless parameter a_o is large, that is, in the limit of very high circulating pulse power [see Equation (C4), Appendix C].

In evaluating the use of a phase area displacement wiggler in the Stanford storage ring (Appendix C), very high steady state circulating power levels ~100GW were found to be necessary. The ratio

$$\left(\frac{\Delta\gamma_{rms}}{\Delta\gamma}\right)_{PAD} = \frac{\Gamma}{a_o}$$

was estimated to be 1/4, with $\Gamma \sim 250$ and $a_o \sim 1000$.

Let $\dot{a}_o/a_o \approx L_w/\ell = 5$, where ℓ is the scale distance over which a_o varies, and let $f \approx 1/6$. Then

$$\left(\frac{\Delta\gamma_{rms}}{\Delta\gamma}\right)_{CON} \approx \frac{24.5}{a_o}$$

and if

$$\left(\frac{\Delta\gamma_{rms}}{\Delta\gamma}\right)_{CON}$$

is to be 1/4, the magnitude of a_o is

$$a_o \approx 98 \quad .$$

This would represent 100 times less circulating power than for the phase area displacement case. For this value of a_o, the parameter $\varepsilon_o \sim 0.5$, and the adiabaticity condition is only marginally satisfied. A somewhat larger value of a_o may be necessary, but nevertheless, smaller than that ($a_o \sim 1000$) required with a phase area displacement wiggler. Thus, the use of a conventionally tapered wiggler with adiabatic trapping and detrapping could reduce considerably the required peak circulating power.

In addition, it should be noted that growth from low noise levels would be easier for conventionally tapered wigglers since they typically have higher linear gain than phase area displacement wigglers.

REFERENCES

1. A. V. Timofeev, "On the Constancy of an Adiabatic Invariant When the Nature of the Motion Changes," JETP 48, 4, 656 (1978).

2. J. R. Cary, D. F. Escande, J. L. Tennyson, "The Breakdown of Adiabatic Invariance at a Separatrix Crossing," submitted to Phys. Rev. Letters.

   J. R. Cary, D. F. Escande, J. L. Tennyson, "Diffusion of Particles in a Slowly Modulated Wave," IFSR No. 155, Institute for Fusion Studies, The University of Texas at Austin (1984).

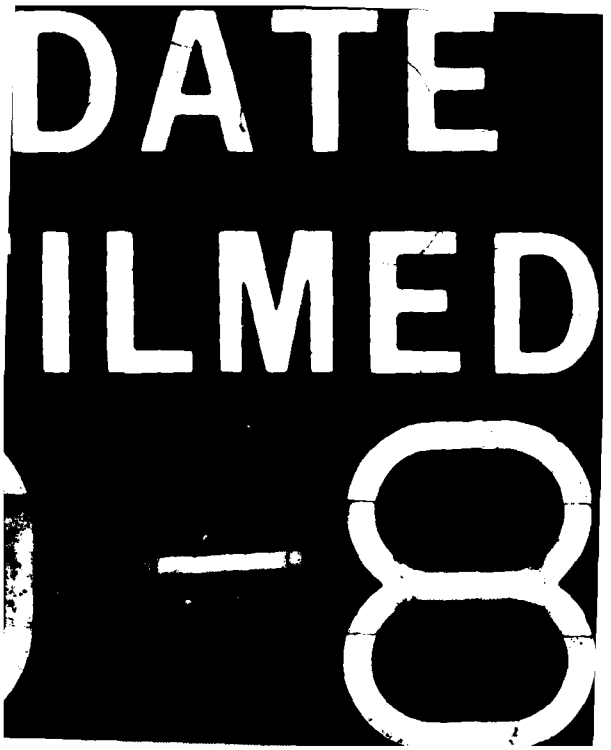
DATE
ILMED
-8